ABSTRACT

Title of Dissertation: ELECTROCHEMICAL COMPRESSION WITH ION EXCHANGE MEMBRANES FOR AIR CONDITIONING, REFRIGERATION AND OTHER RELATED APPLICATIONS

Ye Tao, Doctor of Philosophy, 2017

Dissertation directed by: Prof. Chunsheng Wang, Department of Chemical and Biomolecular Engineering
Prof. Reinhard Radermacher, Department of Mechanical Engineering

The refrigeration industry in the US are facing two main challenges. First of all, the phase down of HFCs in the future would require industries to seek alternative refrigerants which do not contribute to global warming. Secondly, the mechanical compressor in the small scale cooling system with a large energy impact is reaching its limitation due to heat transfer and manufacturing tolerances. Therefore there is an urgent need to develop a highly efficient compression process that works with environmentally friendly refrigerants. And the electrochemical compressor is developed to meet these requirement based on the following reasons. First of all, the electrochemical compressor can achieve an isothermal compression efficiency of greater than 90%. It also operates without moving parts, lubrication and noise. Most importantly, the compressor works with environmentally friendly refrigerants.

In this thesis, three distinct electrochemical compression processes were studied. The first study is focused on modeling a metal hydride heat pump driven by electrochemical hydrogen compressor. The performance of the cooling-generating desorption reactor, the heating-generating absorption reactor, as well as the whole system were demonstrated. The results showed the superior performance of electrochemical hydrogen compressor over mechanical compressor in the system with optimized operating condition and COP. The second study demonstrated the feasibility of electrochemical ammonia compression with hydrogen as a carrier gas. The reaction mechanisms and the compression principle were verified and the compression efficiency was measured to be greater than 90%. The technology can be applied to ammonia vapor compression refrigeration cycle and ammonia storage. The third study is about developing and studying the electrochemical CO_2 compression process with oxygen as a carrier gas. The reaction mechanism was verified and compared for both Pt and $CaRuO_3$ electro-catalysts. And the latter was selected due to better CO_2 and O_2 absorption. The technology can potentially be applied in carbon dioxide transcritical refrigeration cycle and carbon capture.

In conclusion, the electrochemical compression is a promising technology with higher compression efficiency and would bring a revolutionary change to the compressor engineering industry and global refrigeration and air conditioning market. It can also be used in fuel storage and separation based on the selective properties of the ion exchange membrane.

ELECTROCHEMICAL COMPRESSION WITH ION EXCHANGE MEMBRANES FOR AIR CONDITIONING, REFRIGERATION AND OTHER RELATED APPLICATIONS

by

Ye Tao

Dissertation submitted to the Faculty of the Graduate School of the
University of Maryland, College Park, in partial fulfillment
of the requirements for the degree of
Doctor of Philosophy
2017

Advisory Committee:
Professor Chunsheng Wang, Chair, Advisor
Professor Reinhard Radermacher
Professor Yunho Hwang
Professor Michael Zachariah
Professor Taylor Woehl
Professor Peter Sunderland, Dean's representative

Dedication

To my wife Cicy and my daughter Lydia. You are the precious of my life.

Acknowledgements

I would like to express my sincere gratitude to my advisors, Prof. Chunsheng Wang, and Prof. Reinhard Radermacher for their advisory, guidance and support throughout the years. I would also like to thank Dr. Yunho Hwang for his guidance and CEEE for the financial support of my PhD study at UMD. My thanks also go to my colleagues at CEEE and members of Prof. Chunsheng Wang's group. Thank Dr. Hoseong Lee for his guidance at the beginning of my PhD. Thank Prof. Michael Zachariah, Prof. Taylor Woehl, Prof. Peter Sunderland for serving in my defense committee.

I am also very thankful for people who helped me and supported me when I first started here. Tao Cao and Xiaojie Lin, for your help when I first joined CEEE and your friendship during my PhD study. Dr. Yuesheng Ye and Dr. Xiaolong Luo, you offered enormous support during my difficult times and provided me with important guidance. Thanks to Will Gibbons, Chao Luo and Junkai Hu for helping me with the equipment.

My deepest thankfulness goes to my beautiful wife Cicy for her encouragement, support and faith in me. And to my lovely daughter, Lydia, who always bring me joy and happiness when I come home every day. Thank my parents Jun and Jiuhong and my in-laws Sam and Susan for their unfailing love and support. Finally, I would like to thank all my friends at the Maryland Chinese Bible Study Group for your friendship and prayers. Gloria in excelsis deo!

Table of Contents

List of Tables

List of Figures

List of Abbreviations

EC	Electrochemical Compressor
MHHP	Metal Hydride Heat Pump
PEMFC	Proton Exchange Membrane Fuel Cell
AEMFC	Anion Exchange Membrane Fuel Cell
AMFC	Alkaline Membrane Fuel Cell
MEA	Membrane Electrode Assembly
COP	Coefficient of Performance
HFC	hydrofluorocarbons
DC	Direct Current
GWP	Global Warming Potential
PTFE	Poly-tetrafluoroethylene
PMBV	Poly-methyl methacrylate-co-vinylbenzyl
RH	Relative Humidity
BTU	British Thermal Units
HOR	Hydrogen Oxidation Reaction
HER	Hydrogen Evolution Reaction
ORR	Oxygen Reduction Reaction
BET	Brunauer Emmett Teller
XRD	X-ray Powder Diffraction
DI	Deionized
SEM	Scanning Electron Microscope
GC	Gas Chromatography

Chapter 1: Introduction

1.1 Background and Motivation

In the US there are currently an estimated 170 million refrigerators and freezers in use. And the major refrigerants in these cooling appliances are hydrogfluorocarbons (HFCs), which have considerably impact on global warming due to their high global warming potentials (GWPs). In October 15, 2016, leaders in 197 countries gathered in Kigali, Rwanda and agreed on a Montreal Protocol Amendment to phase down HFCs by more than 80% over the next 30 years. Therefore in the future, the US government will come up with legislations to more strictly regulate the operation of HFCs in the refrigeration systems. Currently, industries are seeking alternative refrigerants with low GWPs to replace the HFCs. The currently available alternative refrigerant includes HFOs (R-1234yf for example) or natural refrigerants such as ammonia and carbon dioxide. Among these alternatives, the HFO refrigerant such as R-1234yf is patented by Honeywell and Dupont, which will potentially bring up the cost of air conditioning system and operation. Therefore natural refrigerants such as ammonia and CO_2 become ideal choices of refrigerant because they are cheap to produce and have very low global warming potentials. But both ammonia and CO2 are not as popular for small capacity cooling appliances such as car air conditioning, or window unit because of considerable energy impact of mechanical compressors in the system. The industries are also seeking alternative cooling methods such as solid state cooling to eliminate refrigerant completely. One of the alternative cooling method is the cooling and heating generated by metal hydride reversibly react with hydrogen. The process requires metal hydride to absorb and desorb hydrogen at

different pressure level. To maintain the pressure level, a compressor is needed, which would also bring up the compression efficiency issue. Based on all the aforementioned challenges, there is an urgent need to develop a next generation compressor which operates with a much higher efficiency. Therefore, the electrochemical compressor (EC) is developed to address the aforementioned challenges. The electrochemical compressor is a solid device without moving parts. It operates without lubrication oil, and produces no noise. The EC works with environmentally friendly refrigerants such as metal hydride/hydrogen, ammonia and CO_2, and is potentially much more efficient than mechanical compression.

The EC compresses gas refrigerants with layers of membranes. When a membrane is charged with DC voltage, with the aid of catalyst on both sides of the membrane, gas refrigerants can be converted to ions which are transferred across the membrane from one side to the other, and eventually regenerated on the other side (Figure 1-1).

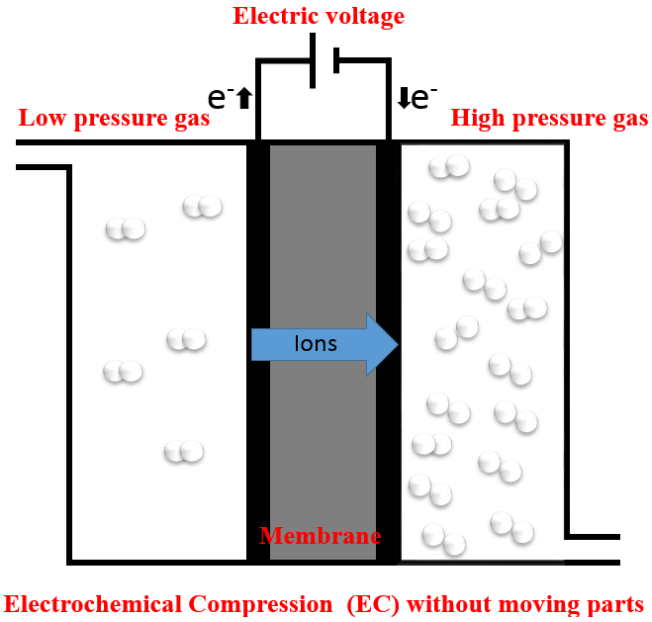

Figure 1-1 Electrochemical compression of gases

Because the entire process is continuous with constant voltage supply, gas molecules are consumed on one side of the membrane and regenerated on the other side, which generates a pressure difference across the membrane. Because the membrane remains stagnant during the entire process, there is no mechanical moving parts, and the process requires no lubrication and no noise is produced during the compression.

1.2 Literature Review on Electrochemical Compression, metal hydride heat pumps and ion exchange membranes

1.2.1 Previous study on electrochemical hydrogen compression and its applications

The concept of electrochemically compressing hydrogen using proton exchange membrane (Nafion) was experimentally studied in 1981 by J. M. Sedlak [1].The process developed back then utilizes a Nafion membrane to separate hydrogen from a gas mixture of hydrogen and nitrogen. With the help of Pt catalyst and a DC voltage charge to the membrane, hydrogen can be converted to protons and electrons on anode. Electrons then travel across the external circuit, while protons are transferred internally through the proton exchange membrane to cathode and combine with electrons to regenerate hydrogen (Figure 1-2).

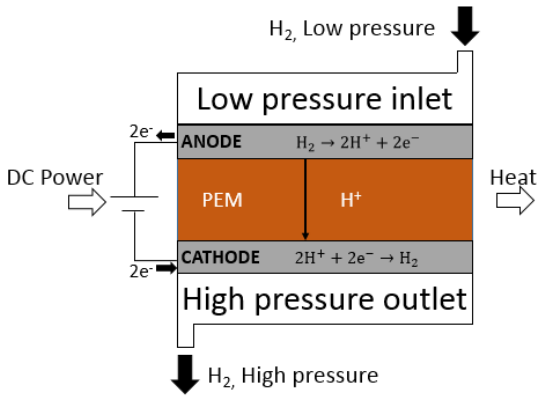

Figure 1-2 Electrochemical compression of Hydrogen

Platinum catalyst was deposited on both sides of the membrane electrode assemblies at a doping amount of 4mg Pt/cm^2. Their experiments were able to achieve hydrogen pressure of 20 atm from the starting pressure of 1 atm with proper membrane support structure. The highest compression efficiency achieved was 87% at 300 mA/cm^2 [1]. But at that time, the development of proton exchange membrane and catalyst is not as advanced as today, therefore their membrane and catalyst performance is limited. And they did not provide any specific design of the electrochemical compression device. Later on in 1998, Rohland and Strobel both studied the electrochemical hydrogen compression for hydrogen storage based on more advanced Pt catalyst and proton exchange membrane. Their motivation of study was to explore the possibility of efficiency improvement of hydrogen EC comparing to small scale mechanical compressors [2,3]. They were able to achieve hydrogen pressure of 43 atm from 1 atm after 18 mins of compression (Figure 1-3).

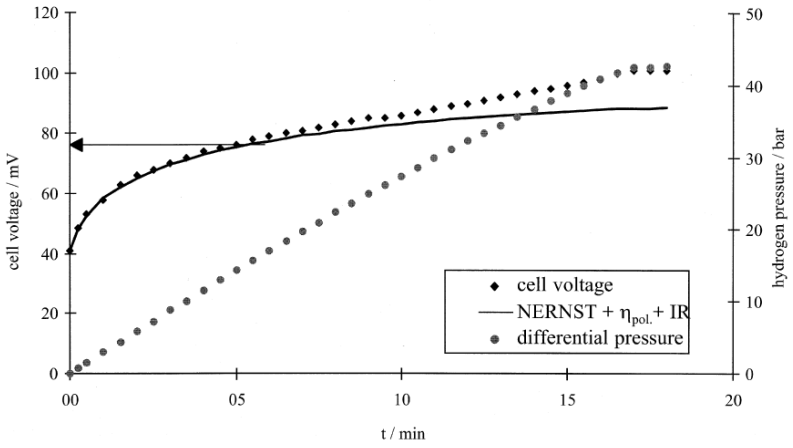

Figure 1-3 Electrochemical compression cell voltage and hydrogen pressure relationship (Rohland, 1997)

The governing equation of electrochemical compression was also proposed, which includes the Nernst potential (Eq. 1-1), polarization voltage (Eq. 1-2) and IR drop (Eq. 1-3). And the total cell voltage is calculated in Eq. 1-4.

$$E_{Nernst} = E_0 + \frac{RT}{2F} ln \frac{P_c}{P_a} \qquad (1\text{-}1)$$

$$\eta = \eta_a + \eta_c \qquad (1\text{-}2)$$

$$U_{ohm} = I * R_i \qquad (1\text{-}3)$$

$$E_{cell} = E_{Nernst} + \eta + U_{ohm} \qquad (1\text{-}4)$$

Where E_0 is zero because the half reactions on both sides of the membrane are opposite. η_a and η_c represents the anode and cathode polarization, which are small for hydrogen oxidation and evolution reactions. The IR drop is resulted by the internal resistance.

It was also pointed out that current density plays an important role in the hydrogen flux across the membrane, but higher current density would lead to reduced performance due to internal IR loss. Therefore the current density must be kept low to minimize the irreversible IR loss, which means the EC is suitable for low power applications [2,3].

The literature review on previous hydrogen EC study by different group is shown in Table 1-1. The EC can compress hydrogen from 1 atm all the way up to 827 atm in one single stage.

Table 1-1: Literature review on hydrogen EC

Group	EC compression pressure achieved (bar)	MEA	Activated area (cm^2)
Rohland et al. (1998)	43	ETEK MEA Nafion 117	100
Strobel et al. (2002)	54	ZSW MEA Nafion 115	100
Grigoriev et al. (2011)	130	Nafion 117	25
Lipp et al. (2012)	827	N/A	200

1.2.2 Previous Study on Metal hydride heat pumps

Metal hydride (MH) cooling and heating technologies are developed with metals or alloys, which can absorb hydrogen reversibly to form MHs. The reaction can be described as Eq. (1-5) (Sandrock, 1999, Hirscher, 2010).

$$M + \frac{x}{2} H_2 \leftrightarrow MH_x + Q \qquad (1\text{-}5)$$

It is clear that there is a thermal effect associated with the process. Where Q is the heat of reaction of hydride formation.

Absorption reaction is exothermic, while desorption reaction is endothermic, based on eq. (1-2). A metal can absorb or desorb hydrogen at given temperature depending on its phase equilibrium plateau pressure (P_m). The absorption process is shown in Figure 1-4. Initially, the metal can dissolve some hydrogen atoms into its lattice to form a solid solution (α phase). When either the hydrogen concentration or the pressure increases further at a given temperature, a MH phase (β phase) starts to form.

Starting at that point, a plateau is observed where both α and β phases coexist [4]. The plateau is similar to the latent heat of a pure substance, such as the latent heat of evaporating water. At low pressure, water evaporates and absorbs heat, at high pressure, water condenses and rejects heat. The Van't Hoff equation below (Eq. 1-6) describes the midpoint plateau pressure in relation with temperature at given enthalpy of formation and entropy of formation [4,5].

$$\ln\left(\frac{P_m}{P_0}\right) = \frac{\Delta H}{RT} - \frac{\Delta S}{R} \tag{1-6}$$

where P_0 is the reference pressure of 1 bar, and R is the gas constant, assuming heat of formation ΔH and entropy of formation ΔS are independent of temperature.

Therefore, the operating pressure can be calculated at any given temperature with the Van't Hoff Equation. Under a given temperature, the metal absorbs hydrogen when the pressure is above the plateau pressure, while below the plateau pressure, the hydride (β phase) is unstable and releases hydrogen.

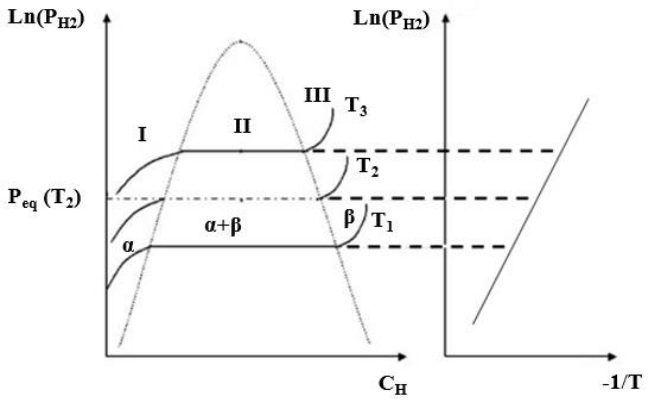

Figure 1-4 Pressure-Composition-Isotherms of Metal Hydride (Hirscher, 2010)

By taking advantage of the unique thermal property of metal hydride react reversibly with hydrogen, researchers over the years have developed metal hydride heat pumps. The heat pump systems have been reviewed by different authors [6,7]. And based on the

operating mechanisms, the metal hydride heat pumps can be divided into two categories: heat driven metal hydride heat pumps, and compressor driven metal hydride heat pumps.

1.2.2.1 Heat driven metal hydride heat pumps (MHHP)

The heat driven MH heat pump is based on transferring hydrogen between two or more reactors at different temperature level, exploiting the different absorption and desorption pressures and temperatures of each reactor to generate heating and cooling [7]. The heat pump can be used to upgrade from low temperature waste heat to high temperature heat. As shown in Fig. 1-5, low temperature MH reactor A and high temperature MH reactor B are connected. Each reactor contains a different MH material. During the operation, MH reactor A releases hydrogen by taking up waste heat at low temperature. Hydrogen released flows to the other reactor which absorbs hydrogen at high temperature to generate useful space heating. The cooling process takes place when the high temperature MH reactor B is cooled by rejecting heat to the air and absorbs hydrogen, which reduces the hydrogen pressure of the system and causes low temperature MH reactor A to desorb hydrogen and generates useful space cooling. But this type of the MH heat pump usually has COP less than 1 [8]. The literature review for heat driven MHHP is shown in Table 1-2 [7]. As shown in the Table, $LaNi_5$ based metal alloy have been widely used in all studies because of its ambient absorption and desorption temperature, which is good for heat pump application, as well as the lattice structure makes it easy to be substituted by different elemental species.

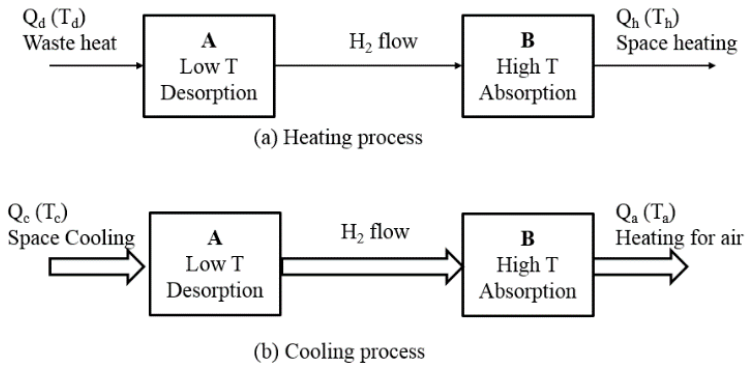

Figure 1-5 Heat driven MH heat pump, using the difference of absorption and desorption pressures of different MH materials

Table 1-2: Previous Study on heat driven MH heat pump [7]

Group	COP	Tcooling/Th source (K)	Capacity (kW)	MH Type
KogaKuin University, 1984	0.4	253/393	1.7	$LaNi_{4.7}Al_{0.3}/MmNi_4Fe$
SRISIA, 1996	0.2	243/473	0.2	$LaNi_{4.5}Al_{0.4}/MmNi_{4.85}Fe_{0.15}$
IKE, University of Stuttgart, 1999	0.6	275/398	0.36	$LaNi_{4.3}Al_{0.4}Mn_{0.3}/La_{0.55}Co_{0.03}Pr_{0.12}Nd_{0.3}Ni_5$
SRISIA, 2002	0.33	277/323	0.15	$LaNi_{4.6}Al_{0.4}/MmNi_{4.15}Fe_{0.85}$
IRCE, Shanghai Jiaotong University, 2007	0.26	293/423	0.085	$LaNi_{4.61}Mn_{0.26}Al_{0.13}/La_{0.6}Y_{0.4}Ni_{4.8}Mn_{0.2}$

1.2.2.2 Compressor driven metal hydride heat pumps

The compressor driven MH heat pump usually places two identical MH reactors [6,7]. A mechanical compressor reduces the pressure of the desorption reactor and increases the pressure of absorption reactor (Figure 1-6) [9]. Thus one reactor desorbs hydrogen

and generates cooling at low pressure and temperature, while the other reactor absorbs hydrogen and generates heating at high pressure and temperature. Figure 1-5 shows that the system is operating under batch mode, when the absorption reactor is saturated with hydrogen and desorption reactor is depleted with hydrogen, the hydrogen flow has to be changed backwards by switching valves, which would potentially create extra room for pipelines and complicate the system design.

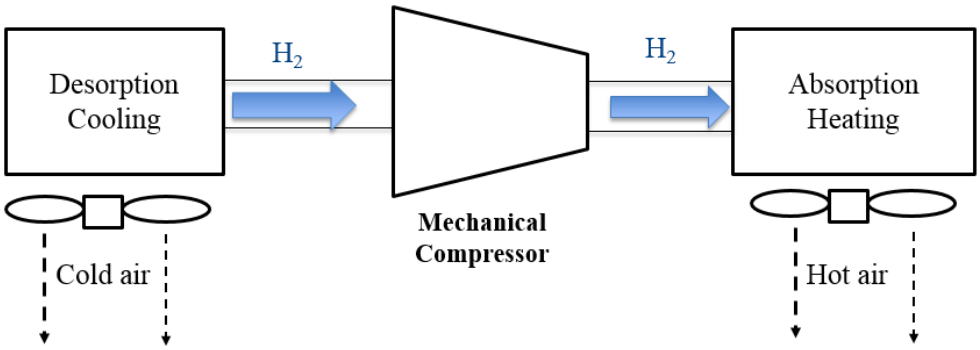

Figure 1-6 Compressor driven metal hydride heat pump, using mechanical compressor to maintain the pressure difference between desorption reactor and absorption reactor

The compressor driven MH heat pump is studied by various groups using a mechanical compressor to maintain the pressure difference by driving hydrogen from one reactor to the other [9-13]. Table 1 lists previous mechanical compressor driven MH heat pump developed by different groups. Among the listed groups, Kim et al and Mazumdar et al did the simulation works, while Park et al and Magnetto et al did the experimental works.

Table 1-3: Summary of previous study on compressor driven metal hydride heat pump

Group	COP	Temperature Lift (°C)	Capacity (kW)	MH Type
Kim et al. (1997)	4.3	8 – 46	3.5	LaNi5
Park et al. (2002)	1.8	6 – 32	1.4	$Zr_{0.9}Ti_{0.1}Cr_{0.55}Fe_{1.45}$
Mazumdar et al. (2004)	2.5	22 – 32	1	$Zr_{0.9}Ti_{0.1}Cr_{0.55}Fe_{1.45}$
Magnetto et al. (2006)	2.6	20 – 45	2	Mm based alloy

Kim et al. (1997) conducted steady state simulation and calculated the COP of LaNi5 system to be 4.3 for a 3.5 kW system with cooling temperature at 8 °C and heating temperature at 46 °C, however, they didn't consider the hysteresis of the MH material, pressure drop during suction and discharge of hydrogen, and heat exchanger effectiveness, so their modeling results might be a bit optimistic. Park et al. (2002) conducted the experiment on $Zr_{0.9}Ti_{0.1}Cr_{0.55}Fe_{1.45}$ and measured the COP to be 1.8 for a 1.4 kW system with cooling temperature at 6 °C and heating temperature at 32 °C. Mazumdar et al. (2004) conducted the transient simulation using $Zr_{0.9}Ti_{0.1}Cr_{0.55}Fe_{1.45}$, taking into account the heat transfer and calculated the COP to be 2.5 with cooling temperature at 22 °C and heating temperature of 32 °C for a 1 kW system. Magnetto et al. (2006) developed a prototype of Mm based alloy that shows COP of 2.6 for a 2 kW system with cooling temperature at 20 °C and heating temperature at 45 °C. However, with all the studies conducted, the mechanical compressor driven metal hydride heat pump has its limitations. The major drawback is the low compressor efficiency in the system makes the compressor a large energy consumer. Currently, small compressors in the capacity range of less than 1 kW of cooling has isentropic efficiency around 65%. There is very little improvement can be done, due to manufacturing tolerances and friction loss. Moreover, the compressed hydrogen

usually contains traces of lubrication oil which is detrimental of the metal hydride reaction process.

1.2.3 The effect of ammonia in proton exchange membranes

As previously mentioned for the electrochemical hydrogen compression, proton exchange membrane (PEM) such as Nafion can be used as an ion conductor to transport protons. To date, hydrogen is the only gas that has been reported transferable across the PEM. A large volume of research has been conducted on PEMs to study the potential contaminants to the membrane. Ammonia in the proton exchange membrane fuel cell (PEMFC) system has been considered as a contaminant [14-17]. Uribe et al found out that traces of NH_3 in the PEMFC anode feedstream causes a decrease in the cell current. And extend of the effect depends not only on the NH_3 concentration in the feed but also the time of exposure [14]. They also measured the NH_4^+ ionic conductivity in the Nafion 105 membrane to be around 0.032 S/cm [14]. They concluded that the PEM conductivity may recover after short period of exposure to ammonia (1 to 3hrs). But the membrane may not recover after long term exposure to ammonia (15 hrs). Soto et al. studied the recovery mechanism of PEM after exposing to a range of 200 ppm NH_3/H_2 to 1000 ppm NH_3/H_2. They found slow recovery rate in the time scale from 2 hrs to 10 hrs. They also proposed the neutralization mechanism of H^+ on NH_4^+ during recovery [15]. Halseid et al., studied the NH_4^+ ion conductivity under different temperatures. Their experimental results show that the NH_4^+ conductivity in Nafion membrane changes from 0.035 S/cm to 0.079 S/cm, under temperatures ranging from 10 °C to 60 °C. They also found out that ammonium ion reduces the conductivity of Nafion 117 membrane by a factor of

3.8 to 3.9, comparing to pure H^+ form Nafion membrane at 25 °C, which is consistent with the finding from Uribe et al [14]. Traces of ammonia introduced into the anode side may reduce the proton conductivity of the PEM by forming NH_4^+, which could displace the H^+ in the membrane. In addition, due to the larger ionic radius of NH_4^+ ions, the ionic conductivity in the membrane goes down [16]. Therefore, previous studies in the PEMFC community have been largely focused on minimizing the NH_3 contamination and crossover. Jung et al. studied the ammonia transport effect in PEM from anode to cathode as a contaminant, and found out that ammonia was able to diffuse across the membrane under humidified condition based on concentration gradient. They tested the membrane under 100-300 ppm NH_3 in N_2 and calculated the flux. They also modeled the diffusion of NH_4^+ in Nafion 117. They also found that with the presence of water, ammonia can dissolve in membrane and quickly reacts with H^+ to form NH_4^+. The NH_4^+ can migrate from one side to the other side of the membrane and converts back to NH_3, which comes out in the gas phase [17]. They concluded that the diffusion of NH_3 in Nafion membrane from anode to cathode logarithmically increases with RHs supplied to the anode. With all the previous studies on the NH_3 contamination in the PEM, it can be concluded that NH_3 does form NH_4^+ ion in the PEM. And there is transport effect due to concentration gradient. My research in this case takes advantage of the NH_4^+ transport effect in the PEM, and developed a membrane compressor to increase the pressure of ammonia using hydrogen as a carrier gas by charging a DC voltage. The electrochemical ammonia compressor development will be discussed in details in Chapter 4.

1.2.4 The effect of carbon dioxide in anion exchange membranes

Anion exchange membrane (AEM) fuel cells have been studied as an alternative for proton exchange membrane fuel cells with potentially better performance and lower cost [18,19]. To date, the AEM fuel cells involve hydroxide ion (OH^-) as the conductive ion. One of the drawback of using hydroxide ion conductive membrane is the development of carbonate/bicarbonate ion in membrane during the operation after exposing to carbon dioxide in the air (Equation 1-4).

$$OH^- + CO_2 \rightarrow HCO_3^- \qquad (1\text{-}4)$$

The resulted carbonate/bicarbonate ion has a lower mobility in the membrane comparing to hydroxide ion, and leads to reduced performance. Report shows that the conductivity of carbonate/bicarbonate ions in the AEM is in the range between 0.002 S/cm to 0.015 S/cm depending on the operating temperature of the fuel cell [20]. The conductivity of hydroxide ions, on the other hand, is in the range of 0.009 to 0.021 S/cm [21]. Based on all the previous study, it is clear that CO_2 can be transferred in the form of CO_3^{2-} or HCO_3^- ions in the anion exchange membranes. And a few studies have done in the past to explore the CO_2 transportation in either carbonate fuel cell as well as using the membrane as a medium for transferring CO_2 across [19, 22, 23]. Vega and Kitchin both studied the effect of CO_2 transfer in the AEM by charging the AEM with a voltage, and the resulted current density ranges from 6 mA/cm^2 at 1.2 V and 10 mA at 1.5 V of charge. FuelCell Energy developed the reverse cycle of molten carbonate fuel cell for CO_2 capture. But it requires heating up the MCFC system to at least 650 °C and is a very energy intensive process. Vega et al. explored the Carbonate cycle in the AEM fuel cell generated by $CaRuO_3$ catalyst, and showed

superior performance than state of the art Pt catalyst [22]. Rotating disk electrode experimental data on $CaRuO_3$ shows that with the presence of both CO_2 and O_2, reduction current is larger than the same condition without CO_2, which means $CaRuO_3$ catalyst shows a better performance with CO_2 presence in the anion exchange membrane fuel cell running under carbonate cycle (Figure 1-7) [22].

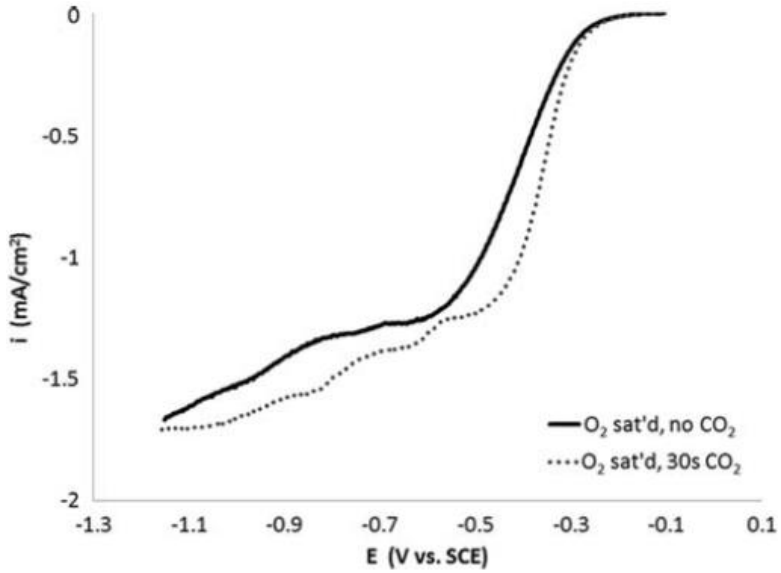

Figure 1-7: The O_2 reduction current measured with and without CO_2 for $CaRuO_3$ catalyst in rotating disk electrode at 900 RPM [22]

1.2.5 Summary

Based on what have been explored in the field of electrochemical hydrogen compression, it is clear that hydrogen can be successfully compressed using the proton exchange membrane. The current density for hydrogen electrochemical compression needs to be kept at a low level to reduce the IR loss. The electrochemical hydrogen compression shows higher compression efficiency than conventional mechanical compressor and creates a potential for future studies for heat pump applications.

Metal hydride heat pump were extensively studied by different groups. The heat pumps can be categorized into two groups, the heat driven metal hydride heat pump and compressor driven metal hydride heat pump. The heat driven metal hydride heat pump requires coupling of two metal hydride reactors at different plateau pressure and temperature for each heating and cooling cycle. The heating metal hydride reactor is driven by another metal hydride hydrogen desorber heated by waste heat, whiling the cooling metal hydride reactor is driven by another metal hydride hydrogen reactor which absorbs hydrogen at higher temperature. The COP of heat driven metal hydride heat pump is usually less than 1, which leaves a lot of rooms for improvement. The compressor driven metal hydride heat pump, however, couples a metal hydride hydrogen desorber and a metal hydride hydrogen absorber with a mechanical compressor with both reactors running in batch mode. The compressor reduces the pressure of the desorber and increases the pressure of the absorber. And the system produces cooling and heating at the same time. The compressor driven MHHP has a much higher COP than the heat driven system.

Ammonia has been considered as a contaminant in the PEM fuel cell. A hydrogen stream with ammonia in ppm level supplied to the anode of the fuel cell can decrease the PEMFC performance by reducing the PEM proton conductivity. The proton conductivity was reported to be reduced to around ¼ of the original value. And researchers in the past have discussed the presence of NH_4^+ ions in the PEM, which sets the theoretical foundation of transporting ammonia in the form of NH_4^+ across the membrane.

Carbon dioxide was reported to be an issue in anion exchange membrane fuel cell which conducts OH^-, because the formation of HCO_3^- and CO_3^{2-} both have reduced mobility in the membrane and lead to reduced AEM conductivity. The presence of CO_2 in AEM in the form of HCO_3^- and CO_3^{2-} ions made the transport of CO_2 across the membrane possible. A few groups in the past have studied the aforementioned transport of CO_2 and showed preliminary results. The results mainly shows a competition of both HCO_3^- and CO_3^{2-} in the membrane due to the adoption of Pt catalyst on both sides of the AEM. There has also been some study on the $CaRuO_3$ catalyst performance to generate CO_3^{2-} in AEMFC for better reaction kinetics and fuel cell performance.

1.3 Selected Compressor Performance Review in Vapor Compression Cycle

1.3.1 Small size compressors in the market

The aim of my research is to develop an electrochemical compressor with 1 kW of cooling which is superior to currently existing similar sized compressors in the market running at similar conditions. Therefore, a literature review is conducted on the state of the art technology. There are a few small sized compressors in the market which works for system with 1 kW of cooling capacity are listed in Table 1-4 and Table 1-5 showing compressors in similar working conditions [24-29].

Table 1-4: Baseline compressor performance at 5 °C evaporating temperature and 45 °C condensing temperature [24, 25, 26]

Compressor type	Cooling Capacity/Volume ratio (W/L)	Refrigerant	COP
Aspen Q-series rotary Compressor Q4-24-5111	142	R-134a	2.46
Embraco miniature linear compressor	554	R-600a	2.55
Danfoss reciprocating Compressor FR6G	60	R-134a	2.6

Table 1-5: Baseline carbon dioxide compressor performance at -10 °C evaporating temperature and 35 °C condensing temperature

Compressor Type	Cooling Capacity (W)	Refrigerant	COP
Copeland Compressor ZO Scroll	3000	R-744	1.7
Danfoss Compressor TN1406	877	R-744	1.39
Frascold Compressor D_SK3	4125	R-744	1.56

As shown in Table 1-2, the smaller sized compressors with R-134a and R-600a (isobutene) operating at 5 °C cooling and 45 °C have COP around 2.5. Ammonia as a refrigerant is only adopted in large scale refrigeration units and water chillers, usually in the hundreds or thousands of kW range. Smaller sized compressors in less than 1 kW range working with ammonia so far have not been designed and developed in the market. The proposed electrochemical ammonia compressor is expected to have a COP around 5.1 and will be discussed in details in Chapter 4. The CO_2 compressors are being manufactured by major companies like Copeland, Danfoss and Frascold. There are small scale compressors with cooling capacities in the kW range. Since CO_2 as a refrigerant requires much higher operating pressure, which needs the compressor in the system to work harder, the overall system COP is reduced to less than 2.0 [27-29]. The compressor power consumption remains a challenge in the state of

the art CO_2 refrigeration system and creates a lot of room for improvement. The CO_2 electrochemical compressor proposed in this thesis is expected to have a much higher operating COP with an improvement in compression efficiency and proper compressor cooling. The CO_2 EC will be discussed in details in Chapter 5.

1.3.2 Compressor cooling

As being discussed earlier, the compressor is the largest energy consumer in a vapor compression refrigeration system. In order to reduce the power consumption of the compressors, the compressor must be cooled. Some previous ways including refrigerant injection in either liquid or vapor phase to the compression chamber to reduce the discharge temperature and improve the system performance [30]. But this technique increases the compressor power consumption because it is compressing excess amount of refrigerant. Therefore, passive cooling technique has been explored [30]. The first option is cooling the compressor motor externally. The second option is making the compression process approach isothermal. The first option reduces both compressor inlet and outlet temperatures (Figure 1-8), and resulted in a COP improvement of 5% with little effect on reducing compressor power consumption, which is also proven to be not a very effective way [30].

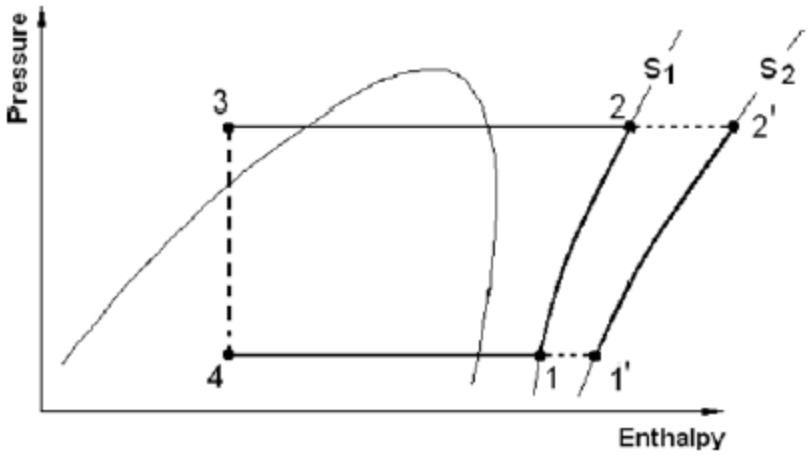

Figure 1-8 External compressor motor cooling pathways [30]

The second option does not change the starting temperature of the compressor but changes the overall compression path (Figure 1-9) to approach isothermal compression. This approach provides more room for energy saving and is calculated to have compressor work reduction by 14%. Among all the refrigerants studied, R-744 (CO_2) has the largest efficiency improvement due to the low molecular mass, and therefore low specific heat capacity among common refrigerants [30]. With all the simulation studies, it seems to be promising to develop an isothermal compression process to reach optimum compressor performance. However, real life experimental studies have expressed concerns about limited compressor surface area for heat removal which makes isothermal compression very difficult to achieve.

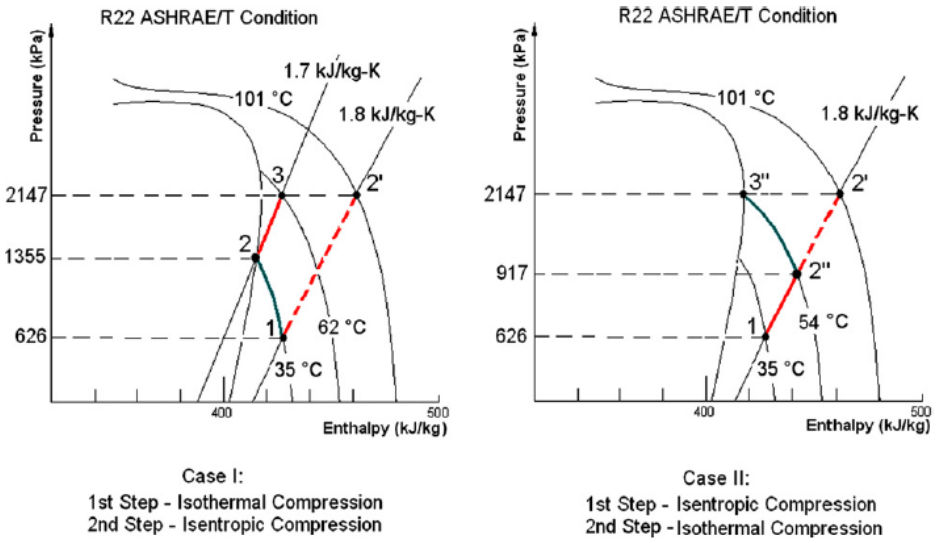

Figure 1-9: Isothermal compression path ways [30]

1.4 Research Gaps

Even though electrochemical compressor for hydrogen has been developed and studied, there is essentially no further research beyond this point in this particular field. There is a lot of room for further research given the high efficiency of electrochemical compression, and unique property of ion exchange membranes. Electrochemical hydrogen compression so far has not been reported in heat pump applications. There is also very limited report in electrochemically compressing ammonia for any time of applications. Carbon dioxide has been reported to be detrimental to anion exchange membrane fuel cell operation due to the formation of less mobile CO_3^{2-} and HCO_3^- . Further research was done on electrochemically transporting CO_2 across the AEM. However, all previous researches that used Pt as electrochemical catalyst and showed low performance. Pt on the other hand is also an expensive catalyst and the cost of scaling up would be prohibiting. Even though research was done on $CaRuO_3$ catalyst and showed superior AEMFC performance in

carbonate cycle. There is no research on electrochemically pumping the CO_2 across AEM by adopting $CaRuO_3$ catalyst, and there is also no compression mechanism study of the process as well.

Therefore, three research directions are explored for this PhD work. The first one would be exploring the feasibility of applying electrochemical hydrogen compression to drive the metal hydride heat pump and evaluate the system performance. The second one is exploring the potential of transferring ammonia in the form of NH_4^+ in proton exchange membrane, given the fact that the existence of ammonium ion (NH_4^+) has been reported in the PEM. The third one is studying the transfer of CO_2 in AEM under carbonate cycle using both Pt and $CaRuO_3$ catalyst. The objectives will be further elaborated in Chapter 1.5.

1.5 Research Objectives

Based on the research directions established, research objectives are set to fill the research gaps in this area. The proposed study aims to develop frameworks including both electrochemical compression system modeling and fundamental understanding of gas transfer through experimental evaluation. This thesis intends to explore the following.

(1) Understanding the fundamentals of electrochemical compressions

(2) Performing the cooling, and heating cycle analysis of electrochemical hydrogen compression for metal hydride heat pumps, modeling the metal hydride heat pump system in terms of COP and cooling/heating capacity

(3) Verifying the feasibility of electrochemical ammonia compression, understanding the reaction mechanisms, testing the single unit electrochemical ammonia compression performance and explore its related applications

(4) Verifying the feasibility of electrochemical CO_2 compression, understanding the reaction mechanisms of electrochemical CO_2 compression with both Pt and CaRuO3 facilitated reaction, design the proper gas distribution channels and explore its related applications

(5) Designing the prototype, scaling up compressor development and analyzing system cycle

This thesis explored the feasibility of first major application of electrochemical hydrogen compression designated for metal hydride heat pump. In addition to that, two important studies of electrochemical compression of ammonia and CO_2 have been conducted to push this field further to real world application. Finally, prototype development and system integration are proposed for future study. In the end, the PhD work presented in this thesis has successfully met the research objectives.

Chapter 2: The fundamentals of electrochemical compressions

2.1 The Fundamental Electrochemistry of Fuel Cells

The electrochemical compression with ion exchange membrane is derived from the principle of fuel cells, and from low temperature proton exchange membrane fuel cell and anion exchange membrane fuel cells in particular for the studies conducted in this thesis. Therefore, it is necessary to discuss the fundamental principles of fuel cells in details. Fuel cells are categorized by the type of electrolyte they use. The electrolyte can be either solid or liquid. This thesis mainly deals with solid electrolyte such as proton exchange membrane and anion exchange membrane. And Chapter 2 is focused on how proton exchange membrane fuel cell and anion exchange membrane fuel cells operate and lay out the connection between fuel cell electrochemistry and electrochemical compression.

2.1.1 Proton exchange membrane fuel cells

2.1.1.1 Fuel cell electrochemistry

A fuel cell is an electrochemical energy converter. It converts chemical energy of fuel directly into DC electricity. Electricity is produced spontaneously as fuel is consumed. Different to an energy storage device, such as a battery, a fuel cell cannot store electricity in any ways. A membrane electrode assembly is the key part of a fuel cell. For the case of proton exchange membrane fuel cells, detailed reaction on the surface of membrane electrode assembly will be explained. As shown in Figure 2-1, hydrogen is supplied to the anode as a fuel and oxygen is supplied to the cathode as an oxidation reactant. At the surface of the proton exchange membrane anode (left),

hydrogen is converted to protons and electrons facilitated by a catalyst in the following reaction [31].

$$H_2 \rightarrow 2H^+ + 2e^- \qquad (2\text{-}1)$$

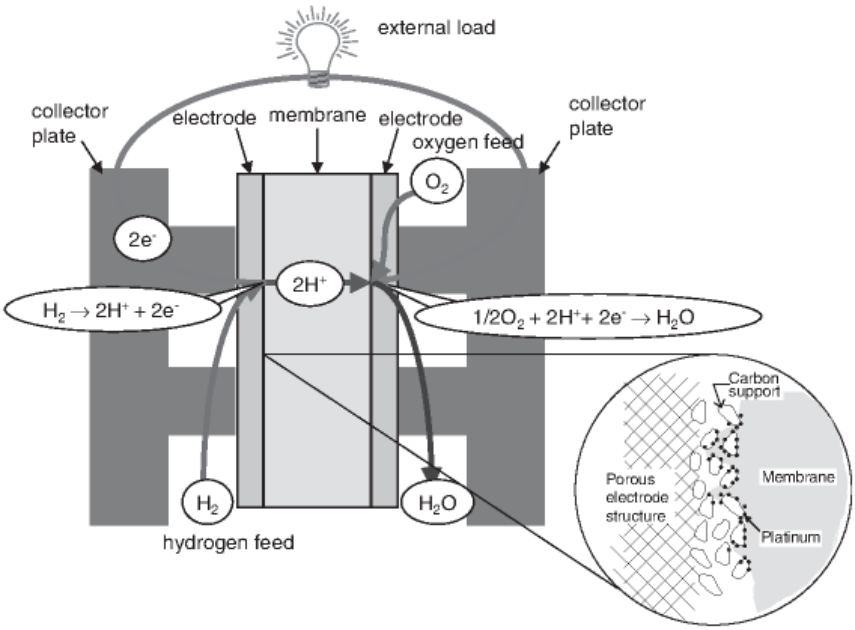

Figure 2-1: Proton exchange membrane operating principle [31]

The electrons will go through the current collector plate and migrates from anode side to the cathode side. The protons are transported through the proton exchange membrane from anode to cathode. On the cathode side, facilitated by the catalyst, oxygen combines with protons and electrons generated from the hydrogen and produce water, which completes the reaction cycle. The entire chemical reaction drives the migration of electrons which creates an electric current for the external load. The current collector plate, the electrode and the membrane have to be in close contact with each other for electrons and proton conduction. Since the electrochemical reactions take place on the catalyst surface at the interface between membrane and electrode, a 'triple phase boundary' needs to be established, which is illustrated in the Figure 2-2.

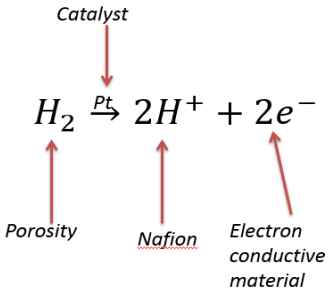

Figure 2-2: Proton Exchange Membrane Fuel Cell Triple Phase Boundary

First of all, the electrochemical reaction takes place in the pores of Pt catalyst. And Pt catalyst particles are supported by larger carbon particles. When protons and electrons are generated, they need to be carried away by proton and electron conductive materials. In this case, the proton conductive material can be electrolyte with chemical structure very similar to the proton exchange membrane. And the electron conductive materials can be the carbon support of the Pt particles and porous carbon electrode (Figure 2-1). Therefore, when making a membrane electrode assembly for PEM fuel cell, a Pt catalyst ink must be prepared which containing Pt catalyst supported by carbon particles and proton conductive electrolyte (Nafion solution). The catalyst ink is then brushed on the surface of carbon electrodes and pressed together with the proton exchange membrane to satisfy the 'triple phase boundary'. If any of the component in the 'triple phase boundary' is missing, the electrochemical reaction in Figure 2-2 is not going to take place. The amount of catalyst and proton conductive electrolyte in the ink can be optimized to generate faster reaction kinetics which gives better fuel cell membrane performance.

The reason that proton exchange membrane conducts proton is due to its unique polymer structure (Figure 2-3). A fuel cell membrane must have high proton conductivity, must provide a barrier for hydrogen (not proton) on the anode coming

into contact with oxygen on the cathode, and must be chemically stable and mechanically stable to withstand a pressure difference [31]. The polymer structure shown in Figure 2-3 contains a poly-tetrafluoroethylene (PTFE) backbone and an ethyl-propyl-vinyl side chain. A sulfonic acid functional group is attached to the side chain. The sulfonic acid (SO_3H) group is ionically bonded with a SO_3^- ion and H^+ ion. The PTFE backbone is hydrophobic and sulfonic acid functional group is hydrophilic. Once the membrane is hydrated, water weakens the bonding between SO_3^- ion and H^+ ion in the hydrophilic functional group, and proton can move freely, which makes the membrane proton conductive.

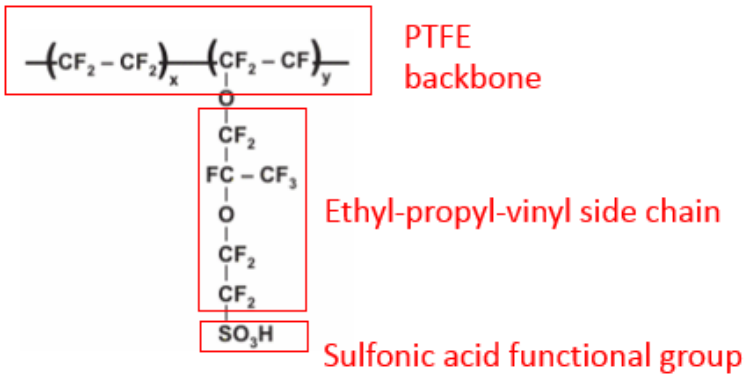

Figure 2-3: Polymer structure of proton exchange membrane (Nafion)

The proton conductivity is directly related to the water content and temperature of the PEM. As previously mentioned, the water molecules weaken the bonding between the SO_3^- and H^+ in the PEM. Therefore, when there is more water molecules in the membrane, the proton conductivity of the membrane will go higher. Figure 2-4 shows the proton conductivity of PEM as a function of water content λ, which is represented by the ratio of water molecules per sulfonate acid group. When λ is less than 5, meaning water molecules in the PEM is little, there is almost no proton conductivity. But when λ is equal to or greater than 5, there is an almost linear relationship between

proton conductivity and water content [31]. Thus it is very important to the keep the PEM hydrated during fuel cell operation for optimal performance.

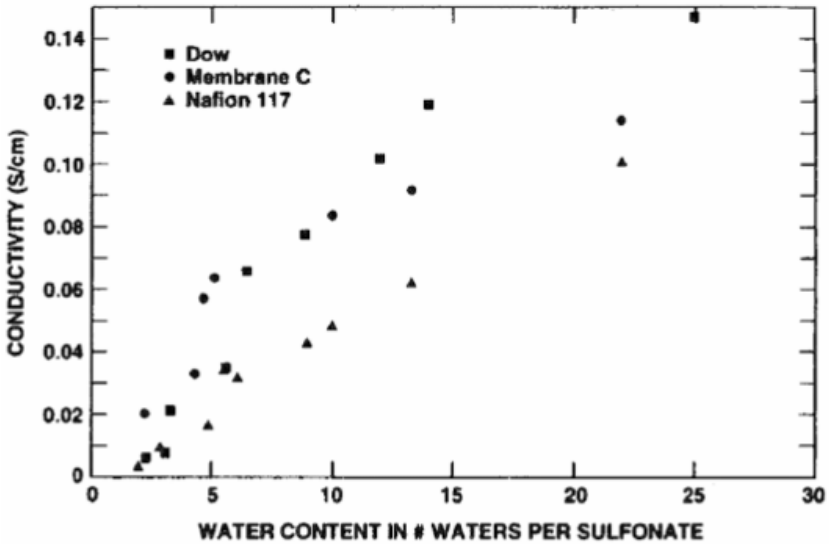

Figure 2-4: Proton conductivity vs water content in PEM [31]

2.1.1.2 Main fuel cell components

A typical PEM fuel cell hardware is composed of the MEA, gaskets, gas diffusion layer and bipolar plate with gas distribution channels (Figure 2-5) [31]. The MEA is sandwiched in between and pressed against gaskets and current collector. The gaskets are usually made of silicon or Teflon to prevent leakage of fuel and reactant gas. The gas diffusion channels are usually an extra layer of carbon cloth for physically supporting the MEA and facilitate gas diffusion through porous channels. Besides carbon cloth, stainless steel mesh can also be used under non-acid electrode environment. The bipolar plate not only serves as the electric conductor but also has gas diffusion channels embedded for distributing of fuel and reactant gas. In order to provide a large voltage output, it requires more fuel cell units to be connected in series to form a stack. All components are bolted together in the stack so that they are in close electric contact with each other.

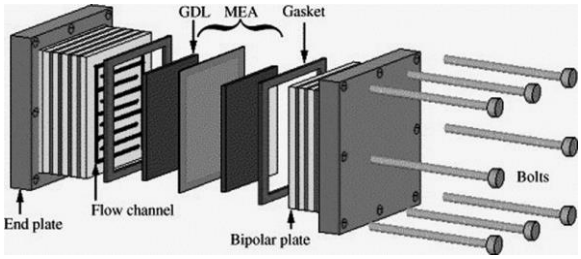

Figure 2-5: Fuel cell hardware structure [31]

2.1.1.3 The Fundamentals of Fuel Cell Thermodynamics

As previously mentioned, a fuel cell is an energy conversion system which turns the chemical energy in the fuel directly to electric energy. If hydrogen is the fuel consumed in the fuel cell, then by combining the anode oxidation reaction and cathode reduction reaction, the overall reaction is simply hydrogen react with oxygen to produce water, or the hydrogen combustion reaction.

$$H_2 + \frac{1}{2}O_2 \rightarrow H_2O \qquad (2\text{-}2)$$

Since hydrogen combustion is an exothermic reaction, energy is produced in the process, which is represented in the form of enthalpy of reaction. In a chemical reaction, the enthalpy of reaction can be calculated by taking the difference between the heat of formation of product and reactant. At 25 °C, the calculated value is equal to -286 kJ/mol by taking values of H_2O, H_2 and O_2 from the thermodynamic table, which is the maximum amount of energy a fuel cell can produce.

$$\Delta H = (h_f)_{H2O} - \left(h_f\right)_{H2} - \frac{1}{2}\left(h_f\right)_{O2} \qquad (2\text{-}3)$$

But in reality, not all the energy released by hydrogen reaction is converted to electricity, with irreversible losses generated in the form of entropy, the valid energy output that can be converted to electricity in a fuel cell can be expressed in the form of change of Gibbs free energy in the following equation.

$$\Delta G = \Delta H - T\Delta S \qquad (2\text{-}4)$$

The production of entropy can again be calculated in the following equation.

$$\Delta S = (S_f)_{H2O} - \left(S_f\right)_{H2} - \frac{1}{2}(S_f)_{O2} \qquad (2\text{-}5)$$

In the end, ΔG=-237.34 kJ/mol at 25 °C and 1 atm, which is the actual amount of energy can be converted to electricity. At different temperature and pressure, the value is different.

The electric work produced by fuel cell with respect to the cell voltage can be expressed in the following equation.

$$W = nFE = \Delta G \qquad (2\text{-}6)$$

Where F is the Faraday's constant, equal to 96500 coulombs/mol, W is the electric work produced in Joule, which can also be denoted as Volt·coulomb, and n is the number of electrons transferred per molecule of hydrogen. By knowing ΔG, n, and F, cell voltage E can be calculated.

$$E = \frac{-\Delta G}{nF} = \frac{237340\ J/mol}{2 \cdot 96500\ C/mol} = 1.23\ Volt \qquad (2\text{-}7)$$

And the theoretical fuel cell efficiency can be calculated by taking the ratio of amount of energy can be converted to electricity and maximum energy released by hydrogen oxidation reaction. The theoretical fuel cell efficiency is therefore calculated to be 83%.

$$\eta = \frac{\Delta G}{\Delta H} \qquad (2\text{-}8)$$

Pressure also play a role on the fuel cell performance. The change of Gibbs free energy in thermodynamics is shown below.

$$dG = VdP - SdT \qquad (2\text{-}9)$$

At constant temperature, the change of Gibbs free energy is derived down to the following.

$$dG = VdP \qquad (2\text{-}10)$$

For ideal gas law, with V representing molar volume,

$$PV = RT \qquad (2\text{-}11)$$

And therefore,

$$dG = RT\frac{dP}{P} \qquad (2\text{-}12)$$

By taking the integral from both sides,

$$G - G_0 = RT\ln\frac{P}{P_0} \qquad (2\text{-}13)$$

Where G-G_0 represents the change of Gibbs free energy from reference state, P_0 is the reference pressure.

For any reaction,

$$jA + kB \rightarrow mC + nD \qquad (2\text{-}14)$$

The change of Gibbs free energy can be calculated as,

$$\Delta G = mG_c + nG_D - jG_A - kG_B \qquad (2\text{-}15)$$

By substituting into previous equation, the Nernst equation can be derived

$$\Delta G = \Delta G_0 + RT\ln\left[\frac{\left(\frac{P_C}{P_0}\right)^m\left(\frac{P_D}{P_0}\right)^n}{\left(\frac{P_A}{P_0}\right)^j\left(\frac{P_B}{P_0}\right)^k}\right] \qquad (2\text{-}16)$$

Therefore for hydrogen and oxygen fuel cell reaction, the Nernst equation is

$$\Delta G = \Delta G_0 + RT\ln\frac{P_{H2O}}{P_{H_2}P_{O_2}^{\frac{1}{2}}} \qquad (2\text{-}17)$$

And by converting to voltage difference,

$$E - E_0 = \frac{RT}{nF} \ln\left(\frac{P_{H_2} P_{O_2}^{\frac{1}{2}}}{P_{H_2O}}\right) \qquad (2\text{-}18)$$

Equation 2-18 shows that when increasing the supply hydrogen pressure on the anode, the fuel cell voltage output will increase. As pressure plays an important role in creating a voltage different in fuel cell, the reserve process is also valid. It means by providing a voltage to the membrane electrode assembly, a pressure difference can be generated across the membrane. This sets the fundamental of electrochemical compression, which will be discussed in details in section 2.2.1.

2.1.2 Alkaline membrane fuel cells

The alkaline membrane fuel cells (AMFC) must be distinguished from alkaline fuel cells, which uses concentrated KOH solution as the electrolyte and operates at 250 °C. The alkaline membrane fuel cells, however, uses solid electrolyte membrane which conducts anions and operates under 50 °C. The AMFC is rather at its beginning developing stage comparing to the long history of PEMFC development, with the first study performed in 2005 by John Varcoe's group at the University of Surrey [32]. The study was initiated to explore the alternatives of alkaline fuel cells and solve the large molecule carbonate salt precipitation problem in the liquid KOH electrolyte. The alkaline membrane, or anion exchange membrane (AEM), has the advantage of minimized solid crystal carbonate salt formation due to no mobile cations in the membrane. Because the cations are essentially part of the polymer functional group, similar to the sulfonic acid functional group in PEM. Therefore, by switching to anion exchange membrane, no crystal carbonate salt will block the electrode layers and reduce the fuel cell performance because of that particular

reason. Different to PEM fuel cell, water is now consumed at the cathode and produced at the anode, but the overall reaction is still the same as PEMFC. The detail reactions on both electrodes are shown as follows.

$$Cathode:\ O_2 + 2H_2O + 4e^- \rightarrow 4OH^- \qquad (2\text{-}19)$$

$$Anode:\ 2H_2 + 4OH^- \rightarrow 4H_2O + 4e^- \qquad (2\text{-}20)$$

$$Overall:\ 2H_2 + O_2 \rightarrow 2H_2O \qquad (2\text{-}21)$$

Hydroxide ion (OH^-) is the conductive ion being transported in the AEM (Figure 2-6). Most of the principles of PEMFC can be applied to the AEMFC, including catalyst, fuel cell structure, ion transport etc.

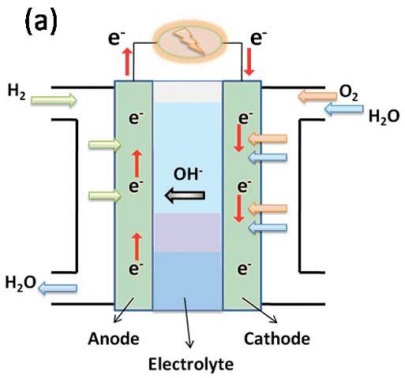

Figure 2-6: Anion exchange membrane fuel cell working mechanism [21]

One of the major difference between PEMFC and AEMFC is the membrane. PEMFC uses a proton exchange membrane which requires acidic environment to operate (H^+ is the ion in the electrolyte), while AEMFC uses an anion exchange membrane which requires alkaline environment to run (OH^- is the ion in the electrolyte). The anion exchange membrane chemical structure involves a polymer binding a cation functional group, poly-methyl methacrylate-co-vinylbenzyl (PMBV), for example (Figure 2-7) [33].

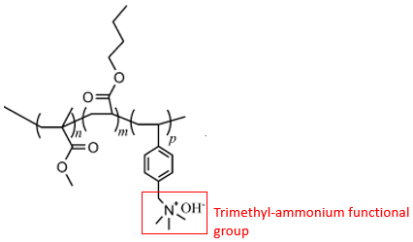

Figure 2-7: Polymer structure of anion exchange membrane fuel cell [33]

Even though salt formation is eliminated in the AEM, one of the major challenge of AEM fuel cell is the involvement of carbonate ions during the fuel cell operation after exposing to air, shown in the following reactions.

$$OH^- + CO_2 \rightarrow HCO_3^- \qquad (2\text{-}22)$$

$$HCO_3^- + OH^- \rightarrow CO_3^{2-} + H_2O \qquad (2\text{-}23)$$

The carbonate and bicarbonate ions have less mobility than hydroxide ions in the AEM and reduces the ionic conductivity of the membrane. However, due to the formation of both HCO_3^- and CO_3^{2-} ions in the AEM, it is possible to transport CO_2 in the forms of those ions. And it sets the fundamental principle of electrochemical CO_2 compression.

2.2 The Electrochemical Compression Principles

2.2.1 The Electrochemical Hydrogen Compression

As previously mentioned in chapter 2.1.1.3, an increase in pressure of the reactant hydrogen gas supplied to the anode side of PEM fuel cell can create a lift on the cell voltage. The reverse process is also valid, meaning by providing a voltage charge to the fuel cell MEA, a hydrogen pressure difference across the PEM can be generated. The reaction process on both the anode and cathode half cells are shown as follows.

$$Anode:\ H_2 \rightarrow 2H^+ + 2e^- \qquad (2\text{-}24)$$

$$Cathode:\ 2H^+ + 2e^- \rightarrow H_2 \qquad (2\text{-}25)$$

In this process, hydrogen is split into protons and electrons on the anode. Proton is transferred across the PEM to the cathode side and combine with electrons to produce hydrogen. And the Nernst equation of electrochemical hydrogen compression can be generated as follows.

$$E = E_0 + \frac{RT}{nF}\ln\frac{P_{H2,cathode}}{P_{H2,anode}} \qquad (2\text{-}26)$$

Where n=2, for each hydrogen, 2 electrons are produced, and E_0 is zero since both half reactions are opposite to each other.

As previously discussed in section 2.1.1.3 about the efficiency of fuel cell, the same principle can be applied to electrochemical hydrogen compression. And the compression efficiency can be calculated by taking the ratio of the theoretical work required to compress hydrogen based on the Nernst equation and the actual work input.

$$\eta = \frac{W_{theoretical}}{W_{input}} \qquad (2\text{-}27)$$

The theoretical work can be calculated from the Nernst equation.

$$W_{theoretical} = nFE = \mathrm{RTln}\frac{P_{H2,cathode}}{P_{H2,anode}} \qquad (2\text{-}28)$$

And the electrochemical hydrogen compression efficiency can be given as

$$\eta = \frac{W_{theoretical}}{W_{input}} = \frac{\mathrm{RTln}\frac{P_{H2,cathode}}{P_{H2,anode}}}{W_{input}} \qquad (2\text{-}29)$$

2.2.2 The Electrochemical Ammonia Compression

As previously mentioned in Chapter 1.2.3, ammonium ion (NH_4^+) can exist in the PEM. Inspired by the proton transport principle in Chapter 2.2.1, ammonia transport in the PEM is proposed for the first time in this thesis and experimentally studied. The principle is to oxidize hydrogen on the anode to produce proton which spontaneously react with ammonia to form ammonium ion on the anode side of the MEA. Under the influence of an electric voltage, ammonium ion is transported from anode to the cathode of the MEA. On the cathode side, ammonium ion is split into proton and ammonia. And hydrogen is spontaneously regenerated after gaining an electron. The detailed reaction mechanism is shown in Figure 2-8. The significance of this study is that it is the first time ammonia being reported to be transferrable in a large amount in proton exchange membrane. It broaden the vision of additional applications of PEM in the fuel cell community.

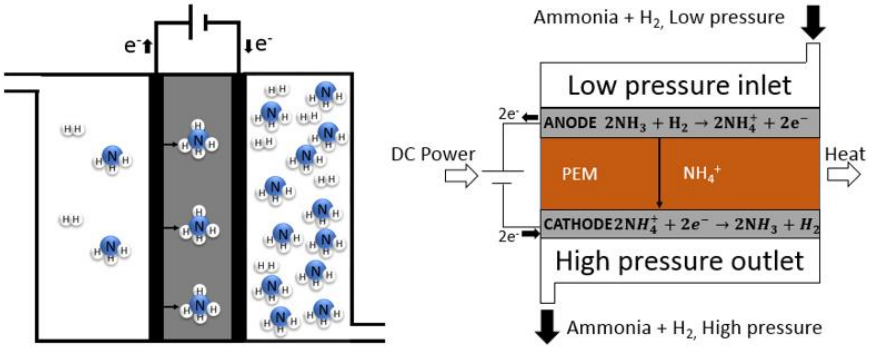

Figure 2-8: Electrochemical ammonia compression mechanism

In order to form ammonium ion in the PEM, hydrogen has to be involved as the carrier gas. The term ‘carrier gas’ was created to describe the transport mechanism in a more visual way. Even though making hydrogen as a ‘carrier gas’ may sound like hydrogen dragging ammonia across the membrane. In reality, the reaction mechanism may involve two spontaneous reaction steps. The first reaction step is the oxidation of

hydrogen to produce protons and electrons at the anode. And the second reaction step is the combination of proton and ammonia to form ammonium ion.

$$Anode\ step\ 1\text{:}\ \frac{1}{2}H_2 \rightarrow H^+ + e^- \qquad (2\text{-}30)$$

$$Anode\ step\ 2\text{:}\ H^+ + NH_3 \rightarrow NH_4^+ \qquad (2\text{-}31)$$

The hydrogen oxidation reaction happens very fast, and ammonia as a base can be easily protonated. Therefore the two reactions are almost spontaneous. When ammonium ion reaches cathode side, it receives electron and quickly regenerate ammonia and hydrogen. That completes the electrochemical hydrogen compression reaction.

$$Cathode\ step\ 1\text{:}\ NH_4^+ \rightarrow H^+ + NH_3 \qquad (2\text{-}32)$$

$$Cathode\ step\ 2\text{:}\ H^+ \rightarrow \frac{1}{2}H_2 \qquad (2\text{-}33)$$

The Nernst equation for electrochemical ammonia compression is derived as follows.

$$E = E_0 + \frac{RT}{nF}\ln\left(\left(\frac{\mathrm{P_{H2,Cathode}}}{\mathrm{P_{H2,Anode}}}\right)^{\frac{1}{2}} * \left(\frac{\mathrm{P_{NH3,Cathode}}}{\mathrm{P_{NH3,Anode}}}\right)\right) \qquad (2\text{-}34)$$

And the compression efficiency can be derived the same way as electrochemical hydrogen compression.

$$\eta = \frac{W_{theoretical}}{W_{input}} = \frac{RT\ln\left(\left(\frac{\mathrm{P_{H2,Cathode}}}{\mathrm{P_{H2,Anode}}}\right)^{\frac{1}{2}} * \left(\frac{\mathrm{P_{NH3,Cathode}}}{\mathrm{P_{NH3,Anode}}}\right)\right)}{W_{input}} \qquad (2\text{-}35)$$

The ammonia electrochemical compression device schematic designed based on PEMFC structure and is shown in Figure 2-9. The end plates containing gas distribution channels are made from graphite for electric conductivity. The MEA used in this study is the commercially available product (Nafion 115). This simple

compression device is solid state without moving parts, demonstrating a huge advantage over state of the art mechanical compressor.

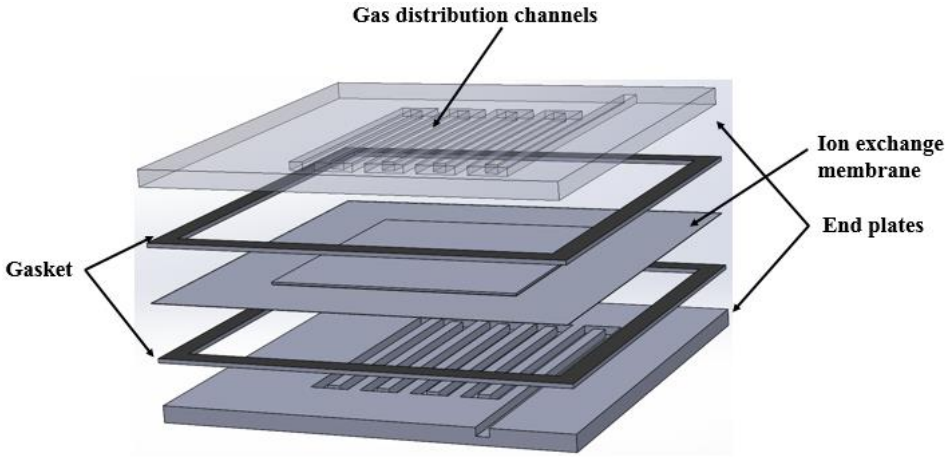

Figure 2-9: Electrochemical ammonia compression experimental device

2.2.3 The Electrochemical carbon dioxide compression

As Chapter 2.1.2 discussed the existence of carbonate and bicarbonate ion in the AEM, it is possible to transport CO_2 across AEM in the form of those ions. AEM fuel cell running under carbonate cycle has been explored by researchers [19]. As a matter of fact, the transporting mechanism of CO_2 in AEM is similar to ammonia transport in PEM, except that CO_2 is transported from the cathode to the anode. When fed to the cathode side of the MEA, depending on the catalyst, CO_2 and O_2 will go through two different reaction mechanisms. In the first reaction mechanism, Pt is used as the catalyst. Similar to what's happening in the AEM fuel cell, O_2 will react with water to form OH^- ion. OH^- ion will then combine with CO_2 to form HCO_3^-.

$$Cathode\ step\ 1: O_2 + 2H_2O + 4e^- \rightarrow 4OH^- \quad (limiting\ step) \qquad (2\text{-}36)$$

$$Cathode\ step\ 2: 4OH^- + 4CO_2 \rightarrow 4HCO_3^- \qquad (2\text{-}37)$$

For this two-step reaction, oxygen reaction with water is the limiting step. Because water is involved as a reactant, the diffusion of water from bulk to the surface of

MEA is a controlling factor. And oxygen reduction reaction is taking place which usually has the slowest reaction kinetics. And on the anode side, the reverse reaction of cathode will take place.

$$Anode\ step\ 1: 4HCO_3^- \rightarrow 4OH^- + 4CO_2 \qquad (2\text{-}38)$$

$$Anode\ step\ 2: 4OH^- \rightarrow O_2 + 2H_2O + 4e^- \qquad (2\text{-}39)$$

In the second reaction mechanism, $CaRuO_3$ is the catalyst. Since Ca is an alkaline metal, CaO can easily absorb CO_2 on the surface, due to acidity of CO_2. RuO_2 on the other hand, is a common oxygen reduction catalyst. Therefore, $CaRuO_3$ facilitates a much more direct reaction mechanism [34]. O_2 will directly combine with CO_2 to form CO_3^{2-}, with no involvement of H_2O. Therefore water does not compete with CO_2 for catalyst absorption.

$$Cathode: O_2 + 2CO_2 + 4e^- \rightarrow 2CO_3^{2-} \qquad (2\text{-}40)$$

$$Anode: \ 2CO_3^{2-} \rightarrow O_2 + 2CO_2 + 4e^- \qquad (2\text{-}41)$$

The overall reaction mechanism for ammonia electrochemical compression is shown in Figure 2-10.

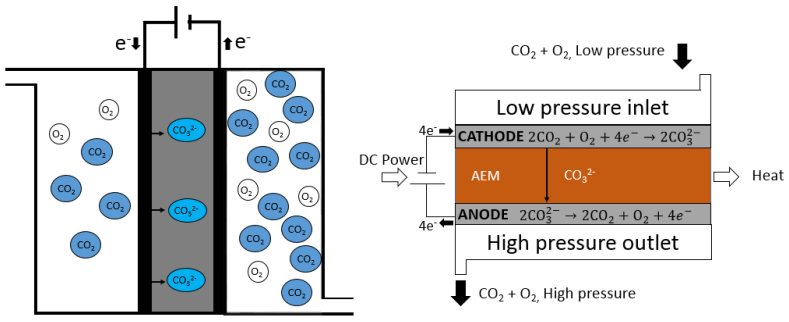

Figure 2-10: Electrochemical carbon dioxide compression mechanism

2.3 Chapter Summary and Conclusions

This chapter discussed about the fundamental electrochemistry and thermodynamics of fuel cells, with PEM fuel cell and AEM fuel cell in particular. The chapter also

layout the connection between fuel cell electrochemistry and electrochemical compressions. It can be concluded that the electrochemical hydrogen compression can be considered as a reserve process of proton exchange membrane fuel cell. The redox process is also similar to the electrolysis of water. The electrochemical ammonia compression process is developed based on the knowledge of ammonium ion (NH_4^+) formation in the proton exchange membrane. It is therefore reasonable to propose that ammonia can be transported across AEM with hydrogen as a carrier gas in NH_4^+ form. The mobilization of carbonate and bicarbonate ions in the electrochemical CO_2 compression process is very similar to the redox reaction taking place in the anion exchange membrane fuel cell. Due to similar electrochemical behavior, Nernst equation derived from fuel cell pressure voltage relationship is the governing equation of electrochemical compression. And the electrochemical compression efficiency can be derived based on the fuel cell energy efficiency equation as well.

Chapter 3: The cycle analysis of electrochemical hydrogen compression for metal hydride heat pumps

3.1 The Process Description for Electrochemical Hydrogen Compressor Driven Metal Hydride Heat Pump

Electrochemical hydrogen compression is adopted to drive the metal hydride heat pump system, replacing the traditional mechanical compressor. The MH heat pump system driven by the EC is similar to the previously developed mechanical compressor driven MH heat pump as two identical MH reactors, one for cooling and one for heating are connected by the compressors in the system. However, in the currently proposed MH heat pump system, the electrochemical compressor reduces the pressure on the desorption reactor and increases the pressure on the absorption reactor. As shown in Figure 3-1, the EC is placed in between two identical $LaNi_5$ MH reactors so that one side generates cooling at low pressure and the other side produces heating at high pressure. Hydrogen is desorbed from the MH reactor, where pressure is below the plateau pressure at low temperature of heat source. Meanwhile, hydrogen is pumped to and absorbed in the MH reactor on the other side where the pressure is above the plateau pressure at temperature of heat sink.

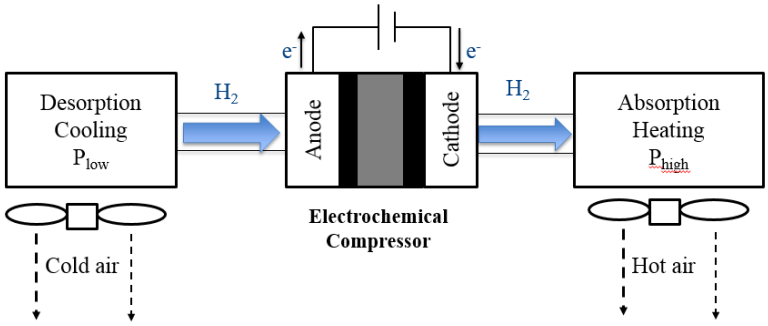

Figure 3-1: Electrochemical hydrogen compressor drives the metal hydride heat pump for cooling and heating

$LaNi_5$ was chosen for modeling, because it is the most commonly used MH for heat pump development as pointed out from the most recent review papers [5, 8]. In addition, $LaNi_5$ and its AB_5 hydride family absorb and desorb hydrogen in room temperature at reasonable pressure range (100-400 kPa) with small hysteresis [4,5].

The uniqueness of choosing EC to be the compressor is that the anode and cathode of the EC are both identical, when both desorption and absorption reactors are running under batch mode, it is possible to switch hydrogen flow direction by switching the positive and negative of power supply. A continuously operating system of the EC heat pump with indoor and outdoor heat exchangers are therefore proposed. As it is shown in Figure 3-2, initially, the reactor on the left (bed 1) is full of hydrogen and reactor on the right (bed 2) is empty of hydrogen. After the EC is turned on, hydrogen pressure is reduced in the left reactor as desorption occurs, so that temperature drops and cooling is generated at T_d (Figure 3-2(a)). This cold reactor is in heat exchange with the indoor heat exchanger. As pressure increases on the right reactor (bed 2), absorption occurs so that temperature increases and heating is generated at T_a. This hot reactor is in heat exchange with the outdoor heat exchanger. When bed 1 is depleted and bed 2 is full, bed 1 (cold) is pre-heated and bed 2 (hot) is pre-cooled by air at room temperature under heat recovery process (Figure 3-2(b)). Finally, as shown in Figure 6(c), the polarity of power supply is switched, so that hydrogen flows from bed 2 to bed 1, bed 2 therefore generates cooling and bed 1 generates heating by switching the heat transfer fluid flow of corresponding indoor and outdoor heat exchangers. The cycle operation of MH is shown on the Van't Hoff Chart (Figure 3-3 a-c).

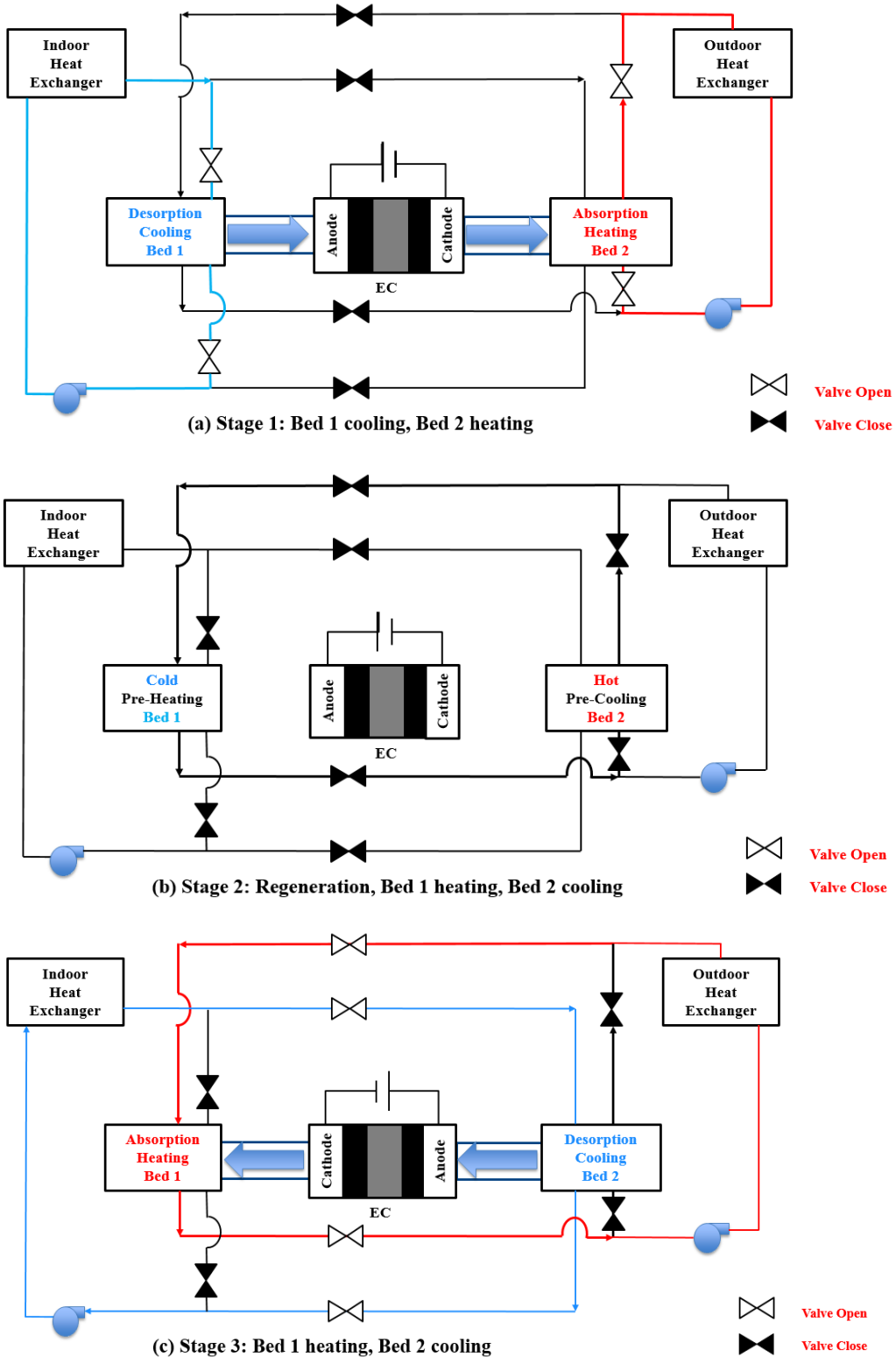

Figure 3-2: Schematic diagram of EC driven metal hydride heat pump system. Stage 1: Bed 1 cooling, Bed 2 heating; Stage 2: Regeneration, Bed 1 heating, Bed 2 cooling; stage 3: Bed 1 heating, Bed 2 cooling

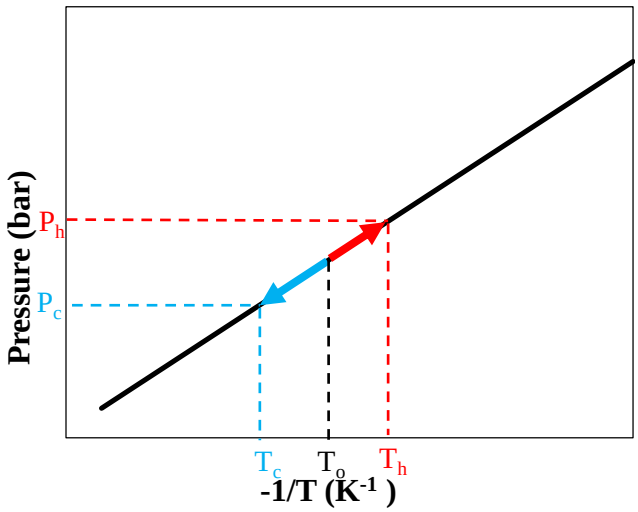

Figure 3-3a: Stage 1, Bed 1 cooling and Bed 2 heating

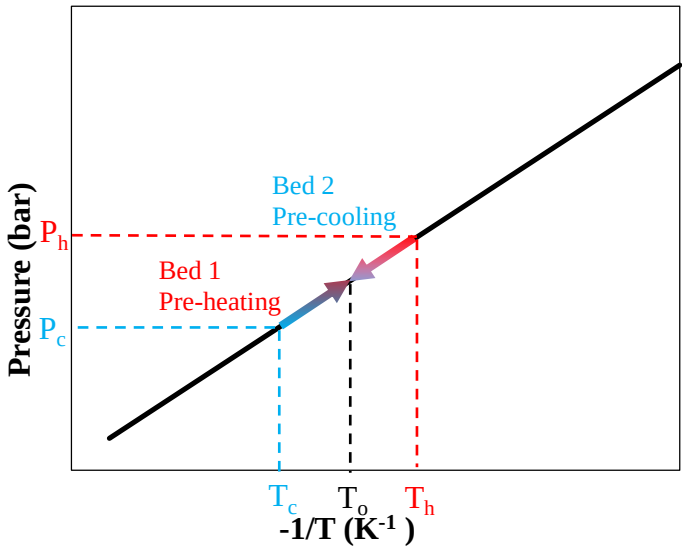

Figure 3-3b: Stage 2, Regeneration, Bed 1 pre-heating and Bed 2 pre-cooling

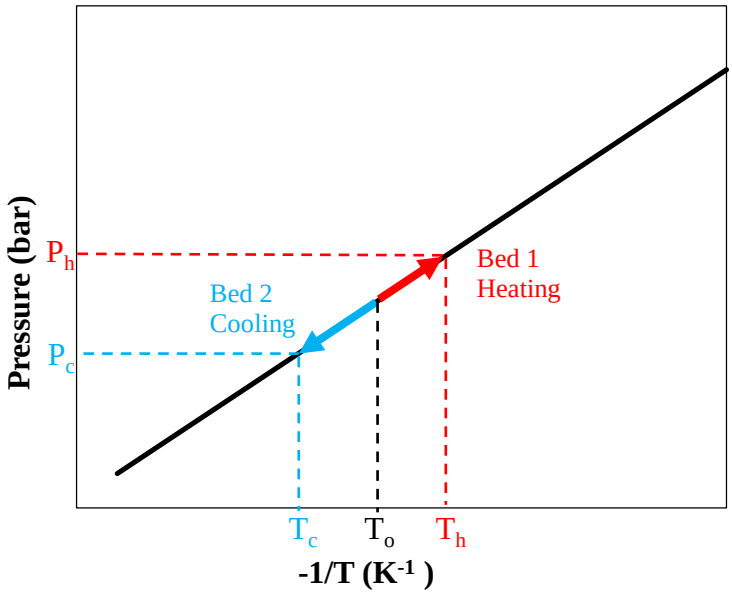

Figure 3-3c: Stage 3, Bed 1 heating, Bed 2 cooling

3.2 Thermodynamic Analysis and Cycle Demonstration

For the analysis of MH heat pump with EC, the thermodynamic model was developed with following assumptions:

- The EC is the only power consumer in the system, power consumed by other parts such as pumps and fans of heat exchangers are neglected.
- Enthalpy of formation (ΔH) and entropy of formation (ΔS) of MH do not change with temperature.
- Metal hydride packing in the reactor is homogeneous, meaning there is no spatial distribution of temperature, and hydrogen concentration in the hydride packing is uniform.
- Modeling is based on system at steady state. Proton transfer across the membrane is only dependent on current density, meaning the Faradaic efficiency of the electrochemical compression process is 100%.

- Back diffusion of hydrogen across the membrane is not considered due to non-significant pressure gradient.
- Electronic resistance on current collectors is neglected because it is very small. Therefore, total cell internal resistance only accounts for membrane ionic and contact resistance.

The relationship between the midpoint of plateau pressure and temperature can be expressed with Van't Hoff's Equation.

$$P_m = \exp\left(\frac{\Delta H}{RT} - \frac{\Delta S}{R}\right) \quad (3\text{-}1)$$

Desorption pressure is calculated by taking into account the plateau slope and hysteresis as shown in the following.

$$\ln P_c = \frac{\Delta H}{RT} - \frac{\Delta S}{R} + f_s(C - C_{eq}) - \ln\left(\frac{P_a}{P_d}\right)_{T_c} \quad (3\text{-}2)$$

$$\ln P_h = \frac{\Delta H}{RT} - \frac{\Delta S}{R} + f_s(C - C_{eq}) + \ln\left(\frac{P_a}{P_d}\right)_{T_h} \quad (3\text{-}3)$$

$$f_s = \frac{\ln P - \ln P_{eq}}{C - C_{eq}} \quad (3\text{-}4)$$

where P_c and P_h are the pressure of desorption (cooling) and absorption (heating), f_s is the plateau slope factor and $C\text{-}C_{eq}$ is the change of hydrogen content in the alloy. For characterization the MH, the pressure at the midpoint of the plateau is taken without considering the plateau slope [4]. $\ln(P_a/P_d)_T$ is the hysteresis factor at given temperature. Hysteresis is represented by the change of Gibbs free energy as follows [4].

$$\frac{\Delta G_{hyst}}{RT} = \ln\left(\frac{P_a}{P_d}\right)_T \quad (3\text{-}5)$$

where P_a and P_d are the absorption and desorption pressure at the given temperature.

The EC suction side and discharge side pressure are calculated in eqs. (3-6, 3-7) based on absorption and desorption pressure plus the pressure drop between desorption reactor and EC inlet as well as absorption tank and EC outlet.

$$P_{suc} = P_c - \Delta P_{suc} \quad (3\text{-}6)$$

$$P_{dis} = P_h + \Delta P_{dis} \quad (3\text{-}7)$$

The MH desorption and absorption temperature are calculated in eqs. (3-8, 3-9) based on cooling and heating temperatures as well as the temperature differences for heat transfer between the reactors and surrounding.

$$T_d = T_c - \Delta T_d \quad (3\text{-}8)$$

$$T_a = T_h + \Delta T_a \quad (3\text{-}9)$$

The amount of MH required for the system is calculated in eq. (3-10) based on the cylindrical reactor volume.

$$m_{MH} = \pi {r_1}^2 * H_R * vr * \rho_{MH} \quad (3\text{-}10)$$

where r_1 is the reactor inner radius, H_R is the reactor length, vr stands for the percentage of reactor volume occupied by MH packing.

The metal hydride and metal hydride container must be sensibly cooled during refrigeration process, and sensibly heated during regeneration process, therefore, this parasitic loss needs to be considered. The entire cooling cycle includes desorption time, sensible cooling down time and regeneration time as in eq. (3-11).

$$t_{cycle} = t_d + t_{cd} + t_{rg} \quad (3\text{-}11)$$

Desorption time is calculated in eq. (3-12) from the amount of hydrogen stored in the MH packing, and the rate of hydrogen flowing out of container. The storage capacity of $LaNi_5$ is taken to be 1.5% by weight [5].

$$t_d = \frac{m_{MH} * 1.5\%}{\frac{dn}{dt} * 2} \qquad (3\text{-}12)$$

The sensible cooling down time (t_{cd}) for MH packing and the reactor is found in eq. (3-13) based on the enthalpy of desorption and hydrogen flow rate.

$$t_{cd} = \frac{(C_{MH} * m_{MH} + C_R * m_R) * \Delta T_{cd}}{\Delta H_d * \frac{dn}{dt}} \qquad (3\text{-}13)$$

where ΔT_{cd} stands for the cooling down temperature.

The regeneration time can be found in eq. (3-14) based on the convection heat transfer between the reactor and the ambient.

$$t_{rg} = \frac{(C_{MH} * m_{MH} + C_R * m_R) * \Delta T_{rg}}{h_x * A_R * \Delta T_{rg}} \qquad (3\text{-}14)$$

where h_x stands for the cylinder convection heat transfer coefficient, it is calculated in eq. (3-15) based on the Zhukauskas relation for flow over cylindrical surface [35]. ΔT_{rg} stands for the temperature change due to regeneration. A_R stands for the surface area of the reactor.

$$h_x = Nu * \frac{k}{D} = \frac{k}{D} C Re^m Pr^n \left(\frac{Pr}{Pr_s}\right)^{\frac{1}{4}} \qquad (3\text{-}15)$$

where Nu is the Nussel number, D is the outer diameter of the reactor, k is the air thermal conductivity, Re is the Reynold's number, Pr is the Prandtl number.

During the regeneration process, both hot and cold metal hydride reactors are either pre-cooled or pre-heated by air at room temperature until thermal equilibrium has been reached. Therefore, the cooling power is calculated in eq. (3-16) by taking the average of total cooling energy generated in terms of cooling cycle time.

$$\overline{Q_c} = \frac{\Delta H_d * \frac{dn}{dt} * t_d * hx_{eff}}{t_{cycle}} \qquad (3\text{-}16)$$

where hx_{eff} is the heat exchanger effectiveness.

The heating power is calculated in the similar manner, as well as considering the time for heating up the metal hydride and the metal hydride container, and the regeneration time.

For modeling the EC, the total cell voltage of EC is expressed in eq. (3-17).

$$U = U_{Nernst} + U_{ohm} + U_{ac} \quad (3\text{-}17)$$

Where U_{Nernst} stands for the Nernst potential, U_{ohm} is the ohmic loss of the cell due to total cell internal resistance, U_{ac} stands for the anode and cathode polarization. For EC, since there is no oxygen which reacts on the cathode side to produce water, the cathode and anode polarization are very small and can therefore be neglected [3, 36]. Thus the above equation is reduced to eq. (3-18).

$$U = U_{Nernst} + U_{ohm} \quad (3\text{-}18)$$

U_{Nernst} can be calculated in eq. (3-19) from the Nernst Equation.

$$U_{Nernst} = \frac{RT_{EC}}{2F} \ln\left(\frac{P_{dis}}{P_{suc}}\right) \quad (3\text{-}19)$$

U_{ohm} of a single EC satisfies the Ohm's law as shown in eq. [31](3-20).

$$U_{ohm} = I_d * R_i = \frac{I}{N*A} * R_i \quad (3\text{-}20)$$

where I_d is the current density of a single EC, I is the total current generated by the power supply, N is the number of ECs connected in parallel, A is the active cell area. A typical value for $R_{i,}$ depending on the thickness of Nafion membrane, is between 0.05 and 0.2 $\Omega \cdot cm^2$ [37]. The lower side value of 0.05 $\Omega \cdot cm^2$ is taken for Nafion 115 membrane with 125 micron thickness. The total power required for the EC is calculated in eq. (3-21) by multiplying the total cell voltage by the total current.

$$W_{EC} = (U_{ohm} + U_{Nernst}) * I \quad (3\text{-}21)$$

The electrochemical compression efficiency is the ratio between Nernst power (W_{Nernst}) and total power input required for the MEA (W_{EC}), based on the analogy of PEM fuel cell power efficiency as shown in eq. (3-22) [31].

$$\eta_{EC} = \frac{W_{Nernst}}{W_{EC}} \qquad (3\text{-}22)$$

where the total power required for the EC is W_{EC}, which is the sum of U_{Nernst} and work generated by internal resistance. Therefore, η_{EC} can be calculated from eq. (3-23).

$$\eta_{EC} = \frac{U_{Nernst} * I}{(U_{ohm} + U_{Nernst}) * I} \qquad (3\text{-}23)$$

which is further reduced to the ratio of Nernst potential and total cell voltage as in eq. (3-24):

$$\eta_{EC} = \frac{U_{Nernst}}{U_{Nernst} + U_{ohm}} = \frac{\frac{RT_{EC}}{2F} \ln\left(\frac{P_{dis}}{P_{suc}}\right)}{\frac{RT_{EC}}{2F} \ln\left(\frac{P_{dis}}{P_{suc}}\right) + I_d R_i} \qquad (3\text{-}24)$$

The similar calculation for EC efficiency is also developed by Wong et al. [38]

The EC power is calculated in eq. (3-25) based on the total amount of energy required divided by the cooling cycle time.

$$\overline{W_{EC}} = \frac{(U_{ohm} + U_{Nernst}) * I * t_d}{t_{cycle}} \qquad (3\text{-}25)$$

The cooling COP of system can therefore be calculated as in eq. (3-26).

$$COP = \frac{\overline{Q_c}}{\overline{W_{EC}}} \qquad (3\text{-}26)$$

3.3 The Simulation Results and Discussion

The hydrogen flow rate across the membrane is only related to the current density for steady state analysis. Therefore, the current density can be treated in analogy to hydrogen flow rate across the membrane. Table 3-1 lists all the design parameters for the steady state simulation. The cross sectional area of 100 cm^2 was chosen for the EC based on the experimental work done by Rohland et al [2]. The membrane resistance was taken assuming thinner membrane is selected for the EC based on the available resistance values. The metal hydride enthalpy of formation and entropy of formation were both taken from existing measurement [5]. The EC operating temperature was chosen according to Moton et al. [39]

Table 3-1: Fixed design parameters for steady state simulation

Parameters	Symbol	Value	Units
Cross Sectional Area	A	100	cm^2
Membrane Internal Resistance	R_i	0.05	ohm·cm^2
Number of ECs in parallel	N	20	ea
Heat of formation	ΔH	30.8	kJ/mol
Entropy of formation	ΔS	0.108	KJ/mol-K
Membrane operating temperature	T_{EC}	343	K
Outdoor temperature	T_h	308	K
Room temperature	T_c	288	K

The effect of current density, mass ratio between MH and reactor, suction and discharge pressure drop, desorption and absorption temperature drop, were studied by keeping other parameters constant at 10 K for ΔT_d, 10 K for ΔT_a, 0.2 for $\Delta P_{dis}/P_{dis}$, 0.1 for $\Delta P_{suc}/P_{suc}$, 1.9 for R_m, 0.05 A/cm^2 for current density, 20 for number of ECs in parallel. Some parameters were selected based on research done by Bedbak et al. (2005) on compressor driven metal hydride heat pump [40]. Other physical properties

for $LaNi_5$ MH and its reactor were taken from the study done by Hopkins and Kim, and are listed in Table 4 [41].

Table 3-2: Physical properties of $LaNi_5$ MH and its reactor

Parameters	Symbol	Value	Units
Thermal conductivity	k	5	W/m-K
Specific heat	C_{MH}	440	J/kg-K
Density	ρ_{MH}	5000	kg/m^3
Reactor inner radius	r_1	0.006	m
Reactor wall thickness	R_{wall}	0.001	m
Reactor Height	H_R	0.35	m
Reactor density	ρ_R	7900	kg/m^3
Reactor specific heat	C_R	385	J/kg-K

Figure 8 shows the effects of current density on system performance at constant mass ratio between MH and reactor [43]. The cooling power increases with current density because the hydrogen flow rate increases.

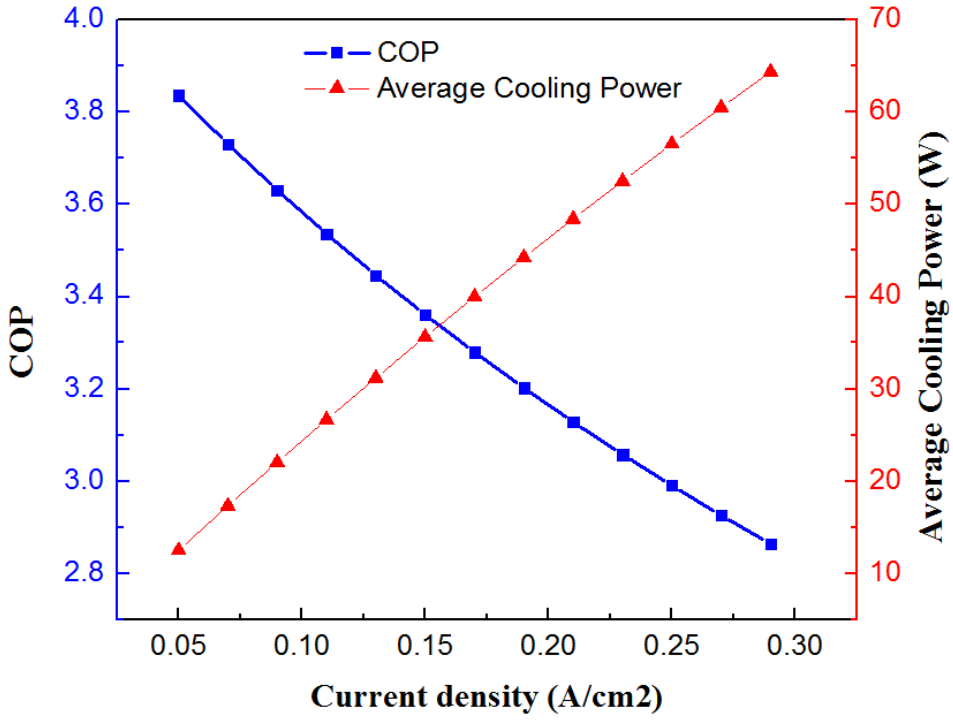

Figure 3-4: Effect of current density on system performance

Meanwhile, the COP decreases. This is due to the increased ohmic loss on the EC unit, and it continuously plays a role on decreasing the compression efficiency of EC, therefore decreases the COP of the system (Figure 3-5).

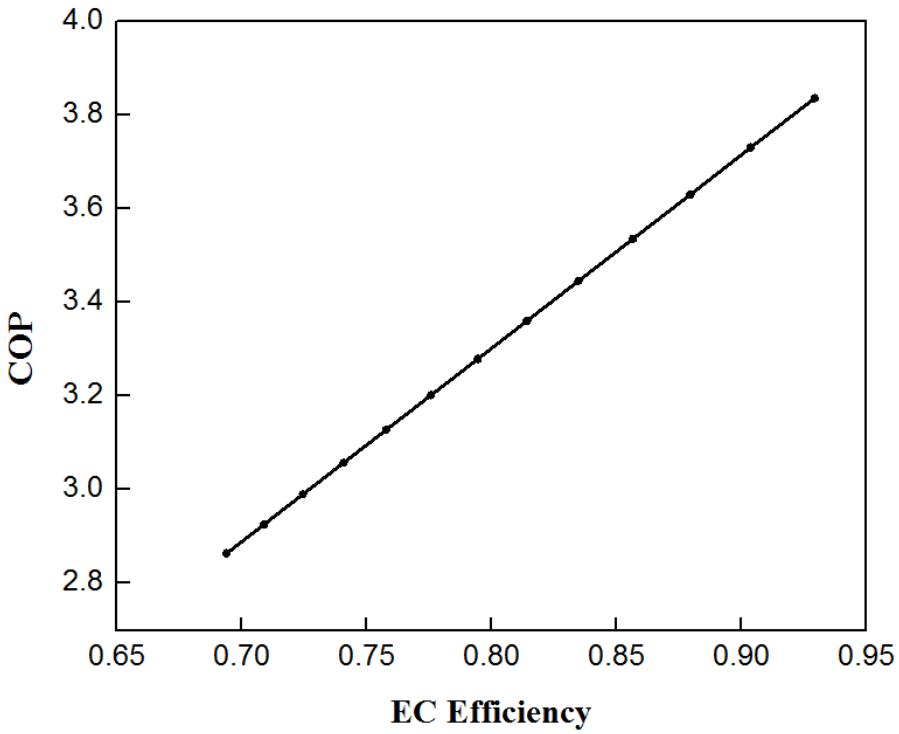

Figure 3-5: Effect of EC efficiency on system performance

Figure 3-6 provides the modeling results of the mass ratio between MH and reactor in terms of system performance by fixing current density. As the mass ratio increases, the cooling power increases.

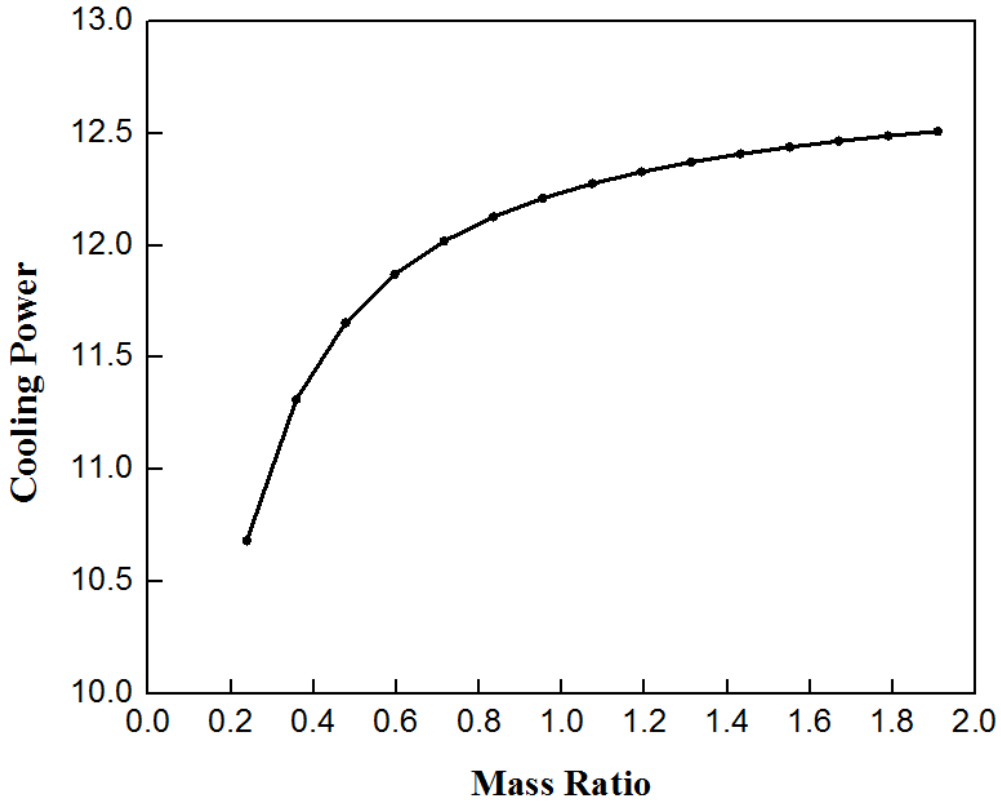

Figure 3-6: Cooling power vs. mass ratio

However, the parasitic loss also increases as more cooling energy is consumed on cooling down the increased MH mass, diminishing return is observed after Rm value of greater than 0.8. After that, the cooling power has no significant improvement. Therefore, there is no point to increase mass ratio by keep increasing the mass of MH material in the cylindrical reactor.

The suction and discharge pressure drops on system performance are shown in Figure 3-7 and Figure 3-8. Increase of suction pressure and discharge pressure drop would increase the pressure ratio, and have a marginal effect on the system performance.

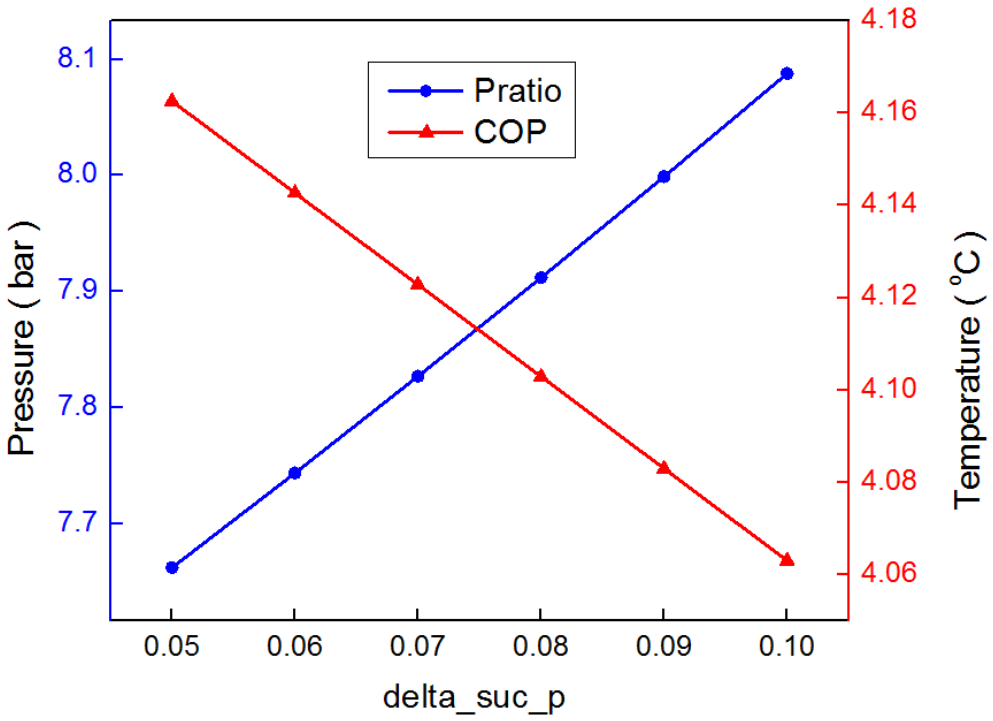

Figure 3-7: Effect of suction pressure drop on system performance

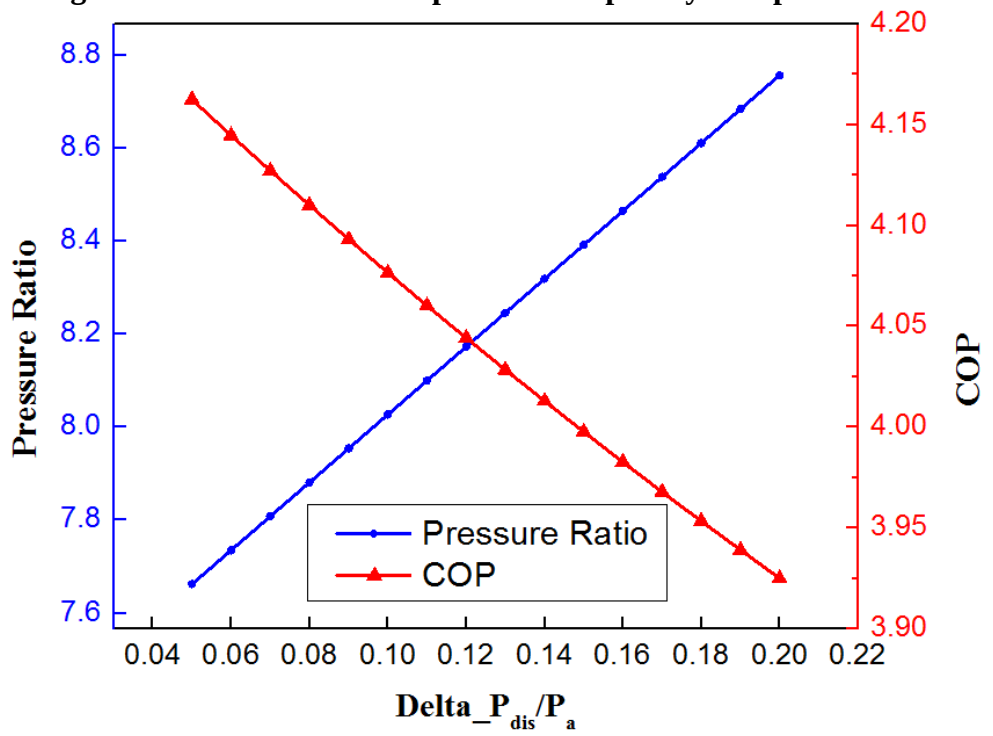

Figure 3-8: Effect of discharge pressure drop on system performance

Figures 3-9a and 3-9b show the effect of temperature difference between desorption reactor and room temperature on system performance. The temperature difference has

a negligible effect on cooling power and suction pressure. However, increase of temperature difference would decrease the system COP significantly, because lowering desorption temperature would lower the EC suction pressure, which increases the EC power consumption.

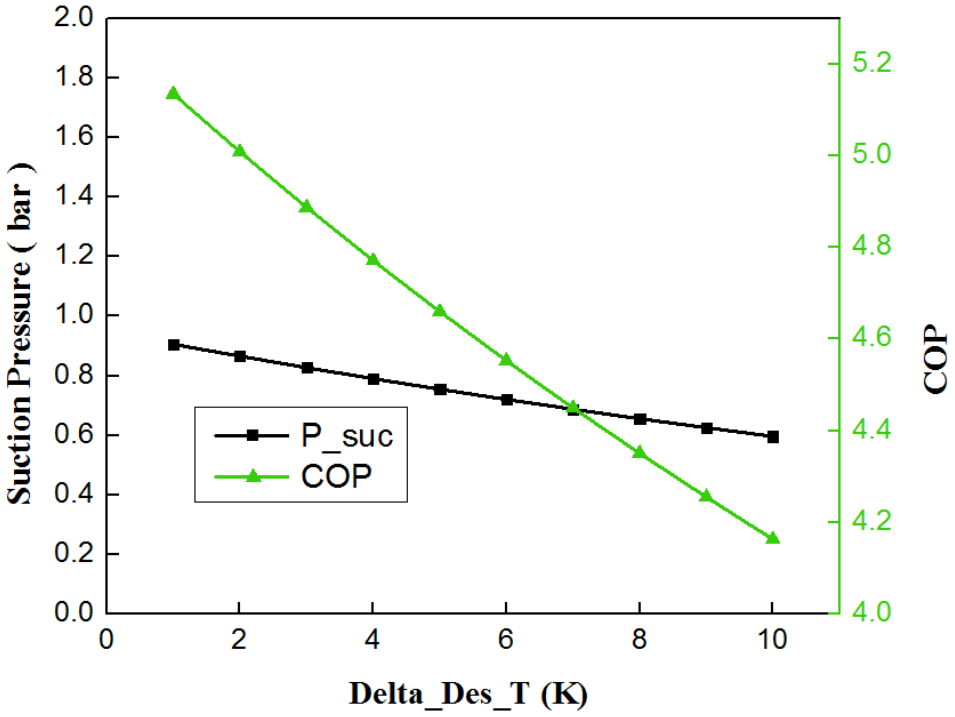

Figure 3-9a: Suction pressure and COP vs desorption temperature drop

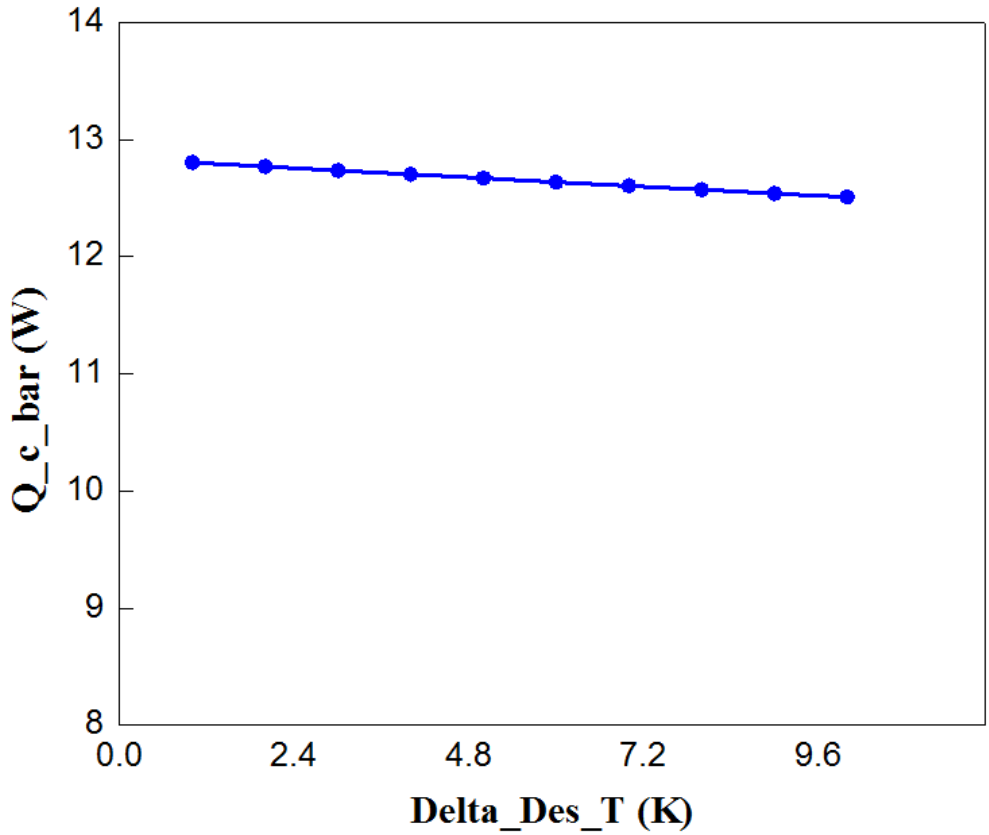

Figure 3-9b: Cooling power vs desorption temperature drop

Figure 3-10a and b shows the effect of temperature difference between the absorption reactor and the heating temperature. Similar to desorption process, the temperature difference has a negligible effect on heating power. The COP of the system, and discharge pressure however, changes significantly as the temperature difference increases.

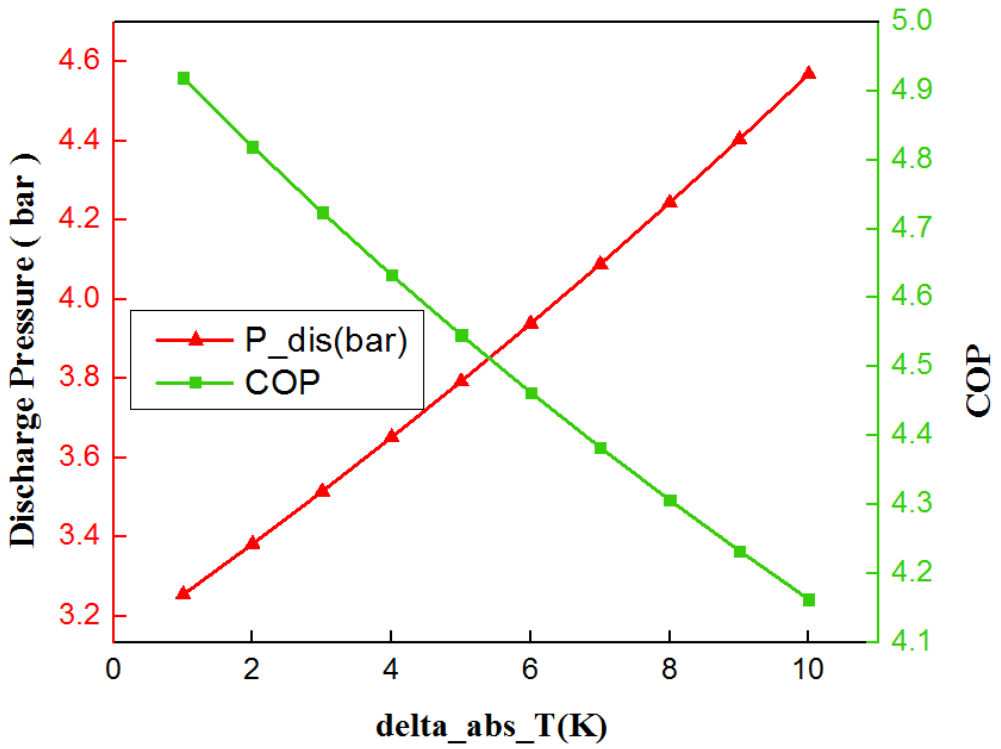

Figure 3-10a: Effect of absorption temperature lift on discharge pressure and COP

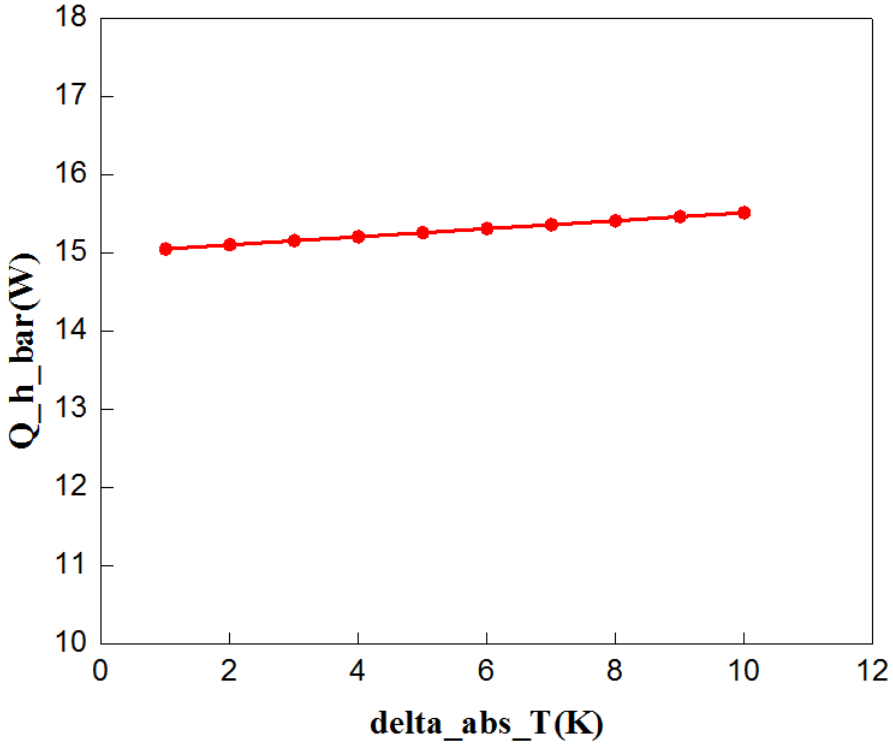

Figure 3-10b: Heating power vs absorption temperature lift

In order to determine the right suction and discharge pressure drops, the reaction kinetics of MH materials, which generates sufficient desorption and absorption rate for desired performance, has to be considered.

Figure 3-11 shows the EC stack volume and cooling power in terms of number of cells the stack consists of. For scaling up the system, MEA stacks need to be connected in parallel to increase the hydrogen flow rate. The volume of EC was calculated and compared with the amount of cooling power. It can be determined that for a heat pump with 100 W of cooling power and COP of 3.4, at cooling and heating temperatures of 5 °C and 45 °C and current density of 0.15 A/cm^2, requires 70 MEAs to form a 100 x 100 x 700 mm stack.

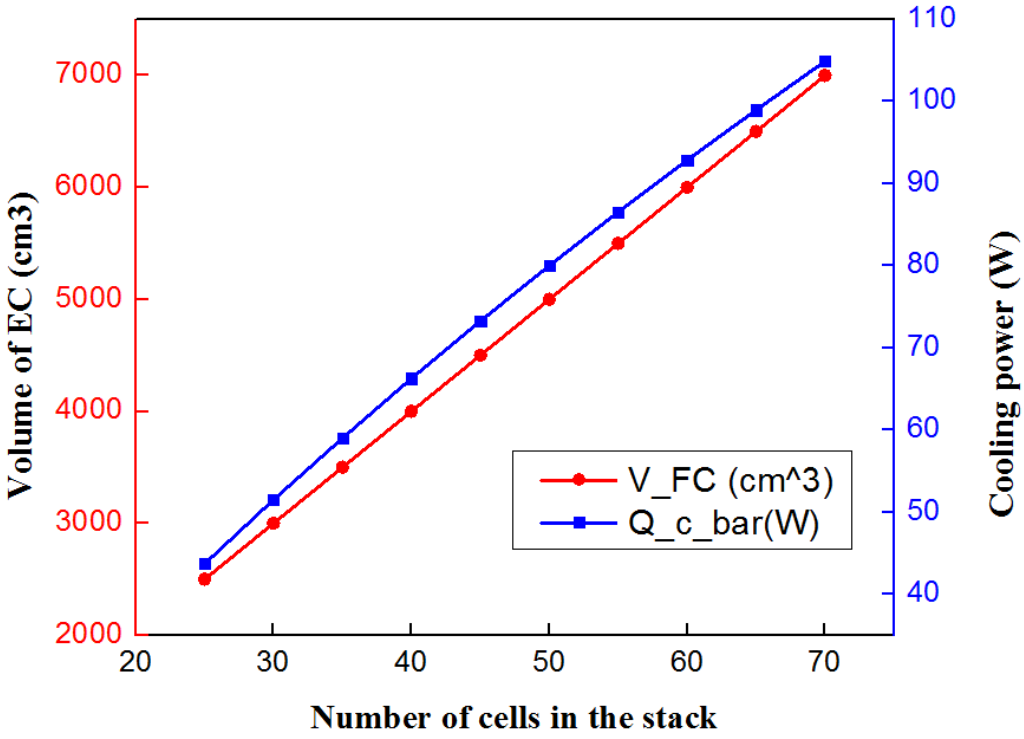

Figure 3-11: Quantitative analysis of EC stack volume and cooling power vs. number of cells in stack

The flow rate control of EC depends on the COP, volume of EC stack and required cooling power because current density generated by external voltage is the driving

force of H_2 transport. As shown in Figure 3-4, an increase of current density increases the cooling power but reduces the COP. A decrease of current density would increase the number of cell in EC stack in order to achieve the same cooling power as compared to higher current density, therefore, it increases the manufacturing cost. Therefore, there is a balance between the initial cost and the performance, and manufacturers need to take both into consideration for scaling up the system.

The life cycle of EC system is mainly constrained by the EC itself. The EC design is very similar to PEM fuel cell. The life cycle of PEM fuel cell includes the production of materials and emissions. Pehnt stated that the production of fuel cell stacks has unneglectable environmental impact [42]. This mainly includes impact caused by the platinum group metal catalyst production and the material and energy consumed for flow field plate production. The emission of SO_2 produced by platinum metal production chain gives major environmental impact. Graphite is the material used for manufacturing the flow field plates. 160 MJ of non-renewable energy is consumed to produce 1 kg of graphite, and it is mainly dominated by the electricity of mining and graphitization [42].

3.4 Chapter Summary and Conclusions

This chapter studied the cycle of electrochemical hydrogen compression in metal hydride heat pumps. A thermodynamic models of EC driven MH heat pump was proposed and studied, and the simulation results were discussed. The $LaNi_5$ alloy was selected as a suitable alloy for the MH reactors. The system performance was evaluated based on different parameters. The simulated results shows that EC efficiency has a great impact on the system COP. For a small scale heat pump with

cooling capacity less than 200 W, the EC operates more efficiently than the mechanical compressor. The EC driven MH heat pump could potentially have a higher COP than the existing MH system. And quantitative analysis shows a heat pump of 100 W cooling power with COP of 3.4 and 5 ºC cooling and 45 ºC heating temperatures and it requires a 10 x 10 x 70 cm^3 stack. For the future, experimental work needs to be performed to measure the real time performance. Since only the thermodynamic model was presented in this paper, in additional to experiments, transient modeling also needs to be performed for better modeling the system performance.

Chapter 4: The electrochemical ammonia compression for vapor compression refrigeration cycle and ammonia storage as a carbon neutral fuel

4.1 The Motivation of Study

The motivation behind the study of ammonia electrochemical compression is its higher compression efficiency and involvement of no moving parts in the process. The aforementioned characteristics are considered very unique and superior over mechanical compression process. Therefore, it may have a wide application in ammonia air conditioning/refrigeration, and ammonia storage. Ammonia is the second most produced chemical in the world. It is considered as a promising carbon neutral fuel for energy storage and delivery because of its low cost, high energy density and facile storage as a liquid [44]. As a hydrogen carrier, ammonia plays important role to advance the frontier of fuel cell electric vehicles and hydrogen economy [45]. Therefore, it is critical to develop a simple and effective ammonia compression process to ensure efficient on-board ammonia storage and delivery. Currently, ammonia can only be mechanically compressed with a low efficiency around 65% for small or medium sized compressors [46]. Electrochemical ammonia compression on the other hand, has a high efficiency of greater than 90%, which offers an opportunity for substantial energy savings. But ammonia is never considered electrochemically compressible due to decomposition.

4.2 The Proposed Ammonia Electrochemical Reaction Mechanism and Experimental Verification

As previously mentioned in Chapter 1.2.3, ammonia has been considered as a contaminant in the PEM fuel cell system. The ammonia contamination is not related

to the Pt catalyst poisoning, according to previous studies, but to the reduction of proton conductivity of Nafion membrane by forming NH_4^+. However, by taking advantage of the NH_4^+ formation in the membrane, the experimental study of this chapter filled the research gap of transferring ammonia in the form of NH_4^+ in PEM, which is not previously reported in the literature. The proposed way of forming NH_4^+ in PEM is introducing hydrogen as a carrier gas on the anode. The overall process is mentioned in Chapter 2.2.2 and discussed in details in the following [47]. When NH_3 and H_2 are fed to the anode, two spontaneous reactions will take place. H_2 is first electrochemically oxidized to H^+ on anode Pt catalyst. NH_3 then combines with H^+ to form NH_4^+.

Anode reaction:

$$H_2 \rightarrow 2H^+ + 2e^- \quad (4\text{-}1)$$

$$2NH_3 + 2H^+ \rightarrow 2NH_4^+ \quad (4\text{-}2)$$

NH_4^+ is then transported across the Nafion membrane under external voltage. At the cathode, NH_4^+ is converted back to NH_3 and H^+, H^+ is then electrochemically reduced back to H_2 on Pt catalyst at higher pressure (reaction 4-3 and 4-4).

Cathode reaction:

$$2NH_4^+ \rightarrow 2NH_3 + 2H^+ \quad (4\text{-}3)$$

$$2H^+ + 2e^- \rightarrow H_2 \quad (4\text{-}4)$$

The standard voltage potential for reactions 4-1 and 4-4 are the same as hydrogen evolution reaction, which is normally smaller than 200 mV. Therefore NH_3 decomposition will not take place [16]. The drag coefficient between NH_3 and H^+ is fixed at 1 due to the formation of NH_4^+ (reaction 2). Therefore, the transfer ratio

between NH_3 and H_2 is 2, since one hydrogen releases two protons. Overall compression reaction is:

$$2NH_3 + H_2\ (P_1) \rightarrow 2NH_3 + H_2\ (P_2) \quad (4\text{-}5)$$

4.2.1 The reaction mechanism verification by gas chromatography

The mechanism of electrochemical NH_3 compression was investigated by feeding a gas mixture of NH_3 and H_2 to the anode side at varied molar ratios (from 1.0 to 4.0). The operating process schematic of electrochemical NH_3 compression is shown in Figure 4-1 in electronic supplementary information, while the testing facility is shown in Figure 4-2.

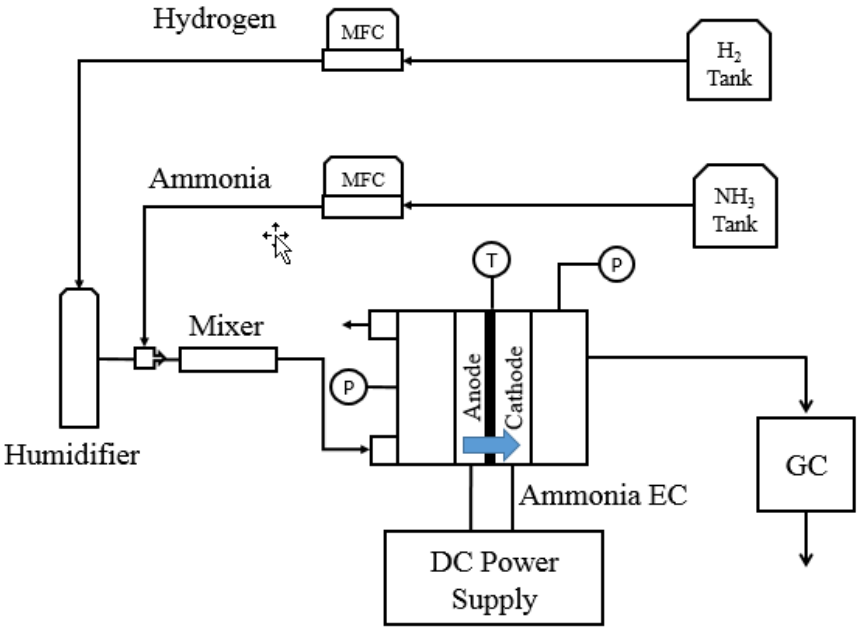

Figure 4-1: The schematic of electrochemical NH_3 compression testing facility for in-situ GC measurement

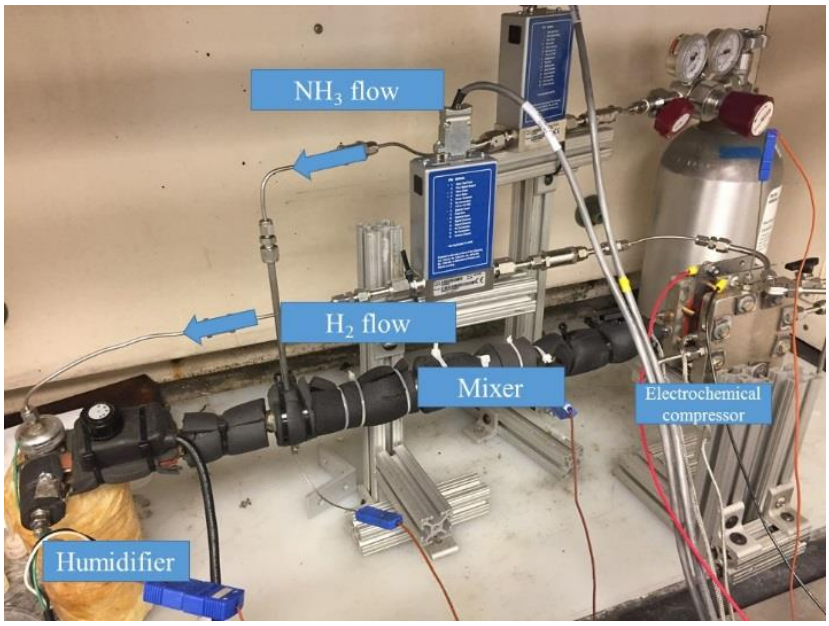

Figure 4-2: Picture of electrochemical ammonia compression testing facility

The electrochemical NH_3 compression is taking place by operating the cell at constant voltage, operated with a back pressure and the outlet gas stream is directed to the gas chromatography (GC) and titration to determine the molar ratio between H_2 and NH_3 (Figure 4-1 and 4-2). GC gives an instantaneous composition of the outlet gas mixture, while titration determines the cumulative amount of ammonia over a period of time (5~10mins). Based on the proposed electrochemical reactions (4-1 to 4-4), the NH_3 and H_2 composition ratio in the EC outlet should always be maintained around 2. As shown in Table 4-1 second column, the measured ratio of NH_3 to H_2 in outlet gas ranges from 2.04 to 2.3 even when the feed gas ratio widely changed from 1.0 to 4.0, which is also backed up by titration measurement (Table 4-2). The slight deviation of outlet gas molar ratio from 2.0 was investigated and it is attributed to NH_3 crossover through Nafion membrane due to concentration gradient of the NH_3 between inlet and outlet.

Table 4-1: Comparison of the mixed gas in the inlet and outlet

Inlet ratio	Outlet gas composition ratio (NH_3/H_2) measured by GC	Outlet gas composition ratio adjusted
4.0	2.30	2.03
2.5	2.16	2.00
2.0	2.04	2.04

Table 4-2: Feed composition in the inlet (anode) and measured composition in outlet (cathode) using titration method

Inlet feed ratio	**Measured gas molar ratio in outlet (NH_3/H_2)**
4.0	2.55
2.5	2.17
2.0	2.06

The amount of NH_3 and H_2 crossover Nafion membrane was measured using gas chromatography (GC) and shown in Table 4-3. The initial ammonia concentration given by the original peak area subtract the ammonia cross over concentration given by the cross over peak area is equal to the ammonia concentration adjusted. And the final gas composition ratio between ammonia and hydrogen is therefore calculated. The adjusted gas ratio in the final column was the measured value after correcting for crossover of NH_3.

Table 4-3: Ammonia composition adjusted based on crossover amount due to concentration gradient

Feed Ratio	H_2 concentration	Original NH_3 concentration	NH_3 concentration adjusted	Original Gas composition ratio	Gas composition ratio adjusted
4:1	0.29	0.67	0.59	2.30	2.03
2.5:1	0.31	0.66	0.61	2.16	2.00

The anode and cathode were both maintained at around 1 atm during measurement. The adjusted ratio of NH_3 to H_2 is around 2.0 (Table 4-1 third column and last column of Table 4-3), which confirmed the compression reaction mechanism. The NH_3 crossover in the Nafion due to concentration gradient is only 10% of total NH_3 transfer. H_2 cross over, however, is even much smaller than NH_3, due to low solubility of H_2 in water (0.00016g/100g of water) comparing to NH_3 in water (53g/100g of water) [48]. The ammonia crossover can be offset by increasing the cathode back pressure. When the compression is taking place at sealed cathode with back pressure, the concentration of H_2 and NH_3 on both sides of the membrane will reach equilibrium at the supplied voltage, satisfied by the Nernst equation. The concentrations on both sides are not expected to deviate from initial values. NH_3 was reported to be electrochemically decomposed to N_2 and nitrogen oxide at potentials over 0.65 V_{RHE} [16]. However the oxidation/reduction of H_2 to protons requires smaller potential, due to the low activation over potential for hydrogen evolution reaction (HER) on the anode and cathode side [36]. Therefore NH_3 does not decompose during electrochemical compression, as evidenced by no traceable N_2 has been detected by the GC. The formation of NH_4^+ fixes the drag coefficient of NH_3 to H^+ at 1, resulting in a constant transfer ratio between NH_3 and H_2 at 2 independent of the temperature.

As shown in Figure 4-3, the transfer ratio stays constant at temperatures ranging from 30 °C to 90 °C based on GC measurement.

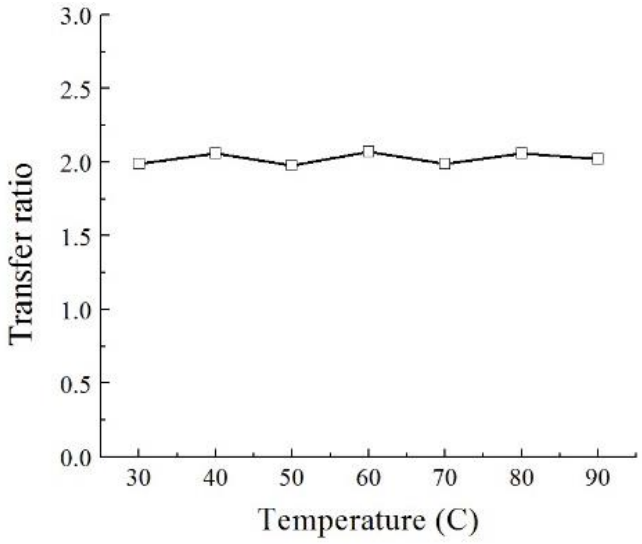

Figure 4-3: NH_3/H_2 transfer ratio vs. temperature

4.2.2 The Reaction Mechanism Verification through Faraday's Equation Based on Flow Rate

The NH_3 transfer rate is also measured in an open cell using titration over time and compared to the calculated rate using Faraday's Law (eq. 4.6) [2].

$$\frac{dn}{dt} = \frac{I}{nF} \qquad (4\text{-}6)$$

where I is the current, n is the number of electrons released per gas molecule (n is 2 for H_2, and 1 for NH_3), and F represents the Faraday's constant. As shown in Table 4-4, the flowrates measured are in the same order of magnitude as compared to the theoretical values. The small discrepancies between the theoretical and measured values are 16-18% for hydrogen and 22-25% for ammonia mainly due to the titration measurement error (shown in the table) and the crossover. The titration measured NH_3 flowrate is about 2 times as much as the measured H_2 flowrate, which further confirms the proposed reactions 1-4.

Table 4-4: Comparison between titration measured flowrate and theoretical

Feed NH_3/H_2 (sccm)	Theoretical H_2 (mol/s)	Theoretical NH_3 (mol/s)	Titration measured H_2 (mol/s)	Titration measured NH_3 (mol/s)
100/50	7.25e-07	1.45e-06	8.77±0.61e-07	1.89±0.13e-06
100/50	7.25e-07	1.45e-06	8.62±0.60e-07	1.86±0.13e-06
100/50	7.25e-07	1.45e-06	8.90±0.62e-07	1.94±0.14e-06

4.3 The Membrane Ionic Conductivity Measurement

The electrochemical compression efficiency is highly dependent on the NH_4^+ conductivity in electrolytes. The NH_4^+ conductivity in Nafion 115 at 30% and 50% relative humidity was measured using standard 4-electrode device (BekkTech BT-112, Figure 4-2, and 4-3).

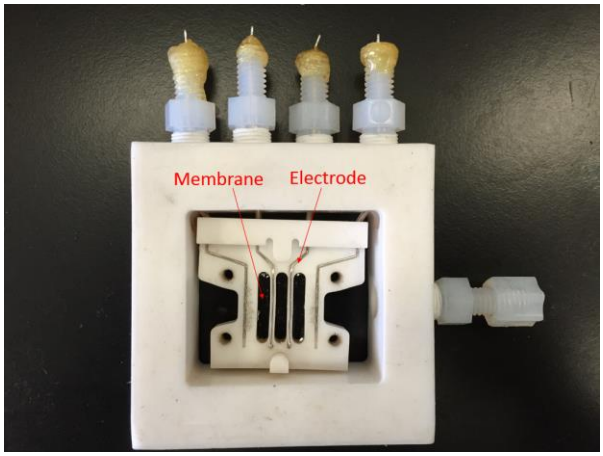

Figure 4-2: The membrane placed in between electrodes in BekkTech BT-112 for NH_4^+ conductivity measurement

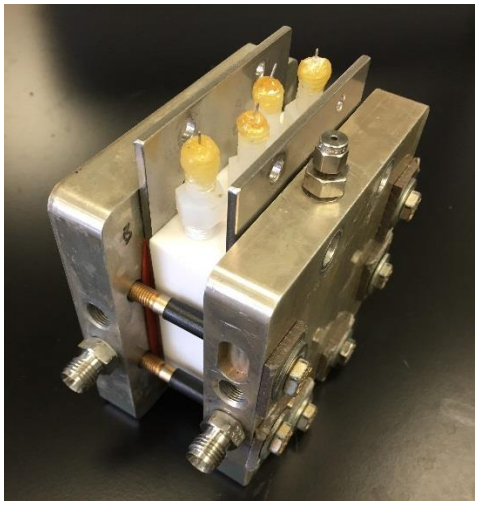

Figure 4-3: The BekkTech BT-112 module is sandwiched in between original electrochemical compression device

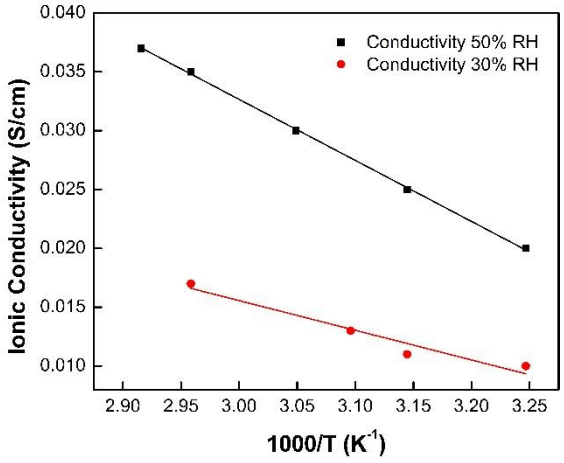

Figure 4-4: The relationship between NH_4^+ conductivity in Nafion and temperature at 30% RH and 50% RH

The NH_4^+ conductivity in Nafion 115 in temperature range between 35 °C and 70 °C at 30% and 50% RH is shown in Figure 4-4. The NH_4^+ conductivity in Nafion 115 is in the range between 0.02 to 0.04 S/cm at 50% RH, which is 4-10 times lower than the conductivity of H^+ in Nafion at the same temperature and RH. This data agrees with the NH_4^+ conductivity in Nafion 105 membrane reported by Uribe et al., which is 0.033 S/cm [14]. The reduced conductivity is due to the larger size of NH_4^+ than that of H^+. Nevertheless, the high NH_4^+ conductivity in Nafion ensure the high kinetics for electrochemical NH_3 compression.

4.4 The Pressure Ratio and Voltage Charge Relationship

The relationship between pressure ratio and voltage for electrochemical compression in a closed system should satisfy the Nernst equation when system reaches the equilibrium, defined in eq. (4-7) [36].

$$U_{Nernst} = E_0 + \frac{RT_{EC}}{nF} \ln\left(\left(\frac{P_{H2,outlet}}{P_{H2,inlet}}\right)^{\frac{1}{2}} * \left(\frac{P_{NH3,outlet}}{P_{NH3,inlet}}\right)\right) \qquad (4\text{-}7)$$

where the partial pressure of compressed hydrogen and ammonia at both cathode and anode were measured and calculated, and n is the number of electrons each gas molecule releases, in our case n=1 since one H^+ combines with one NH_3 to form NH_4^+. T_{EC} = 40 °C is the operating temperature of the device, and E_0 is equal to zero because the half reactions on both sides of the membrane are opposite. Once charging a voltage to an EC with cathode sealed, current should gradually decreases to zero when equilibrium has been reached, and the compression ratio and voltage relationship can be obtained from eq. 4-7. However, for a continuous compression process at a constant voltage, the current gradually decrease to a steady-state value, which represents the flowrate across the EC membrane. The current density decreases with time at four different voltages in continuous compression processes are shown in Figure 4-5, when the anode pressure is maintained around 1 atm.

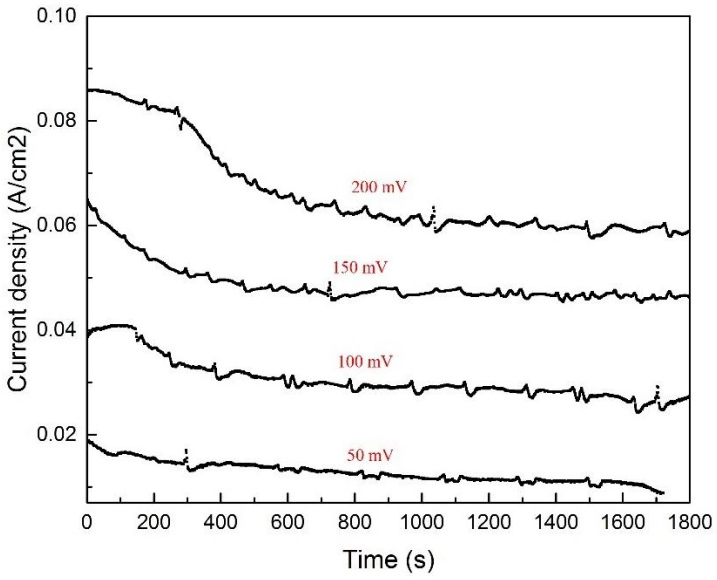

Figure 4-5: Current density vs. time at constant voltage charge (50mV, 100mV, 150mV, 200mV) with cathode back pressure, current density decreases due to cathode pressure built up and eventually stabilizes

Figure 4-6 shows that the natural log scale of partial pressure ratio follows linear increase trend with respect to the cell voltage although the partial pressure ratio is lower than what can be calculated by Nernst eq. 4.7 for a sealed system due to continuous compression flow. The cathode pressure increases with respect to time at each constant voltage operation in continuous compression process is shown in EIS (Figures 4-7 through 4-10).

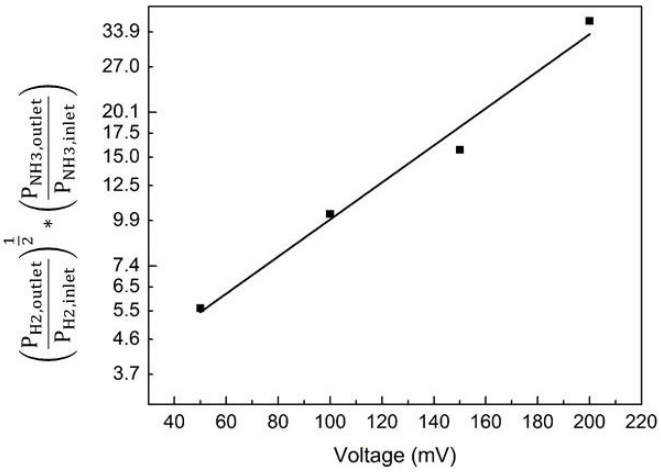

Figure 4-6: Partial pressure ratio vs. cell voltage based on Nernst equation, where P_2/P_1 is the pressure ratio measured from cathode and anode

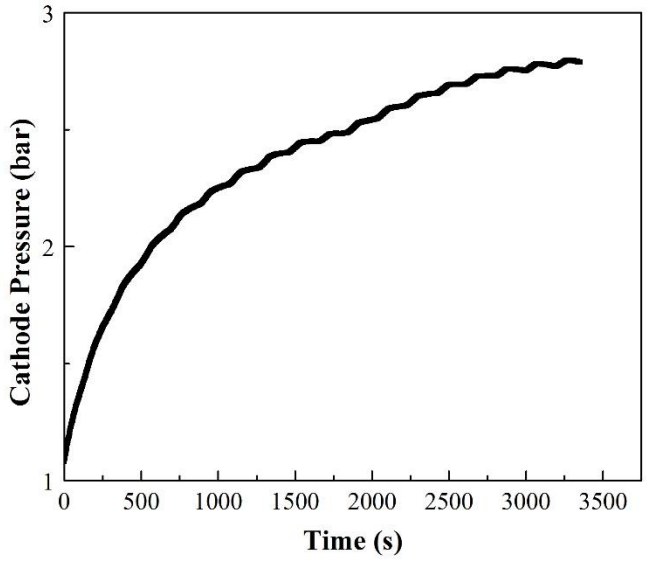

Figure 4-7: Cathode pressure vs. time at constant voltage of 50 mV

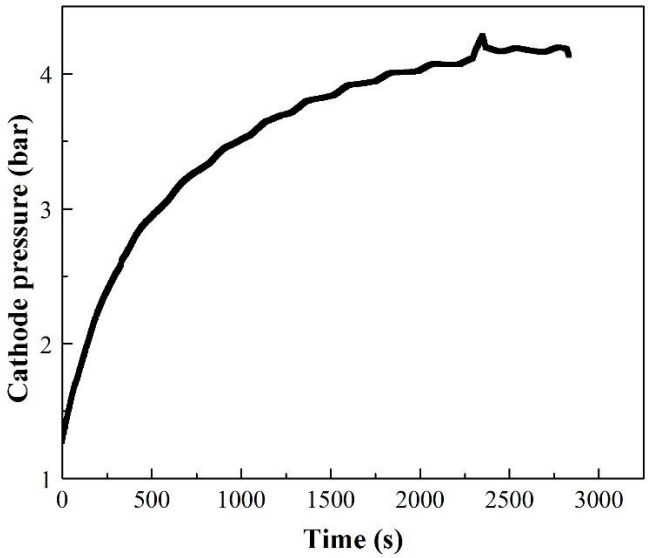

Figure 4-8: Cathode pressure vs. time at constant voltage of 100 mV

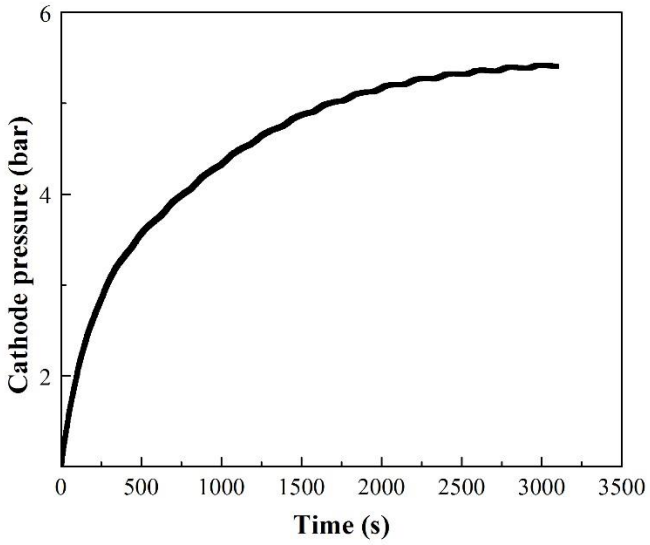

Figure 4-9: Cathode pressure vs. time at constant voltage of 150 mV

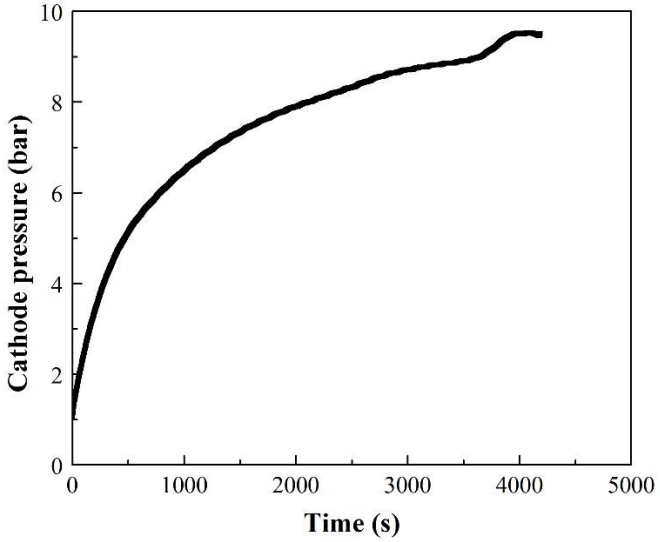

Figure 4-10: Cathode pressure vs. time at constant voltage of 200 mV

4.5 The Ionic Transfer Mechanism Discussion

Three mechanisms, including Grotthuss mechanism, proton hopping and vehicular mechanism (mass diffusion) have been proposed for proton transfer in Nafion membrane [49]. While in anion exchange membrane, hopping and vehicular mechanism were determined for OH^- ions by Chen et al. [50]. Similarly, the transfer for NH_4^+ in Nafion may be also caused by hopping and vehicular mechanism. Grotthus mechanism particularly represents the H^+ mobility in water [51]. Without water, NH_3 alone cannot provide H^+ mobility in Nafion membrane, as evidenced by almost zero current in electrochemical ammonia compression at constant voltage with dry ammonia and hydrogen in Figure 4-11. In contrast, a high current density of 0.07 A/cm^2 is observed at 50% RH (Figure 4-11). It is because water weakens the bonding between NH_4^+ and the Nafion sulfonic acid group ($R\text{-}SO_3^-$).

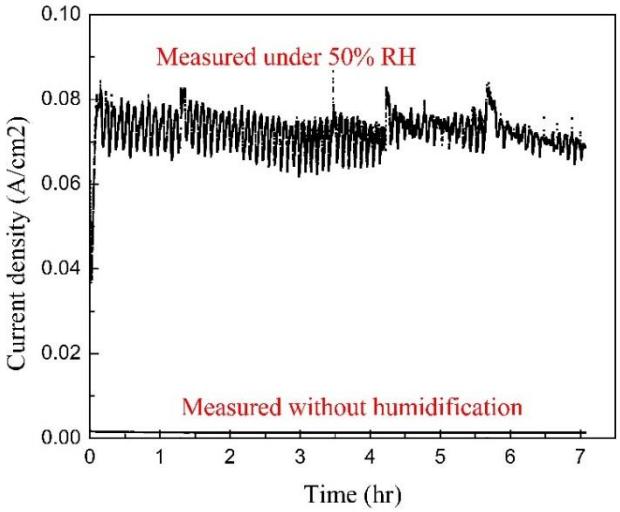

Figure 4-11: Stabilized current density at constant voltage 200 mV measured over time with and without humidification (H_2 and NH_3 supplied to anode)

The Nafion membrane was ion exchanged from H^+ to NH_4^+ by soaking in NH_3 solution, which gives the membrane an alkaline environment. H^+ does not exist in alkaline environment. Therefore, Grotthus mechanism does not play a major role. Instead H^+ only transfers together with NH_3 in the form of NH_4^+. Similarly, NH_3 transfer in Nafion membrane is also facilitated by H^+ by forming NH_4^+. If no H^+ is created by supplying H_2 on the anode, NH_3 alone cannot go through the membrane, which is verified by the very low current density measured by supplying humidified ammonia to the anode (Figure 4-12).

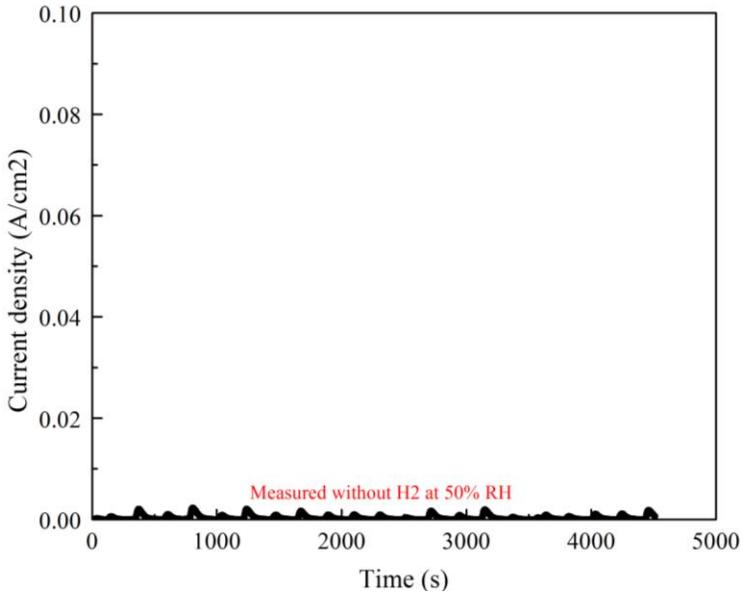

Figure 4-12: Current density of NH_3 flow at constant voltage 200 mV measured over time without H_2 fed to the anode (humidified NH_3 supplied to anode)

Hopping mechanism represents the cation hopping between sulfonic acid groups on the membrane surface [49], which can be the transfer mechanism of NH_4^+. Vehicular mechanism represents the mass diffusion of cations under external voltage influence, which may be one of the mechanisms NH_4^+ undergo as well. The NH_3 in Nafion membrane largely remains in NH_4^+ form if NH_3 and H_2 are continuously supplied to the anode side based on the Le Chatelier's principle (Figure 4-13).

High concentration of NH_3 and H_2 on left side

$$2NH_3 + H_2 \longrightarrow 2NH_4^+ + 2e^-$$

Equilibrium shift to the right

Figure 4-13: The Le Chatelier's principle of NH_4^+ formation in the PEM

4.6 The Electrochemical Ammonia Compression Performance

The compression efficiency at 50 mV of DC voltage charge is shown in Table 4-5, and the detailed calculation is shown in electronic supplementary information. The efficiency would stay the same as EC is scaled up by stacking multiple units in

parallel to increase the flowrates. Therefore the electrochemical ammonia compressor has an advantage over mechanical compressor in terms of efficiency.

Table 4-5: Compression efficiency vs. voltage

Current density (A/cm2)	Voltage charge (mV)	Nernst Voltage (mV)	Cathode pressure (MPa)	Efficiency
0.010	50	47	0.28	93%

The current density and voltage relationship determined by linear voltage sweep at 0.5 mV/s from 50 mV to 200 mV is shown in Figure 4-14. The linear sweep process is continuous without reaching steady state. Similar technique was applied by Strobel et al. to understand the current density and voltage relationship for electrochemical hydrogen compression [3]. In addition, continuous electrochemical compression operation of 7 hours has been achieved with stable performance (Figure 4-11).

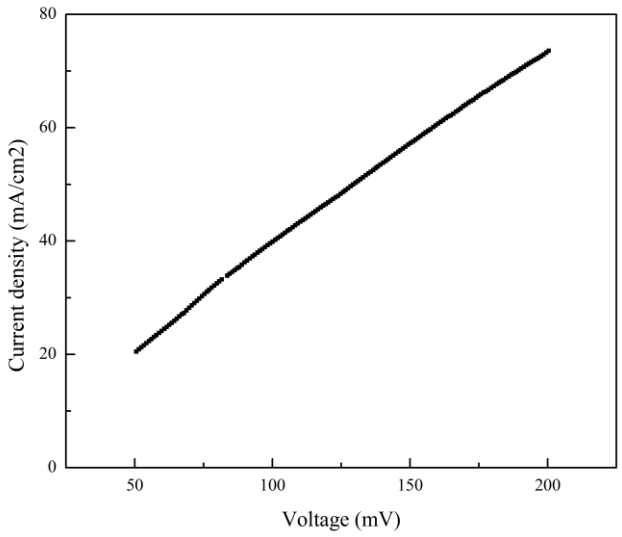

Figure 4-14: Measured current density vs. voltage in a linear sweep at 0.5 mV/s from 50 mV to 200 mV at 50% RH (H2 and NH3 supplied to the anode)

4.7 Potential applications in refrigeration and heat pump

The annual US energy consumption on residential and commercial building is 39 quadrillion BTUs, which is 40% of the total US energy consumption, among which

10% is used for refrigeration [52]. Among all the components in the refrigeration system, the compressor contributes a large portion to the overall system energy consumption. The electrochemical ammonia compression can potentially be used to replace mechanical compressors to create a more energy efficient vapor compression refrigeration system. With the extensive study of single membrane unit electrochemical compression of ammonia, it is possible to scale up the membrane units to form a stack for increasing ammonia flow rate. The scaled up design is shown in Figure 4-15, with two units connected in parallel and cathode discharge channels are placed in between an air cooled microchannel heat exchanger. The reason to place a heat exchanger in between the discharge channels is to cool down the refrigerant in the discharge side and achieve isothermal compression process for a reduced compressor power consumption.

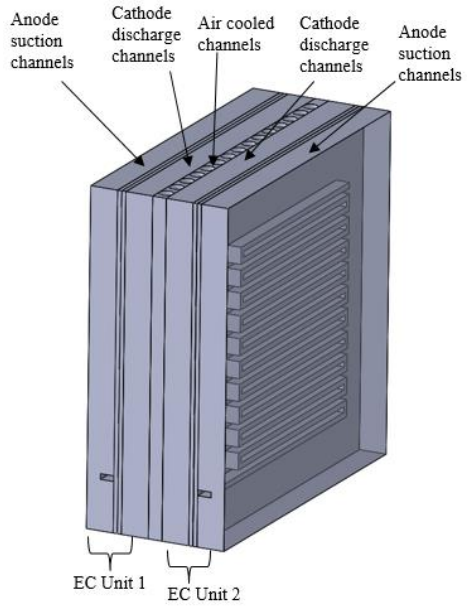

Figure 4-15: Electrochemical ammonia compressor with cooling channels in between two cathode discharge sides

Based on the modeling results, the vapor compression refrigeration system with electrochemical ammonia compressor can achieve a COP of 5.1 at 5 °C evaporating

and 45 °C condensing temperature and 200 W of cooling capacity. Comparing to the currently available small sized compressors with different kind of refrigerants, the ammonia EC has greater COP and competitive capacity to volume ratio (Figure 4-16).

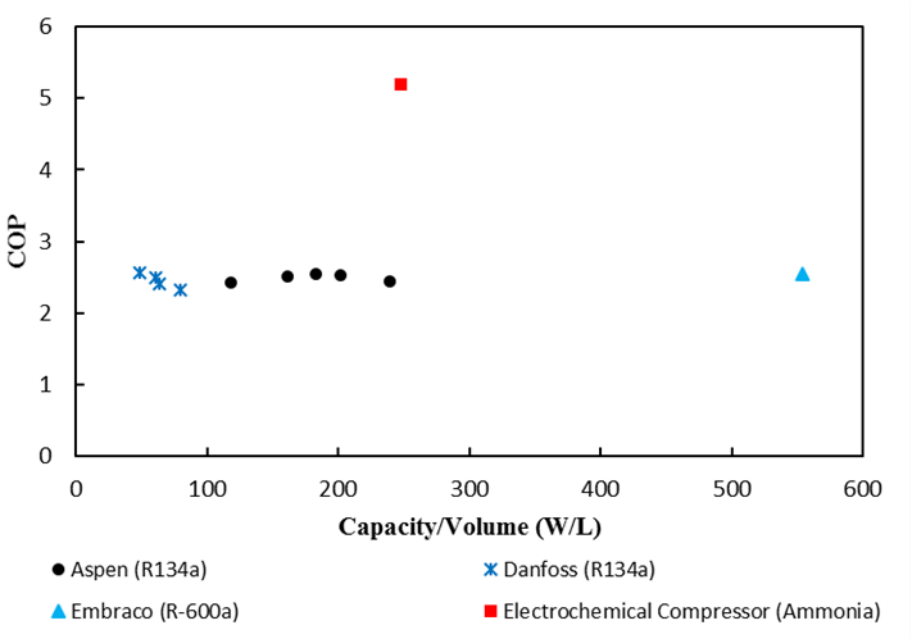

Figure 4-16: EC comparing to state of the art compressors in the market

In conclusion, the electrochemical ammonia compressor can potentially run a much more efficient vapor compression refrigeration system than mechanical compressors. And the developed compressor will also be very competitive in terms of size comparing to currently available state of the art.

4.8 Potential applications in ammonia storage

Ammonia is a carbon neutral fuel which can either be treated as a hydrogen carrier, or directly combusted as a fuel. Nowadays, a large fraction of ammonia is stored as a liquid either under atmospheric pressure by cryogenic cooling at -33 °C, or it is stored under room temperature at an elevated pressure of around 10 atm [53]. Both storage

methods are quite energy intensive. Plus mechanical compressors require lubrication oil to operate, which will potentially contaminate the compressed ammonia. The electrochemical ammonia compression device developed with greater than 90% compression efficiency will have a much higher efficiency and potential application in ammonia storage. The technology can potentially provide substantial energy savings. The targeting market will be portable scale ammonia storage such as automobile fuel tank or fuel cells. Currently, for small scale ammonia compression, especially compressor power consumption less than 1kW range, the ammonia compressor does not exist. The electrochemical ammonia compressor can fill the gap in this market. One potential challenge is the separation of hydrogen and water from ammonia. Since hydrogen is used as a carrier gas to transfer ammonia across the membrane, a mixture of both gases is generated on the cathode side of the membrane. Therefore hydrogen must be separated from ammonia. And during the transferring process, membrane must be humidified to maintain ionic conductivity. Therefore some amount of water (<1%) may also be carried over to the cathode side. Water can mix easily with ammonia and creates a challenge for maintaining ammonia purity for storage. Possible solutions of separation technique are introduced to address the aforementioned issue. In order to separate hydrogen from water and ammonia, phase separation approach is proposed. Because hydrogen always remain in gas form under room temperature and moderate pressure, it can be separated by liquefying ammonia, which takes place at relatively moderate pressure of 10 atm. In the laboratory, I have achieved ammonia pressure as high as 20 atm by electrochemical compression. Therefore, hydrogen in the gas phase can be removed in the electrochemical ammonia

compression system. As far as separating water from ammonia, a moisture trap can be placed at the outlet of the electrochemical compressor to remove moisture in the humid ammonia stream. The moisture trap will contain desiccant material CaO for water removal, which is a standard industrial desiccant chosen to remove moisture and produce anhydrous ammonia. The reason CaO is chosen is because ammonia as a base can react with acidic desiccant such as concentrated sulphuric acid. Also CaO is considered as cheap and easy to acquire.

In conclusion, electrochemical ammonia compression can play an important role in ammonia storage, for its high compression efficiency, no moving parts design and operation without lubrication oil.

4.9 Chapter Summary and Conclusions

This chapter discussed the electrochemical ammonia compression in details. The proposed reaction equation shows that ammonia and hydrogen are both transferred across the membrane in the ratio of 2 to1. The proposed reaction was verified using gas chromatography to measure the concentration ratio of both gases in the discharge stream, and titration method to measure the amount of both gases with phenolphthalein as the pH indicator. The PEM ionic conductivity was measured at 30% and 50% RH. The measured results show that NH_4^+ ionic conductivity is 4 to 10 times lower than the H^+ conductivity in the Nafion membrane. The pressure ratio and voltage charge relationship is verified with Nernst equation. The natural log relationship shows that a discharge pressure ratio of 10 can be achieved at 200 mV of voltage charge. The ionic transfer activity in the PEM was discussed and concluded that NH_4^+ transfers in the membrane via hopping and vehicular mechanism. The

single membrane unit can achieve a compression efficiency of 93% at 50 mV. The ammonia EC can be applied in both air conditioning and heat pump systems with a simulated COP of 5.1 at 5 °C evaporating and 45 °C condensing. The scale up design is proposed for the vapor compression refrigeration system. It can also be applied for ammonia storage by liquefying ammonia at room temperature and 10 atm. The process can be achieved in one stage and hydrogen and moisture in the mixture stream can be separated by phase change and CaO desiccant. Overall, the ammonia EC technology shows a promising performance and sets the foundation for future scale up development.

Chapter 5: The study of electrochemical carbon dioxide compression for trans-critical refrigeration cycle and carbon capture

5.1 The Comparison between Electro-Catalysts

The study of electrochemical reactions of both CO_2 and O_2 on the surface of the electro-catalysts is very important for membrane CO_2 transfer. In this chapter, two electro-catalysts are studied. The first one is platinum, which is a very common electro-catalyst used in fuel cell reactions. The platinum catalyst has the advantage of facilitating fast redox reactions for hydrogen oxidation reaction (HOR) and hydrogen evolution reaction (HER). Therefore it is widely adopted on the anode of hydrogen fuel cells. The cathode reaction in PEM fuel cell is the oxygen reduction reaction, which is usually the limiting step of the fuel cell reaction kinetics because it is much slower than the anode HOR. There are publications available to fabricate platinum based alloys for better oxygen reduction reaction kinetics, which are beyond the scope of this thesis study. The specific electro-catalytic situation for the study of electrochemical CO_2 compression is that oxygen reduction is taking place on the cathode which would combine either with water to form OH- (Eq. 5-1), or with CO_2 to CO_3^{2-} (Eq. 5-3).

$$O_2 + 2H_2O + 4e^- \rightarrow 4OH^- \qquad (5\text{-}1)$$

$$4OH^- + 4CO_2 \rightarrow 4HCO_3^- \qquad (5\text{-}2)$$

$$O_2 + 2CO_2 + 4e^- \rightarrow 2CO_3^{2-} \qquad (5\text{-}3)$$

Therefore if the catalyst has low selectivity of CO_2 over H_2O, then more OH^- would form to compete with the direct CO_3^{2-} formation. In fact, if more OH^- is formed, then the anion can readily combine with CO_3^{2-} to form HCO_3^-. The involvement of water

in the overall reaction would require more presence of water on the cathode side, which creates a limiting factor for the cathode reaction. Platinum is facilitating more water reaction with oxygen to form OH^-, due to the weak interaction between platinum and CO_2 [22]. And the reaction mechanism of Pt facilitated electrochemical compression of CO_2 will be discussed in chapter 5.3.

The understanding is that even though ORR is slow on the cathode side, it is still feasible to develop a catalyst which prefers to absorb both O_2 and CO_2 instead of O_2 and H_2O. And $CaRuO_3$ is developed to improve the reaction kinetics based on the aforementioned absorption preference. The reason that $CaRuO_3$ catalyst has more advantage than Pt is because Ca is an alkaline metal, and CaO favors CO_2 over H_2O for absorption. RuO_2 on the other hand is a good catalyst for oxygen reduction. Therefore the combination of both CaO and RuO_2 would make the catalyst facilitate the combination reaction between O_2 and CO_2 more easily on the catalyst surface, which means reaction 5-2 can take place more frequently than 5-1. Additionally, operating the AEM under pure carbonate ions would extend its lifetime since carbonate ions have lower nucleophilic strength comparing to OH^-, which attacks the functional group and causes membrane degradation through Hoffman elimination [54]. Also due to the higher valence of CO_3^{2-}, the ion exchange capacity of the AEM is slightly increased [56]. A higher ion exchange capacity leads to better AEM performance [56]. The superiority of $CaRuO_3$ catalyst over Pt catalyst for the particular CO_2 and O_2 electrochemical reaction can be reflected by the difference between current measured. Figure 5-1 shows the current measured both at 1.2 V of voltage charge for Pt and $CaRuO_3$ catalyst at same surface area per gram.

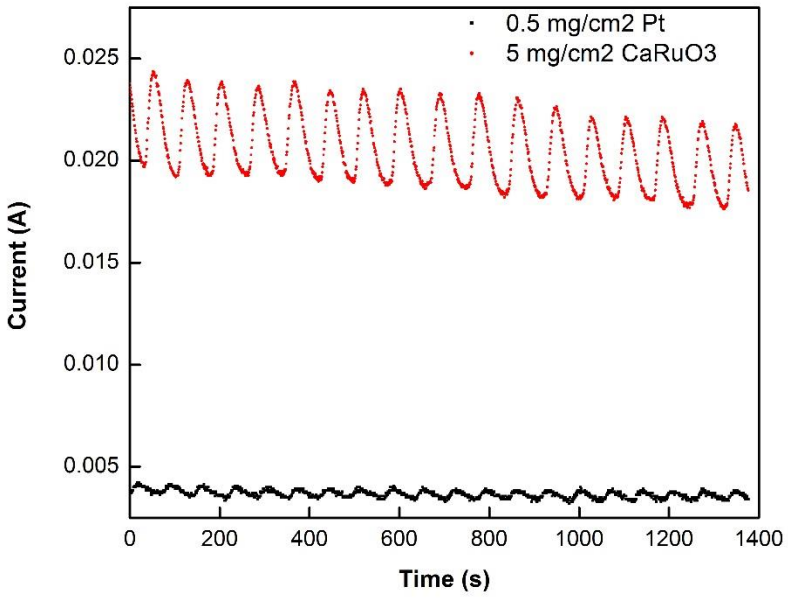

Figure 5-1: The current density comparison between Pt and $CaRuO_3$ with 150 m^2/g surface area

In order to make it a fair comparison, catalytic activity needs to be compared at the same amount of surface area. Pt catalyst is the commercially available product with surface area of 150 m^2/g. The laboratory synthesized $CaRuO_3$ surface area is measured to be 15 m^2/g by BET. Therefore the amount of $CaRuO_3$ needs to be ten times as much as the amount of Pt doped on the surface of the MEA to make it a fair comparison. As a result, the loading amount for $CaRuO_3$ coated MEA needs to be ten time as much as the loading amount of Pt coated MEA. And Figure 5-1 shows that the catalytic activity for $CaRuO_3$ is higher than Pt at same operating conditions. Additionally, it is also necessary to study the reaction mechanism of $CaRuO_3$ facilitated electrochemical compression of CO_2, which will be further discussed in chapter 5.3.

5.2. The development of $CaRuO_3$ catalyst and MEA fabrication

5.2.1 CaRuO3 catalyst synthesis and characterization

Previously, studies have been done on $CaRuO_3$ in AEMFC for carbonate cycle operation [34] with superior performance than Pt. And the synthesize techniques were previously introduced. The catalyst for this study was developed based on the work done by [34]. One selected synthesize methods was conducted for this study. In this method, $KMnO_4$ is used as a strong oxidizing agent and mixed with 1 M KOH solution to prepare 1 mM potassium permanganate solution. CaO and $RuCl_3$ were mixed in a 1:1 molar ratio and dissolved in the potassium permanganate solution. The solution is placed in a stainless steel reaction vessel and heated to 200 °C for 48 hours. The resulted precipitated product was washed with DI water and ethanol and dried overnight at 80 °C. The catalyst synthesized is analyzed with XRD (Figure 5-2). The XRD shows the lab synthesized CaRuO3 material is identical to the literature standard. Meanwhile, the surface morphology was observed with SEM (Figure 5-3).

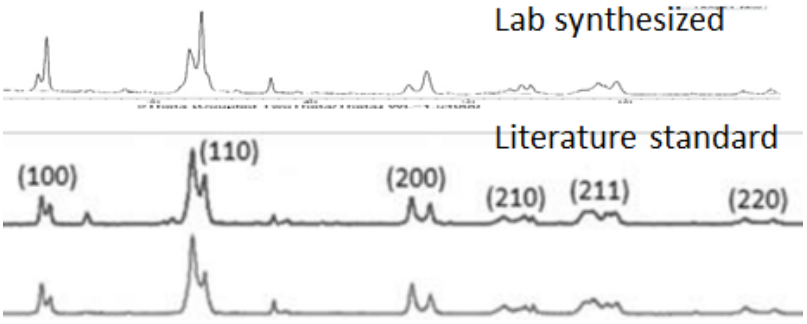

Figure 5-2: Lab synthesized $CaRuO_3$ versus literature standard

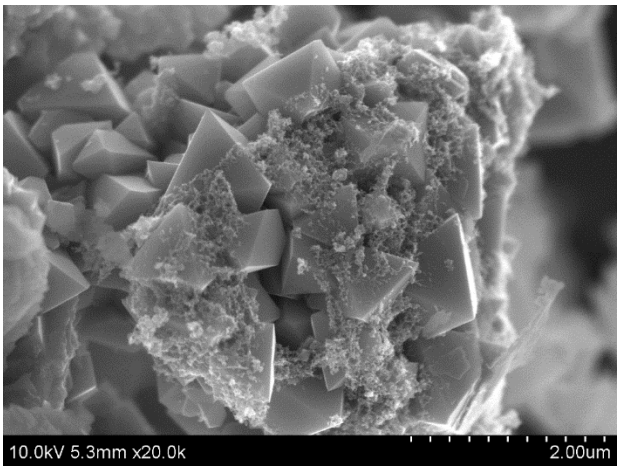

Figure 5-3: The SEM image of synthesized CaRuO3 catalyst

The surface area of developed catalyst was then measured with BET and the resulted surface area is 15 m^2/g. With surface area measured, the doping amount of CaRuO3 on the surface of carbon cloth electrode is determined to be 5 mg/cm2.

5.2.2 Preparation of catalyst ink

Fumatech anion exchange membrane was used in our experiments as the anion exchange membrane. The membrane was pre-treated by ion exchanging from Cl^- state to CO_3^{2-} state by soaking in Na_2CO_3 solution for 24 hours. Fumion binder solution was used for making the catalyst ink. The catalyst ink was prepared by mixing $CaRuO_3$ with 5% ionomer solution in isopropanol. The solution was then sonicated for 30 mins to form a ink suspension. The ink solution in suspension form was brushed on the surface of 2.5*2.5 carbon cloth with loading amount of 5 mg/cm2 to make anode and cathode electrodes. The prepared electrodes were then pressed against the anion exchange membrane with pound force of 500 psi. The prepared membrane electrode assembly is shown in Figure 5-3.

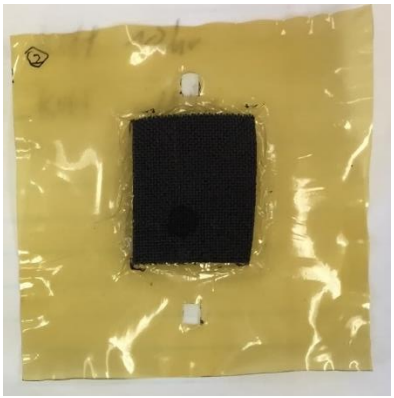

Figure 5-4: Membrane electrode assembly prepared with anion exchange membrane and carbon cloth electrodes

$CaRuO_3$ catalyst not only has a better catalyst performance than Pt for CO_2 and O_2 reduction reaction, but also lower cost, which is about ¼ of the cost pure Pt sold in the market.

5.3 The proposed reaction mechanism and verification

As previously mentioned in chapter 5.1, Pt and $CaRuO_3$ are both catalysts studied in electrochemical CO_2 compressions. But each catalyst facilitates a different reaction path, which essentially leads to the combination of oxygen preferably with either H_2O or CO_2. Therefore it is important to study both catalytic reaction mechanism and verify the proposed reaction pathway in eq. 5-1, 5-2 and 5-3. The experiments were performed with similar experimental setup in Figure 4-1 and Figure 4-2. The electrochemical CO_2 compressor is charged with 1.2 V of DC voltage and the discharge gas stream is collected by the GC. The GC is running in situ and the sample line is directly connected to the discharge side of the compressor. The calibration curve of CO_2 and O_2 concentration is shown in appendix B. The GC measures the relative concentration of CO_2 and O_2 and the concentration ratio is calculated. The goal is to verify if the measured concentration ratio is backed up by the ratio of

stoichiometric coefficient of CO_2 and O_2. Therefore, the CO_2 and O_2 concentration ratio in the discharge stream should be 4 for Pt facilitated reaction and 2 for $CaRuO_3$ facilitated reaction. Table 5-1 shows the measured concentration ratio of CO_2 and O_2 on the discharge side with four trials for each catalyst. The concentration ratio measured with Pt as catalyst varies around 4.0, with average value equal to 3.7, which shows the stoichiometric coefficient of CO_2 and O_2 in reaction equation 5-1 and 5-2 is validated. The reason that the average value is slightly less than 4.0 is because the Pt catalyst can still absorb some amount of CO_2 to trigger reaction 5-3, and leads to a slightly lower CO_2 concentration in the discharge side. On the other hand, the concentration ratio measured with $CaRuO_3$ as catalyst varies around 2.0, with average value equal to 2.1, showing the stoichiometric coefficient of CO_2 and O_2 in reaction equation 5-3 is validated. Of course, the average is slightly higher than 2.0, meaning $CaRuO_3$ does absorb some amount of water to trigger reaction 5-1, and leads to a higher CO_2 concentration in the discharge side. This theory is backed up by analysis done by Vega et al., reporting the carbonate selectivity for Pt was 1.78, while for $CaRuO_3$ was 7.33 [34].

Table 5-1: The measured concentration ratio in the discharge side for both catalysts

Catalyst	Voltage charge (V)	CO_2 Flow	O_2 Flow	Discharge side gas composition		Concentration ratio
				CO_2 concentration	O_2 concentration	
Pt 2 mg/cm^2	1.2	50	50	0.24	0.88	**3.6**
	1.2	50	50	0.21	0.73	**3.4**
	1.2	50	50	0.23	0.88	**3.8**
	1.2	50	50	0.16	0.61	**3.9**
$CaRuO_3$ 2 mg/cm^2	1.2	50	50	0.41	0.88	**2.1**
	1.2	50	50	0.44	0.86	**2.0**
	1.2	50	50	0.4	0.89	**2.2**
	1.2	50	50	0.4	0.88	**2.2**

5.4 The AEM ionic conductivity measurement

The ionic conductivity for HCO_3^-, CO_3^{2-} and OH- ions were measured with device shown in Figures 4-2 and 4-3. The AEM cannot be operated at elevated temperature more than 50 °C, therefore, the experiments were conducted at room temperature with 100% RH. The AEM was submerged in 1 M Na_2CO_3, $NaHCO_3$ and NaOH solutions respectively for 24 hours to exchange the original Cl^- ion to CO_3^{2-}, HCO_3^- and OH^- ions. The measured results are calculated and shown in Table 5-2. Due to larger ionic radius and lower ionic mobility of HCO_3^- and CO_3^{2-}, the conductivity of both ions in the AEM is lower than OH^- [55]. The carbonate and bicarbonate ions also lowers the pH of the membrane environment, avoiding nucleophilic attack of OH^- to the membrane. Just by comparing between HCO_3^- and CO_3^{2-}, the HCO_3^- conductivity is slightly higher due to smaller ionic radius. Even with slightly higher ionic conductivity, the

current generated by voltage charge in CO_3^{2-} form of AEM is still higher than HCO_3^- form, because of better electro-kinetics of $CaRuO_3$ and higher ion exchange capacity of CO_3^{2-}.

Table 5-2: The ionic conductivity of three types of ions in AEM

Ion	Conductivity (S/cm)	Ionic Radius (pm) [57]
CO_3^{2-}	0.019	178
HCO_3^-	0.024	156
OH^-	0.029	133

5.5 The Carbon Dioxide Flowrate Measurement and Compression Ratio

The carbon dioxide flowrate can be measured with titration method using phenolphthalein as the pH indicator and NaOH as titrate. The measured flowrate value is compared with theoretical flowrate calculated based on Faraday's equation (Table 5-3).

Table 5-3: The CO_2 measured flowrate versus theoretical calculated values

Feed CO_2/O_2 (sccm)	Current (A)	Measured Flowrate (mol/s)	Theoretical Flowrate (mol/s)
50/50	53	2.51±0.18E-07	2.75E-07
50/50	24	1.19±0.08E-07	1.24E-07
50/50	18	9.18±0.64E-08	9.33E-08

The results indicate that the measured flowrate is in the same order of magnitude of theoretically calculated values based on the Faraday's equation. The measured CO2 flowrate across AEM is less than measured ammonia flowrate across PEM due to lower CO_3^{2-} mobility in the AEM which leads to lower ionic conductivity.

Figure 5-5 shows the compression ratio vs. voltage relationship. Again, due to the lower ionic conductivity of CO_3^{2-} in AEM, the compression ratio is considered as lower than ammonia compression ratio generated by ammonia EC. And higher voltage needs to be supplied to drive the CO2 EC. In the end, the $CaRuO_3$ catalyst needs to be further improved in order to reduce the voltage charge for a significant flowrate and compression ratio.

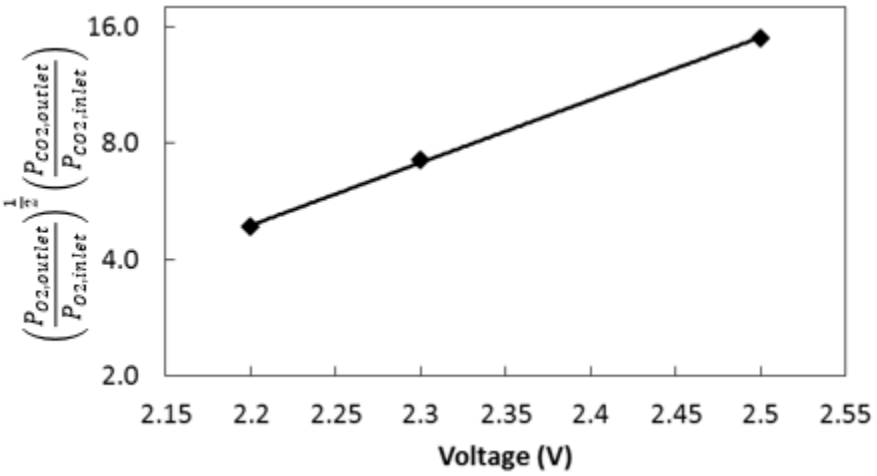

Figure 5-5: Compression ratio versus voltage charge for CO_2 EC

5.6 The Design of Gas Distribution Channels in the Electrochemical CO_2 Compressor

The gas distribution channels are embedded in the anode and cathode plate for the electrochemical CO_2 compressor. These are crucial part of the compressor design as significant pressure drop or pressure lift will take place inside of these channels. The materials of anode and cathode plates (some time named bipolar plates) also makes a significant difference for operation. In PEM fuel cells, graphite is the most common materials for bipolar plates for decades [58], simply because graphite is stable under acidic environment in the PEMFC. In recent years, people started using stainless steel

plates coated with inert materials for fuel cell operations [59-61]. For electrochemical CO_2 compression, oxygen is used as carrier gas and we need to take into consideration the large pressure difference across the membrane due to the thermodynamic properties of CO_2. Therefore the bipolar plates in electrochemical CO_2 compression is studied and discussed in this chapter.

5.6.1 The corrosion problem and the solution

The electrochemical CO_2 compression operate in basic condition and the voltage charge applied to the bipolar plates is greater than or equal to 1.2 V. Graphite is stable under basic environment, but a serious corrosion issue is detected when operating graphite at a voltage greater than 1.2 V. Figure 5-6 shows the graphite corrosion in the anode activated area.

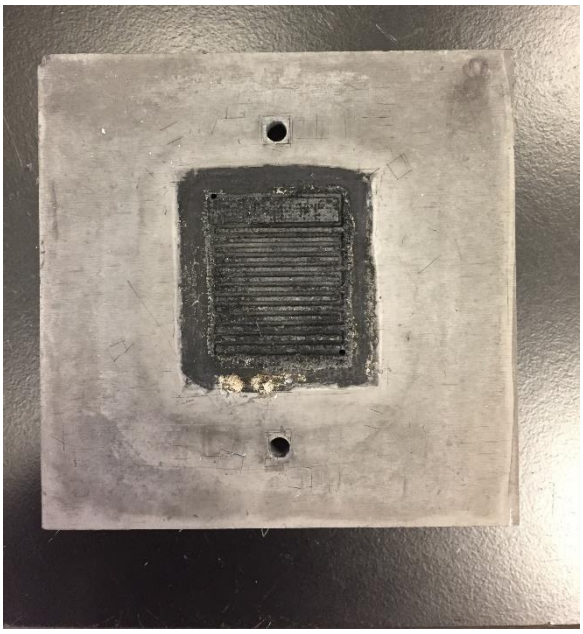

Figure 5-6: Graphite anode plate corrosion in the activated area (gas distribution layers can be seen at the center)

The corrosion happens because the graphite (carbon) readily reacts with oxygen on the cathode under the DC voltage charge to generate CO_2 (Eq. 5-4).

$$C(graphite) + O_2 \rightarrow CO_2 \qquad (5\text{-}4)$$

The drawback of using graphite is not only the corrosion issue which eventually deteriorates the plate structure, but also generates excess amount of CO_2 that creates bias on the anode discharge stream CO_2 concentration measurement. Therefore it make stainless steel the obvious choice for the material of bipolar plate. Because it is stable under voltage charge range between 1.2-1.5 V. A stainless steel bipolar plate is designed and voltage charging test shows very minimal corrosion problem in oxygen operating environment (Figure 5-7). And Figure 5-8 shows the original graphite bipolar plate is replaced by thinner stainless steel plate in the CO_2 EC. Stainless steel also has the advantage of reduced cost and increased mechanical durability.

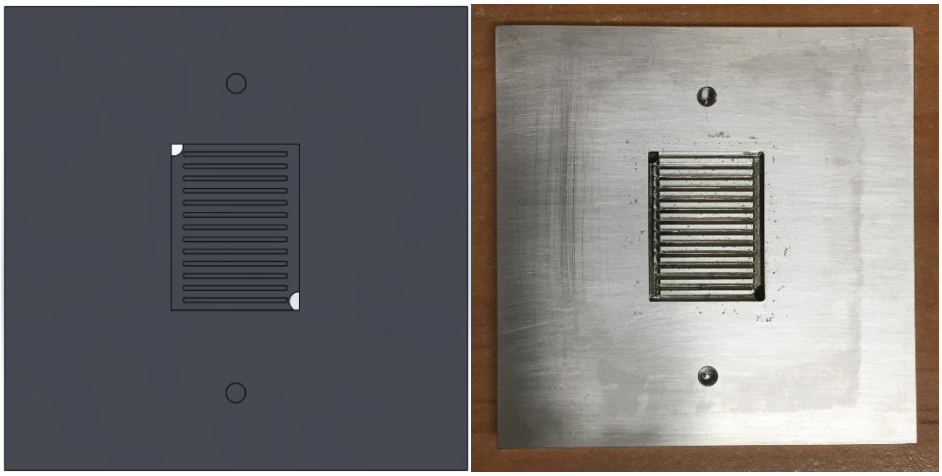

Figure 5-7: The stainless steel bipolar plate with gas distribution channels, Solidworks design (left) and the machined plate (right) with minimal corrosion issue detected

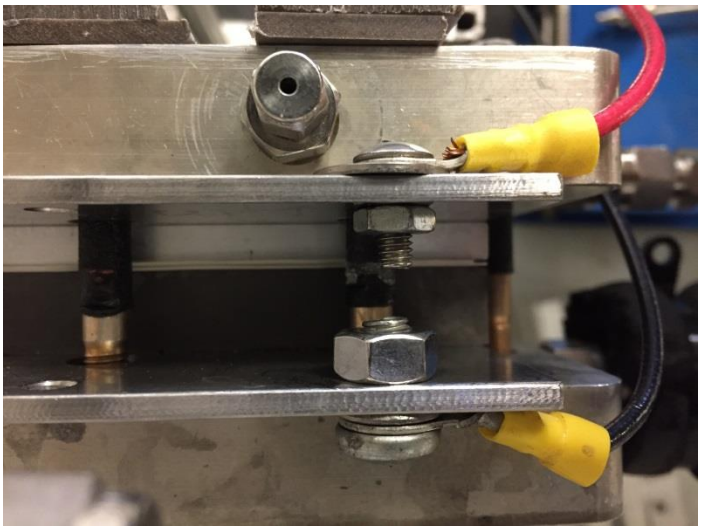

Figure 5-8: The discharge side stainless steel channel in the CO_2 EC

5.6.2 The selection of gas distribution channel design

Once the bipolar plate material is determined to be stainless steel, the next step is to design the gas distribution channels embedded in the plate. In PEM fuel cell, different gas distribution channel designs are studied, and the most common designs are serpentine channels and parallel channels [31]. But the fuel cell operates with an open channel design, meaning the anode and cathode plate each has an inlet and an outlet so that fuel can always be supplied to the membrane electrode assembly abundantly. For the case of electrochemical CO_2 compressor, though there has never been any design previously proposed, it has to be only an inlet on the cathode plate for gas intake and an outlet in the anode plate for gas discharge. And the gas distribution channel width needs to be adjusted to reflect the pressure drop and fluid distribution alone the way. Based on all that, it is necessary to have a proper design for the gas distribution channels in both anode and cathode of the electrochemical compressor. The cathode gas distribution channel is shown in Figure 5-9. As shown in the figure, since the cathode is the suction side, serpentine channel is selected to make sure there

is only one way for gas flow for better distribution on the surface of MEA. The width of the channel gets wider as it is getting close to the suction link to accommodate the flow change and pressure drop.

Figure 5-9: The cathode channels with serpentine design and reduced width to accommodate flow change along the way

The anode gas distribution channels are shown in Figure 5-10. Because the anode is discharge side of the compressor, parallel channels are selected to accommodate higher discharge pressure lift and flow distribution. The merging channel needs to get wider approaching the discharge line to accommodate the increased mass flow and pressure drop.

Figure 5-10: The anode gas distribution channels with parallel design and wider merging area for pressure drop and flow distribution

5.7 The Exploration of carbon dioxide Electrochemical Compressor Stack Cooling Techniques

The electrochemical compression process requires energy input into the compressor in the form of voltage charge, which heats up the device and brings up the temperature of CO_2 discharged. And increased discharge temperature of compressed fluids would eventually degrades the performance of the compressor by increasing its energy consumption. A proper compressor heat removal technique during the compression process could lead to energy savings as high as 28% [62]. Traditionally, ideas about injecting the refrigerant in liquid or vapor phase to the compressor chamber have proved to be effective to reduce the discharge temperature and improve the compressor performance [30]. But the drawback of this idea leads to additional work requirement to compress extra amount of refrigerant. Other ideas about externally cooling the motor or actively cooling the shell have been proposed also [30]. But the compressor usually has limited surface area for heat removal which makes it very

challenging to cool it down. The electrochemical compressor, however, has large membrane surface areas for heat removal and can potentially be modified by inserting heat exchangers for proper compressor cooling to approach isothermal compression. Even though it is very challenging to make the refrigerant stay at constant temperature during the compression process, inter-stage cooling can still be achieved with multiple stage of compression coupled with heat removal, which will be discussed in details in chapter 5.7. In this chapter, different heat exchanger designs are explored for compressor thermal management.

5.7.1 The Review of Heat Exchangers Used in PEM Fuel Cells

Convective air cooling of the cathode side is commonly used in small fuel cells. However, this requires an open structure at the cathode sides, and may increase the volume of the stack [63, 64]. The gas distribution channel in the discharge side of the electrochemical compressor can be made of either graphite or steel. Then the heat generated in the discharge side of the compressor can be removed by heat exchangers installed adjacent to the discharge side. Here we propose applying three types of heat exchangers based on similar applications in the PEMFC.

First type is open channel design. Air is flowing through these open channels to cool down the high temperature discharge gas. Cooling channel size depends on the heat load to be removed and pressure drop allowed. A separate cooling plate can be inserted in between two cathode discharge sides, so that heat is removed or channel geometry can be embedded in cathode wall. This cooling strategy was used for PEMFC stacks in the range between 100 W to 2 kW [65]. The advantage of this method is that air is the only working fluid involved, which reduces the complexity of the EC

system. Schmidt et al. applied this technique on a 35-unit automobile fuel cell stack with active cooling area of 310 cm^2 [66]. Cooling air temperature ranges from 25°C to 50-80 °C from inlet to outlet. They proved the feasibility of air cooled stacks. Sohn et al. built a 500 W PEMFC stack with air cooling and find out that with optimized design and operation, cooling fan consumes only 10 W of power [67]. Matian et al. proposed thinner cooling channel plates to reduce the stack size, but found out that there is a tradeoff between plate thickness and pressure drop and recommends an optimization [68].

Second option is using the microchannel flat tube. The microchannel heat exchanger is recognized as the next generation heat exchanger over the conventional fin-tube heat exchangers due to its improved heat transfer on the refrigerant side, a reduced air side flow resistance and a reduced volume. The major difference to the open channel heat exchangers is that the microchannel heat exchanger requires higher density fluids than air due to its smaller flow area. The smaller tube diameter, however, increases the heat transfer area and improves the system performance. Garrity et al.[69] did an experimental study on 56-channel aluminum microchannel evaporator cooling plate on PEMFC cathode side with HFE-7100 as refrigerant. The channel has a cross sectional area of 1x1 mm and length of 115 mm. The study concluded that microchannel plate has a thermal capacity of 32 kW/m^2 at mass flow rate of 30 g/s, and is able to completely handle the heat flux rejected by the PEMFC, with refrigerant pressure drop ranging from 200 to 800 Pa. It is also indicated that the microchannel evaporator requires an external heat sink for refrigerant condensation which would potentially increase the complexity of the system.

Third option is using the metal foam heat exchanger. The metal foam has the advantage of large heat transfer area per volume. Boomsma et al. [70] showed that the metal foam heat exchanger has thermal resistance 2 to 3 times lower than the commercially available heat exchangers and consumes the same pumping power. Odabaee did an experimental study on metal foam heat exchangers with size of 5 x 100 x 100 mm and 95% porosity for PEMFC thermal management and found out that the air cooled metal foam heat exchanger requires half of the pumping power compared to water cooled fuel cell systems for the same amount of cooling capacity at same operating conditions and created a uniform temperature distribution across the cathode plates [71]. For heat flux of 1 kW/m^2, the air flow rate was 0.0024 kg/s and the approach temperature was 1.7°C. However, there is also concerns about the increase of pressure drop across the heat exchanger which will increase the fan power requirements.

5.8 The potential application of carbon dioxide Transcritical Refrigeration Cycle

5.8.1 The performance comparison between carbon dioxide EC and the state of the art

The CO_2 EC can potentially be used to replace mechanical compressors in the CO_2 transcritical refrigeration cycle. The currently available CO_2 compressors in the market have COPs less than 2. The electrochemical compressor on the other hand has COP of 3.9 (Figure 5-11). The calculation also shows that the capacity to volume ratio of the CO_2 EC is competitive comparing to smaller capacity compressors in the market. Therefore the CO_2 EC has a high performance potential than the currently state of the art mechanical compressors.

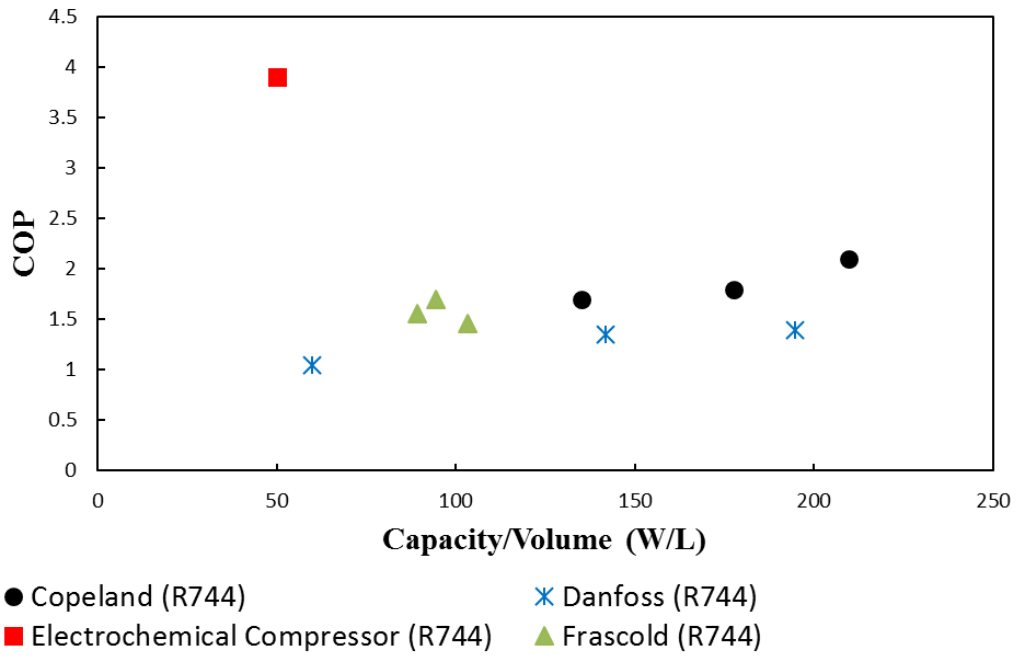

Figure 5-11: Electrochemical CO_2 compressor performance comparing to the state of the art

One of the challenges is that the pressure difference across the membrane is large for CO_2 compression. In mechanical compressor, for a compression ratio of 4, the pressure on the suction side can be 30 bar, and the pressure on the discharge side can be as high as 120 bar. For the electrochemical compressor there is multiple stages of compression, the pressure difference can be distributed across several layers of membranes, which means the membrane has to be mechanically supported to withstand 20 to 40 bar of pressure difference. Currently one way to support the membrane is to use fine stainless steel mesh together with stainless steel bipolar plates. The meshes are placed next to each of the anode and cathode side in between the MEA and the gas distribution channels, and the feasibility is still yet to be tested in the future.

5.8.2 The Isothermal Compression Potential

The potential to reach isothermal compression is discussed in this study. As previously mentioned in chapter 5.5, it is very difficult for mechanical compressors to achieve isothermal operating condition due to limited surface area for heat removal. The electrochemical compressor compresses refrigerant with layers of membranes. The refrigerants are discharged over a surface area of 100 cm^2, which provide large area for heat removal. The isothermal effect is especially effective for CO_2 compressor because CO_2 has a low molecular mass and can generate a significant temperature reduction. The P-h chart of the entire CO_2 transcritical refrigeration cycle is shown in Figure 5-12. The superheated refrigerant leaving the evaporator is going through three separate inter-stage cooling to achieve the final gas cooler temperature, before entering the expansion valve. The compressor power consumption has therefore been reduced, and the system COP is improved.

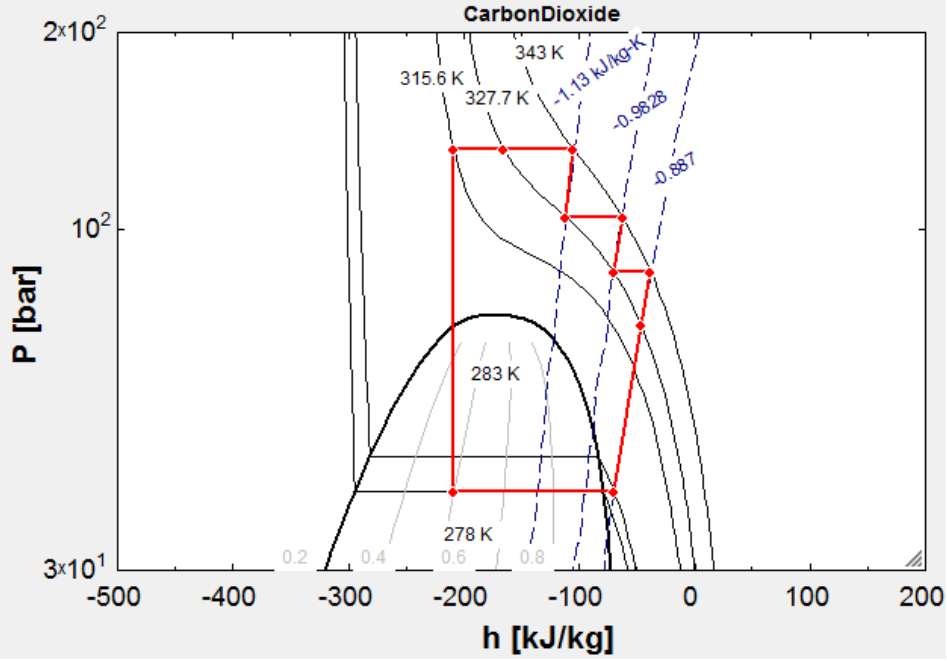

Figure 5-12: CO_2 transcritical refrigeration cycle with three compressor inter-stage cooling

5.9 The potential application of carbon dioxide EC for carbon capture

The electrochemical CO_2 compressor can be used for carbon capture. Because it is able to separate CO_2 from the flue gas stream in addition to compressing the CO_2 to a high pressure. In oil and gas production plant, a large amount of steam is produced for oil recovery [72]. The steam is generated from the boiler by burning natural gas, which produces flue gas in the meantime. Flue gas is usually composed of carbon dioxide, water vapor, nitrogen and oxygen, as well as traces amount of carbon monoxide, sulfur oxides (SOx) and nitrogen oxides (NOx). Therefore it is possible to treat flue gas stream with CO_2 EC for separating and compressing CO_2 for carbon capture. Before the stream enters the CO_2 EC, it has to be treated to remove SOx and NOx to prevent potential catalyst poisoning. But the removal of CO is not necessary since ruthenium oxide is an excellent CO oxidation catalyst [73]. The proposed setup for EC carbon dioxide capture is shown in Figure 5-13. The inlet is designed to be serpentine open channel for continuous gas flowing, and the outlet is one end open for gas discharge.

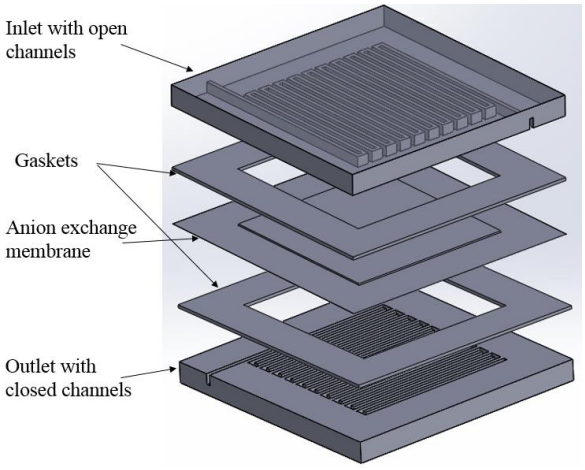

Figure 5-13: Electrochemical CO2 compressor for carbon capture

5.10 Chapter Summary and Conclusions

In this chapter, fundamental chemistries of electrochemical CO_2 compression is studied. At the beginning, Pt and $CaRuO_3$ catalysts are compared for electrochemical reactions on the surface and catalytic performance. The $CaRuO_3$ catalyst is synthesized in our lab and membrane electrode assemblies are fabricated for performance testing of both catalysts. And $CaRuO_3$ has shown superior performance than Pt for this particular reaction between CO_2 and O_2, due to its higher selectivity towards CO_2 than water. The proposed reaction mechanisms for CO_2 and O_2 on the surface of both Pt and $CaRuO_3$ are verified via GC. For the application of electrochemical compression, proper gas distribution channels for both cathode and anode plates are designed. Corrosion problems were detected for graphite bipolar plates and were successfully resolved by switching to stainless steel plates. The compressor stack cooling techniques are also explored based on PEM fuel cell literature. And finally, the CO_2 EC is explored for potential refrigeration and carbon capture application with proper cycle analysis and device modification. Overall, CO_2 EC will have a much higher compression efficiency than its mechanical counterparts and produces better system performance. It also provides the new opportunity for compressor cooling due to its unique structure, which was considered as challenging in current industry.

Chapter 6: Conclusions and Future Work

6.1 Conclusions

In this thesis, three distinct studies on electrochemical compression were performed to address the current challenges in the mechanical compression processes for air condition and refrigeration industry. The first study focuses on the simulation study of electrochemical compression of hydrogen with metal hydride for heat pump applications. The hydrogen EC was coupled with two metal hydride reactors running in batch mode. The compressor reduces the pressure in desorbing metal hydride reactor which generates cooling and increases the pressure in the absorbing metal hydride reactor that generates heating. As a result, hydrogen is pumped from the desorbing reactor to the absorbing reactor. When the desorbing reactor is depleted with hydrogen and absorbing reactor is filled with hydrogen, a heat recovery cycle will take place to preheat and precool both reactors. And finally the EC switches the hydrogen flow direction so that the metal hydride absorption and desorption will continue at corresponding reactors. The metal hydride heat pump cycle was modelled to show that the hydrogen EC demonstrates superior performance than conventional mechanical compressor driven system with cooling capacities less than 200 W. And quantitative analysis shows a heat pump of 100 W cooling at 5 ºC evaporating and 45 ºC condensing yields a COP of 3.4. The second study focuses on electrochemical compression of ammonia for refrigeration and fuel storage purposes. In this study, ammonia was electrochemically compressed by proton exchange membrane with hydrogen as a carrier gas. Hydrogen was present to protonate ammonia to form NH_4^+ ion, which will be transferred across the PEM under an external voltage potential. And when NH_4^+ reaches the cathode side of the membrane, it will be deprotonated to

form NH_3 and H_2 at an elevated pressure. The proposed reaction shows that for each molecules of H_2 transfer across the membrane, 2 molecules of NH_3 was transferred along, and the transfer coefficient was proven to be strictly maintained independent of temperature and pressure. The NH_4^+ ion conductivity in PEM was measured to be ¼ of the regular proton conductivity. The Nernst equation was satisfied with electrochemically compressing NH_3 to a higher pressure at four different voltage charges. And the ionic transfer mechanism in the PEM is believed to be hopping and vehicular mechanism. The ammonia EC compresses with an efficiency of 93% which results in an improved COP of 5.1 at 5 °C of evaporating and 45 °C of condensing at 200 W of cooling capacity based on modeling results. And the EC can potentially be deployed for ammonia storage as a carbon neutral fuel. The third study focuses on electrochemical compression of CO_2 with anion exchange membrane for vapor compression refrigeration cycle and carbon capture. First of all, $CaRuO_3$, an electro-catalyst which selectively absorbs both CO_2 and O_2 on the surface for enhanced kinetics were synthesized in the lab, and the proposed electrochemical reaction mechanism is verified with GC. Then $CaRuO_3$ was compared with Pt in terms of reaction kinetics, and showed superior performance for the same catalytic surface area. Due to the specific requirement of CO_2 compression, gas distribution channels in the EC were designed and the bipolar plates were machined with stainless steel to replace the original graphite plate. And because of the high discharge temperature of CO_2, proper compressor thermal management was explored and discussed with selection of heat exchangers. Finally, potential applications of CO_2 EC in trans-critical refrigeration cycle with isothermal compression and carbon separation and

capture from flue gas were discussed. In all three studies, electrochemical compression of gases in ion exchange membrane was explored in depth. The results show that the EC is a promising technology with much higher compression efficiency, and operates without moving parts and lubrication. Finally, the proposed EC cooling technique opens another door for compressor cooling, which is considered very difficult in the current state of the art.

6.2 Future work and recommendations

6.2.1 Future work for hydrogen EC heat pump

As hydrogen EC metal hydride heat pump was modeled in a system level, it is clear that an EC stack can be built with measurable amount of hydrogen flowrate for a 200 W cooling system. The hydrogen delivery manifold needs to be designed for parallel EC units in the stack. And the heat pump needs to be tested is a system level with EC implemented. The proposed metal hydride heat recovery process needs to be tested with experimental study. And one of the key future developments will be the design and implementation of an effective metal hydride heat exchanger with large heat transfer coefficient. Also the effective thermal conductivity of metal hydride bed needs to be improved with proper heat transfer design inside the reactor matrix. There has been some previous designs on the MH heat exchangers [9, 11, 74]. Another issue of MH that needs to be further looked into is the fatigue problem during absorption and desorption reaction, which means the metal hydride alloys will break after multiple reaction cycle. And the resulted particles have poor thermal conductivity comparing to the hydride alloys [9]. In conclusion, the metal hydride reactors with proper thermal management needs to be explored further.

6.2.2 Future work for ammonia EC

The key future developments for ammonia EC would be building of the compressor stack, and separation of hydrogen and water from compressed ammonia. The preliminary compressor stack building is discussed in Chapter 4.7. Proper flow distribution manifold needs to be developed for delivering ammonia and hydrogen to the inlet of each EC unit in the stack. And microchannel flat tube heat exchanger embedded in the compressor needs to be tested for stack cooling. Finally, the flowrate of the constructed stack needs to be measured and the EC performance will be both modeled and evaluated in the system level. The ammonia EC in the vapor compression refrigeration system needs to be tested for COP and cooling capacity. The proposed compressor cooling technique also needs to be fully tested for its effectiveness. And the ammonia EC for fuel storage application needs to be tested for compressor efficiency, compression ratio and ammonia liquefaction under room temperature.

6.2.3 Future work for carbon dioxide EC

The future work for electro-chemical CO_2 compression involves the improvement of $CaRuO_3$ catalyst. The catalyst developed in the lab was synthesized with sealed reaction vessel under 200 °C, which could potentially enlarge the particle size of the catalyst. Because the catalyst particles may agglomerate under pressurized environment. The synthesized particles in the lab have surface area around 15 m^2/g, which is considered as low. To reduce the particle size and increase the surface area, the catalyst may ideally be synthesized at 200 °C in atmospheric pressure under reflux condition in $KMnO_4$ solution [22]. The process needs to be constantly monitored

for 48 hours for safety. Ball milling has been tried to increase the overall surface area and turned out to be not successful. Even though ball milling was able to reduce the particle size, it crushes the particle inner pores and results an even smaller surface area (Figures B-5 and B-6). Therefore, another proper method needs to be explored to reduce the particle size and maintain the particle porosity. Ultimately, the surface area needs to be increased in terms of m^2/g for enhanced reaction kinetics.

The electrochemical CO_2 compression stack needs to be built for a complete system analysis. The preliminary scaled-up EC stack design is proposed in chapter 4.7. And the gas diffusion channel design for CO_2 EC is discussed and shown in chapter 5.4.2. These proposed designs need to be built and tested for their effectiveness in the EC compressor stack.

6.3 Contributions

6.3.1 List of Major Contributions

- Reaction fundamental of electrochemical compression
    - Developed the understanding of surface electrochemistry, compression efficiency and mechanism
- Electrochemical hydrogen compressor driven MH heat pump
    - Proposed thermodynamic cycle analysis and heat recovery
    - Simulated the heat pump operation with cooling, heating capacity and COP
- Electrochemical ammonia compression for vapor compression refrigeration cycle and fuel storage
    - Proposed and experimentally verified ammonia electrochemical compression mechanism with hydrogen as a carrier gas
    - Measured the NH_4^+ ionic conductivity in PEM
    - Determined the pressure ratio and voltage charge relationship and verified with Nernst Equation
    - Proposed the ionic transfer mechanism of NH_4^+ in PEM
    - Measured the electrochemical ammonia compression performance
    - Proposed potential applications for ammonia vapor compression refrigeration cycle and ammonia fuel storage
- Electrochemical CO_2 compression for trans-critical refrigeration cycle and carbon capture

- Compared both $CaRuO_3$ and Pt catalyst for the electrochemical compression process
- Fabricated membrane electrode assemblies with both $CaRuO_3$ and Pt catalyst and tested the performance
- Proposed and experimentally verified the electrochemical compression mechanism of CO_2 and O_2 at the surface of the catalyst coated anode and cathode
- Measured and compared the ionic conductivity of CO_3^-, HCO_3^- and CO_3^{2-} in AEM
- Designed stainless steel gas distribution channels in CO_2 electrochemical compressor to replace graphite
- Proposed electrochemical compressor stack cooling technique with selection of heat exchangers
- Proposed and explored the potential applications for CO_2 trans-critical refrigeration cycle and carbon capture

6.3.2 List of Publications

Peer-reviewed Journal Papers:

Y. Tao, W. Gibbons, Y. Hwang, R. Radermacher, C. Wang, Electrochemical ammonia compression, *Chemical Communications,* 2017, 53, 5637-5640.

Y. Tao, H. Lee, Y. Hwang, R. Radermacher, C. Wang, Electrochemical compressor driven metal hydride heat pump, *International Journal of Refrigeration*, 2015, 60, 278-288.

Y. Tao, Y. Hwang, R. Radermacher, C. Wang, Electrochemical Carbon Dioxide Separation and Storage using Carbonate Selective Perovskite Oxide Catalyst, *In Preparation.*

Conference Papers:

Y. Tao, Y. Hwang, R. Radermacher, C. Wang, Performance investigation on electrochemical compressor with ammonia, *International Compressor Engineering Conference,* West Lafayette, IN, USA (July, 2016) **Awarded for 1st Place Best Student Paper**

Y. Tao, H. Lee, Y. Hwang, R. Radermacher, C. Wang, Experimental investigation on electrochemical ammonia compressor, *Gustav Lorentzen Natural Working Fluids Conference,* Edinburgh, UK (September, 2016)

Y. Tao, Y. Hwang, C. Wang, R. Radermacher, The integration of ammonia electrochemical compressor in vapor compression system. *IEA Heat Pump Conference,* Rotterdam, the Netherlands (May, 2017)

Invention Disclosures:

R. Radermacher, **Y. Tao**, M. Beshr, Heat pump using metal hydride and electrochemical hydrogen compressor, US Patent Application 62/380200, 2016.

C. Wang, R. Radermacher, **Y. Tao**, Y. Hwang, Novel methods and devices for electrochemical compression CO_2, University of Maryland, **committed by Sanhua Holding**, PS-2016-169.

C. Wang, R. Radermacher, **Y. Tao**, Y. Hwang, Ammonia Electrochemical Compression and Power Recovery for Vapor Compression Cycle, University of Maryland, PS-2016-093.

C. Wang, R. Radermacher, **Y. Tao**, Y. Hwang, Carbon Dioxide Electrochemical Compression and Expansion for Vapor Compression Cycle, University of Maryland, PS-2015-094.

R. Radermacher, **Y. Tao**, M. Beshr, Electrochemical Expander, University of Maryland, PS-2014-092.

R. Radermacher, **Y. Tao**, M. Beshr, Brayton Cycle using Electrochemical Compression, University of Maryland, PS-2014-093.

R. Radermacher, **Y. Tao**, M. Beshr, Ericsson Cycle using Electrochemical Compression, University of Maryland, PS-2014-094.

R. Radermacher, **Y. Tao**, M. Beshr, Vapor Compression Cycle using Electrochemical Compression and Expansion, University of Maryland, PS-2014-095.

Appendices

Appendix A: Additional ammonia EC experimental data

Ammonia GC calibration curves

The GC calibration curves were developed for measuring the concentration ratio of ammonia and hydrogen on the discharge side of the electrochemical compressor. They were prepared by running ammonia and hydrogen mixture with known concentration through the GC. And they were plotted in terms of known composition versus GC peak areas.

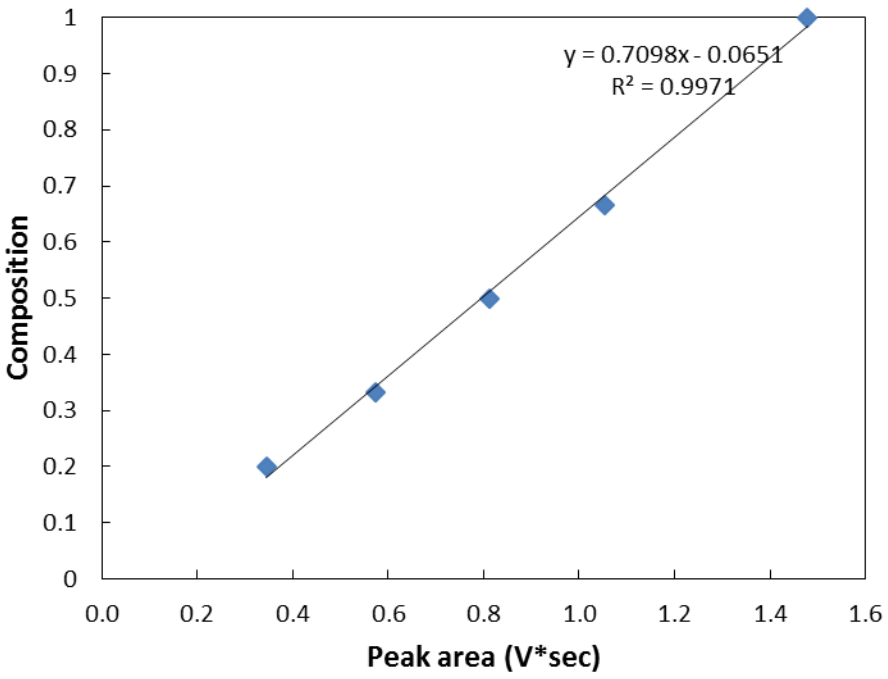

Figure A-1: Hydrogen concentration GC calibration curve

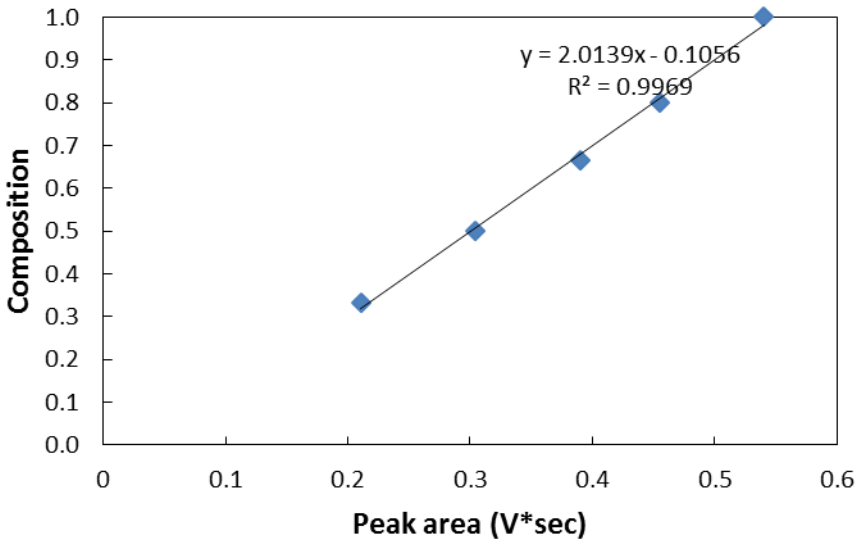

Figure A-2: Ammonia concentration GC calibration curve

Ammonia EC performance at different relative humidity

The compressor performance was evaluated at three different relative humidity. The performance was given in terms of current voltage linear sweep (Figure A-3). The RHs can be controlled by the heater and humidifier and measured at operating temperature of 30 °C, 50 °C and 60 °C. As shown in Figure A-3, the increase of relative humidity leads to increase of current which is reflected by the compressor performance at the same voltage charge. The best performance is achieved at the highest operating temperature and highest RH, because the Nafion membrane resistance decreases and RH increases as the temperature increases. But the EC operating temperature has to stay below 100 C to avoid any dehydration of the membrane.

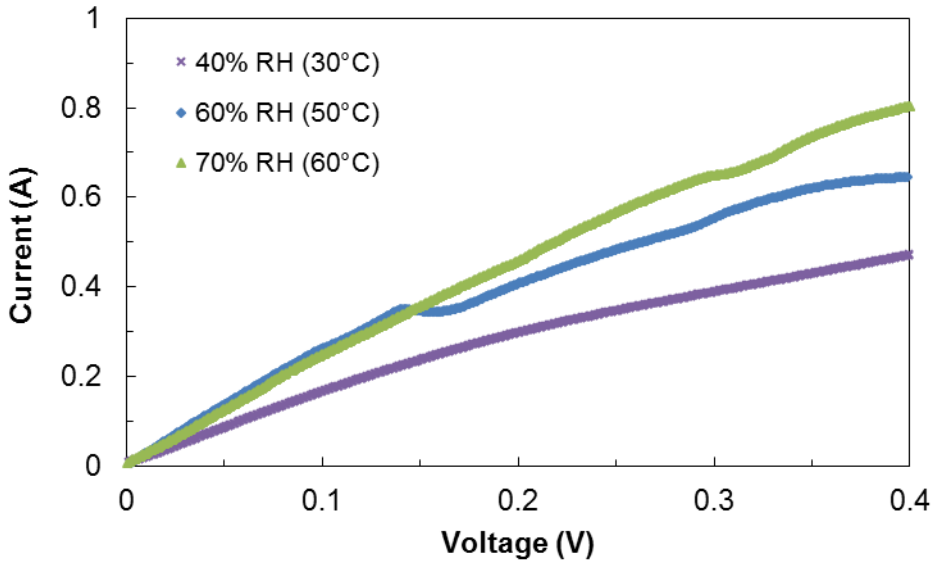

Figure A-3: Current density linear scan in terms of voltage at three RHs

Closed loop analysis with single unit electrochemical ammonia compressor

In order to test the compressor prototype performance for the potential vapor compression cycle application, a closed loop analysis was performed to test the EC performance in real conditions with discharge line valve partially opened. As previously described, the EC builds up pressure by pumping gas molecules across the MEA, therefore the discharge side flow back to the suction line needs to be regulated. The closed loop analysis gives real time performance of the EC. At this moment, the single unit EC prototype has only very limited flow rate. In order to have flow rate that is measureable, the EC needs to be scaled up by increasing the MEA surface area and number of stacks. The system was pulled vacuum before charging 2 bar of mixture of H_2 and NH_3 at 1:2 ratio. Figure A-4 shows the closed loop design of EC with suction line and discharged line marked. The suction line uses 6.4 mm diameter tubing and 50 cc cylinder for gas reservoir. The discharge line uses 3.2 mm diameter tubing. Figure A-5 shows the closed loop schematic of the ammonia EC. Both suction

side (anode) pressure and discharge side (cathode) pressure were measured by pressure transducers. The MEA needs to be humidified to be able to transport both H_2 and NH_3, so that the refrigerant loop was heated by a tape heater to keep temperature constant at 60ºC to have reasonable RH of 70% for enough membrane humidification. For the real refrigeration system, the tape heater can be removed and a suction line humidifier would be installed to maintain the humidity of the MEA. The humidity is required at a high level in order to maintain the ionic conductivity of the proton exchange membrane for high ammonia transfer rate. Water is not interacting with the working fluid but only serves as a need for the membrane to conduct ammonium ions. The EC performance at different voltage charges was measured in terms of pressure drop and current.

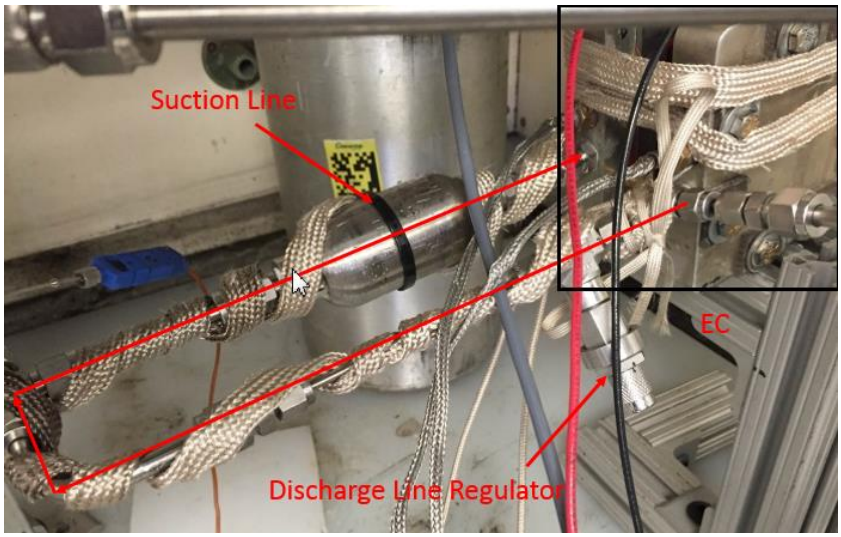

Figure A-4: Closed loop analysis with suction and discharge line shown.

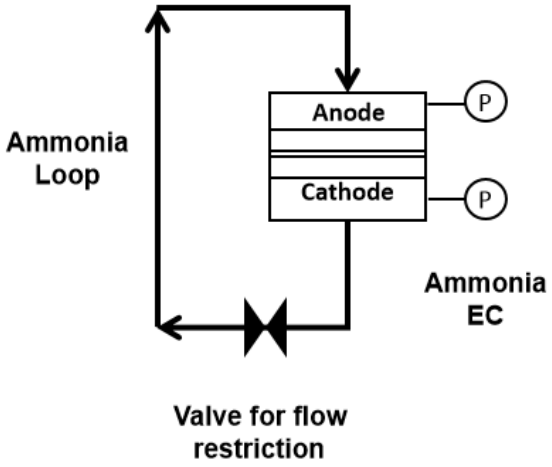

Figure A-5: Schematic of EC closed loop

The EC single cell was charged with a voltage for 1,500 seconds and the current was measured as well as the pressure lift from the suction side to the discharge side. Figure A-6 shows the current versus voltage graphs. As the voltage charge increases, the current increases as well. The EC was able to maintain constant pressure lift at fixed voltages. The flow rate across the EC can be calculated based on the current by using the Faraday's Law.

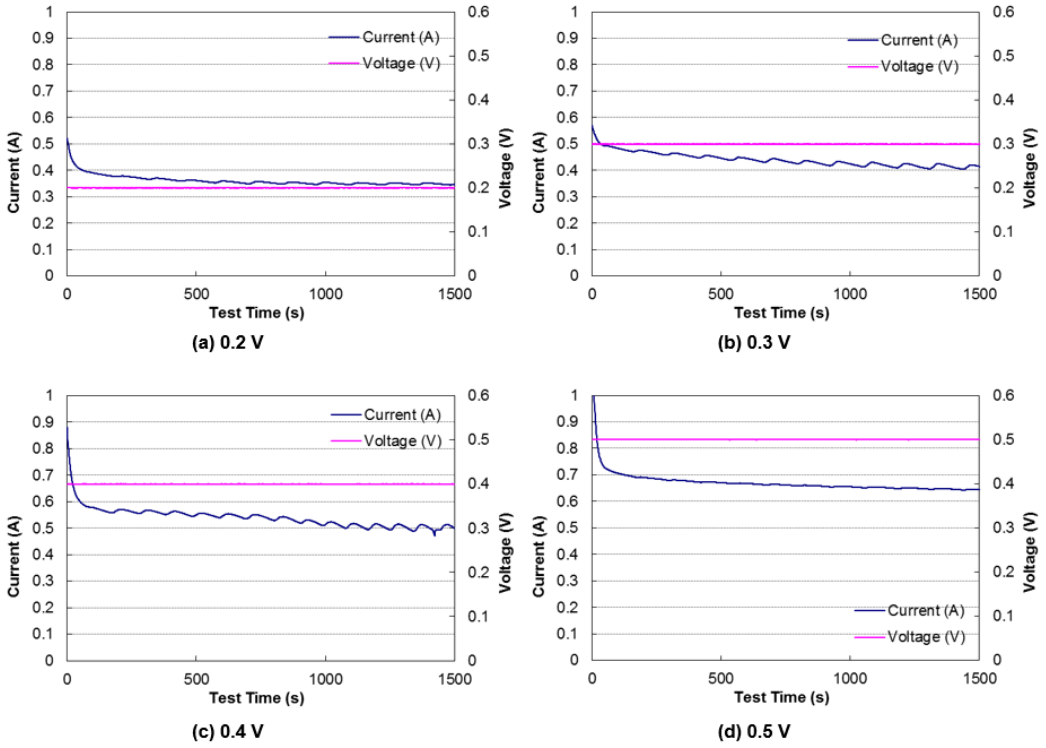

Figure A-6: Current versus voltage at voltage charge

The pressure lift was measured at the suction line and discharge line by partially opening the metering valve. Table A-1 shows the pressure lift with respect to different voltage charge. The pressure lift of a single EC unit is very low. However, it is expected to increase linearly as the number of units in the stack increases for scaling up. The evaporating and condensing temperatures of ammonia are 5°C and 45°C at 5 bar and 18 bar, respectively. For the future development, 1 EC with multiple units in the stack for the required pressure lift will be built and tested for a 200 W cooling system.

Table A-1: Pressure lift versus voltage charge

Voltage (V)	Pressure lift (kPa)
0.2	19
0.3	23
0.4	26
0.5	30

Ammonia EC compression efficiency

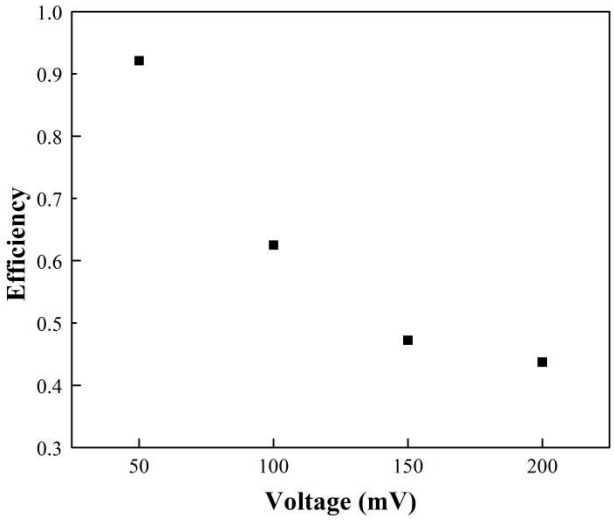

Figure A-7: Ammonia EC compression efficiency at 50 mV, 100 mV, 150 mV and 200 mV

Appendix B: Additional CO_2 EC experimental data

CO_2 GC calibration curves

The GC calibration curves for CO_2 and O_2 were generated by running samples through GC at given concentration. Because the concentration of discharged CO_2 will be in the range between 60% and 80%, and the concentration of discharged O_2 will be in the range between 20% and 40%; the calibration process can be conducted in the concentrations of these range.

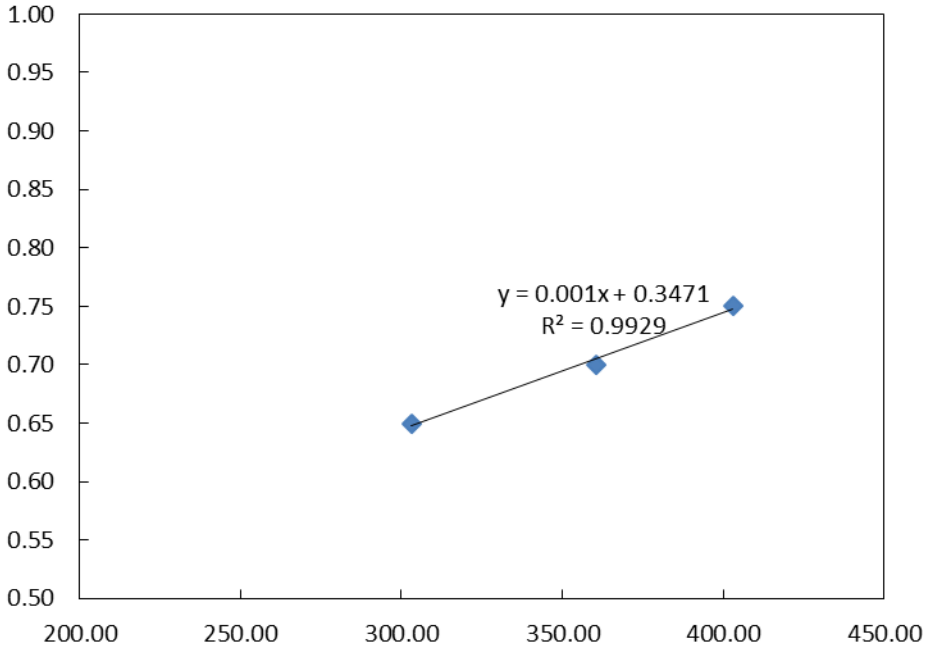

Figure B-1: CO_2 GC calibration curve

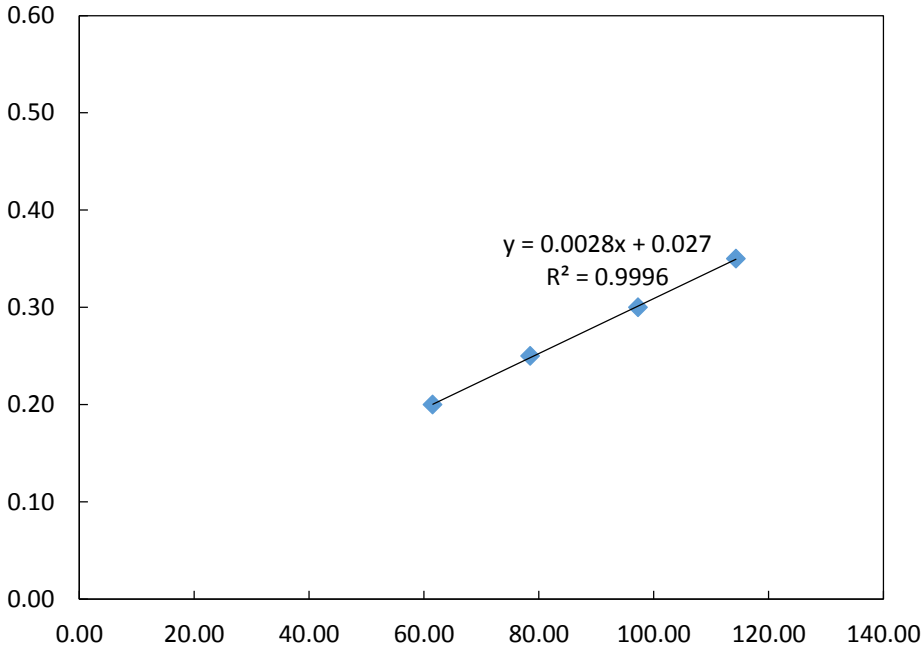

Figure B-2: O_2 GC calibration curve

The SEM of CaRuO3 catalyst particles

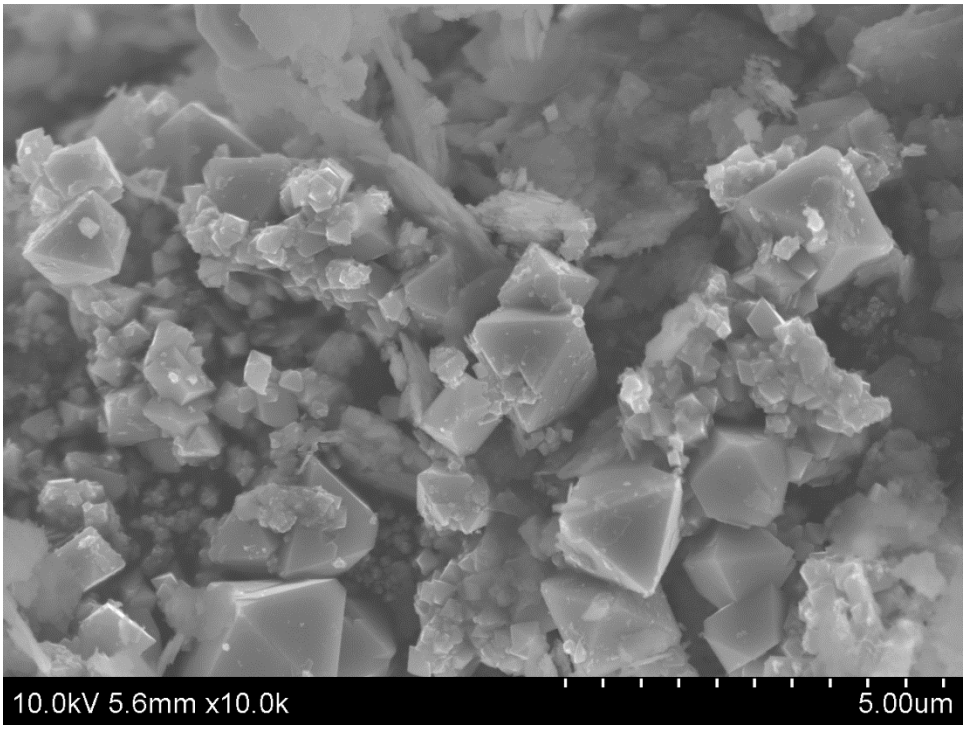

Figure B-3: SEM of $CaRuO_3$ at 5 micron scale

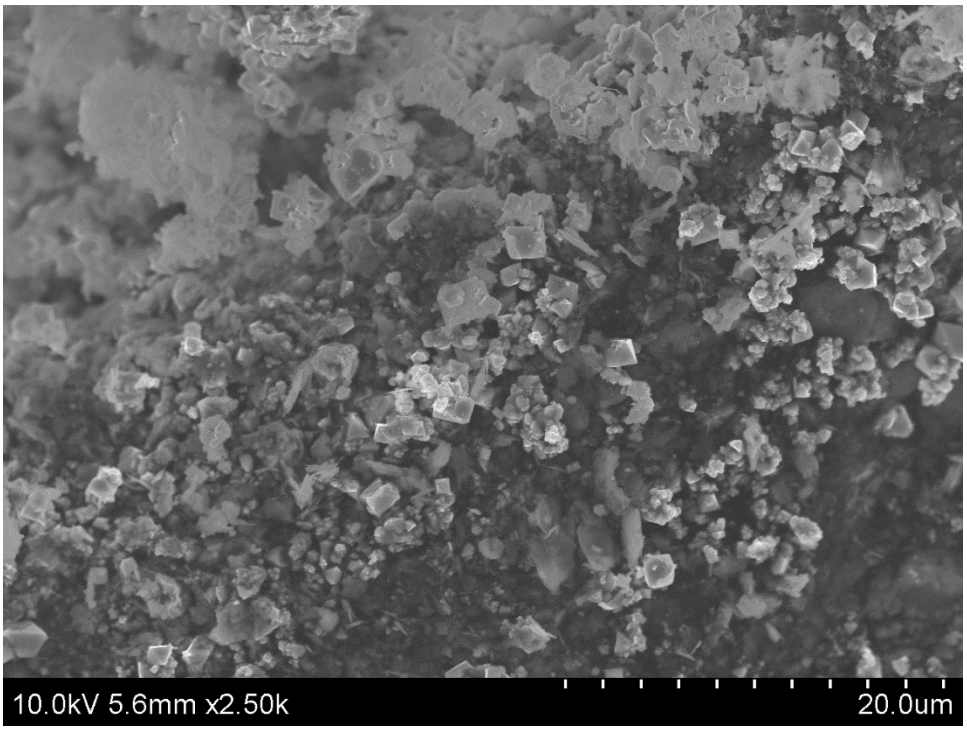

Figure B-4: SEM of $CaRuO_3$ at 20 micron scale

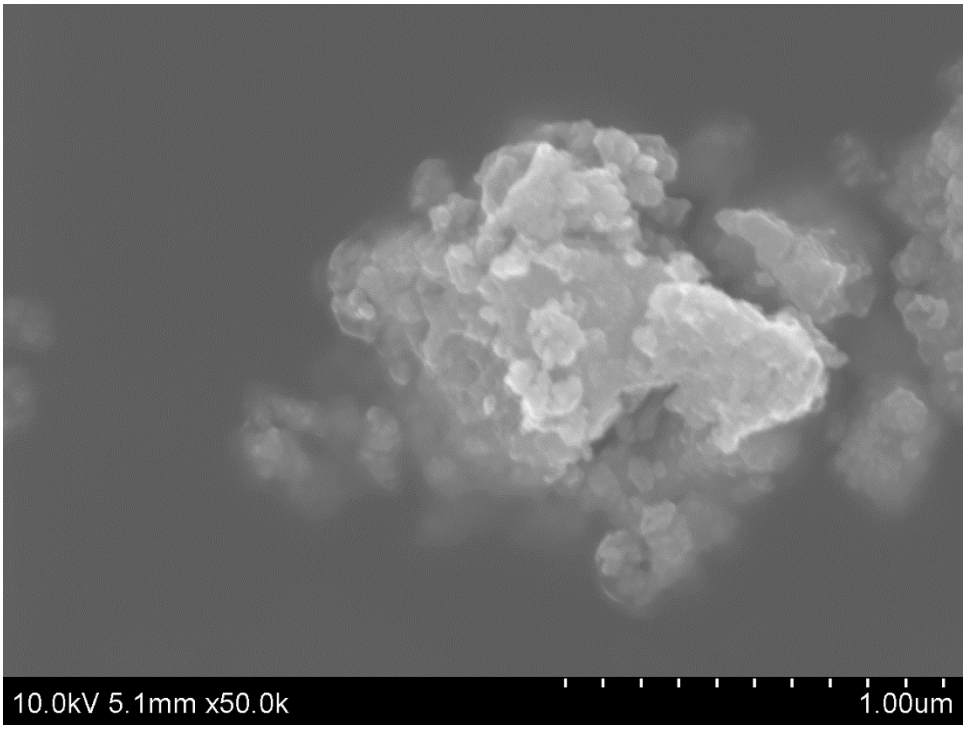

Figure B-5: Ball milled CaRuO3 at 1 micron scale

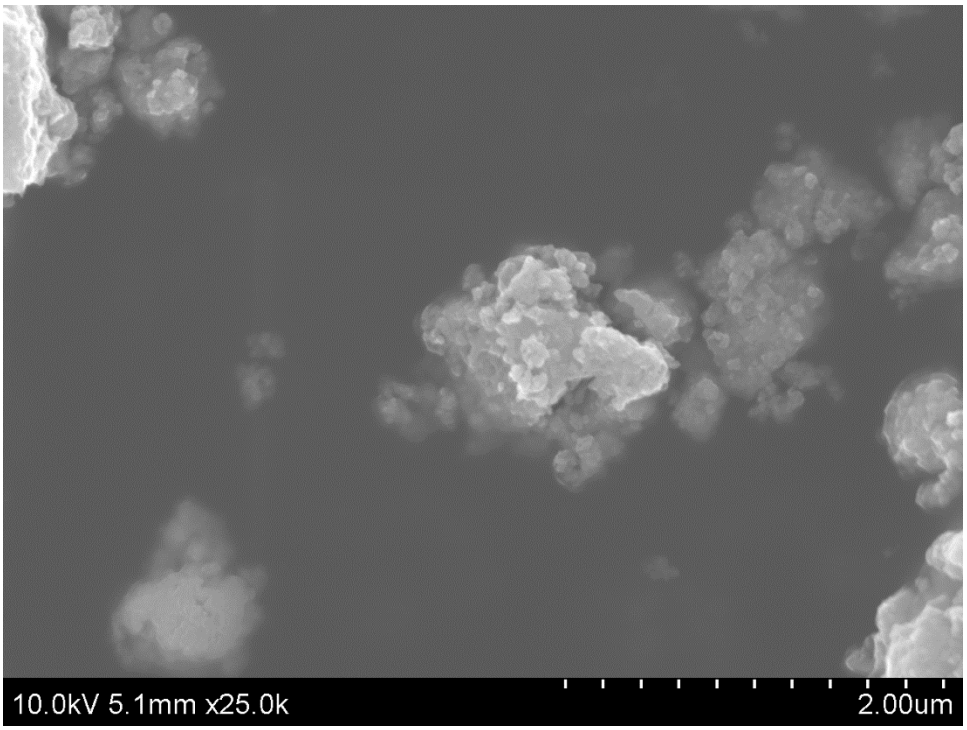

Figure B-6: Ball milled CaRuO3 at 2 micron scale

CO_2 partial pressure compression ratio

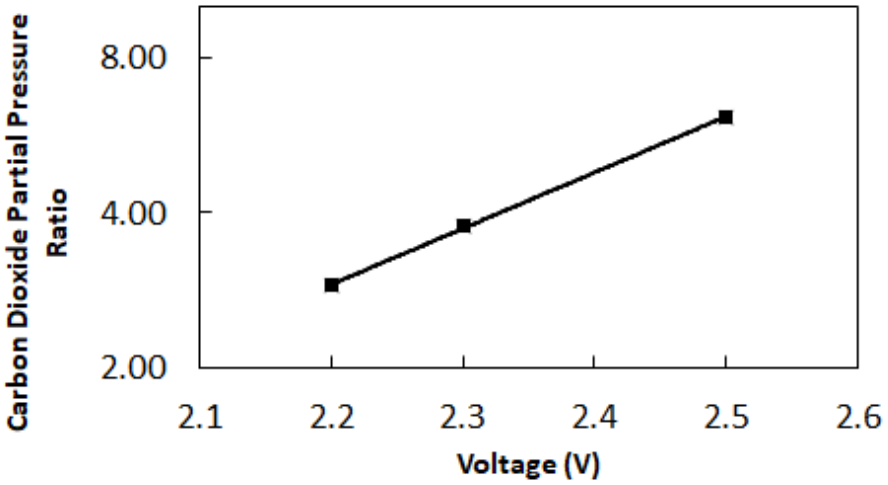

Figure B-7: CO_2 partial pressure compression ratio vs. voltage charge

Bibliography

1. Sedlak, J., Austin, J., LaConti, A., 1981. Hydrogen recovery and purification using the solid polymer electrolyte electrolysis cell. International Journal of Hydrogen Energy 6, 45-51.
2. Rohland, B., Eberle, K., Strobel, R., Scholta, J., Garche, J., 1998. Electrochemical hydrogen compressor. Electrochimica Acta 43, 3841-3846.
3. Strobel, R., Oszcipok, M., Fasil, M., Rohland, B., Jorissen, L., Garche, J., 2002. The compression of hydrogen in an electrochemical cell based on a PE fuel cell design. Journal of Power Sources 105, 208-215.
4. Hirscher, M., 2010. Handbook of Hydrogen Storage: New Materials for Future Energy Storage, WILEY-VCH Verlag GmbH&Co. KGaA, Weinherm.
5. Sandrock, G., 1999. A panoramic overview of hydrogen storage alloys from a gas reaction point of view. Journal of Alloys and Compounds 293-295, 877-88.
6. Takeda, H., Kabotomori, T., Ohnishi, K., 2009. Metal hydride air-conditioning. Energy Carriers and Conversion Systems, Encyclopedia of Life Support Systems, 2, 249 – 263.
7. Muthukumar, P., Groll, M., 2010. Metal hydride based heating and cooling systems: A review. International Journal of Hydrogen Energy 35, 3817-3831.
8. Zhong, Y., Glanville, P., 2014. Metal-hydride adsorption systems for space conditioning in commercial and residential buildings. Proceedings of the ASME 2014 International Mechanical Engineering Congress and Exposition, November 14- 20, 2014, Montreal, Quebec, Canada.
9. Kim, K., Feldman K. Jr., Lloyd G., Razani A., 1997. Compressor-driven metal-hydride heat pumps. Applied Thermal Engineering 17, 551-560.
10. Park, J., Jang, K., Lee, P., Lee, J., 2001. The operating characteristics of the compressor-driven metal hydride heat pump system. International Journal of Hydrogen Energy 26, 701-706.
11. Park, J., Han, S., Jang, H., Lee, S., Lee, P., Lee, J., 2002. The development of compressor-driven metal hydride heat pump (CDMHHP) system as an air conditioner. International Journal of Hydrogen Energy 27, 941-944.
12. Mazumdar, S., Gopal, M., Bhattacharyya, S., 2004. Performance of compressor driven metal hydride cooling systems under different operating conditions. International Refrigeration and Air Conditioning Conference, Purdue University, IN.
13. Magnetto, D., Mola, S., Dacosta, D., Golben, M., Rosso, M., 2006. A metal hydride mobile air conditioning system. SAE International, 2006-01-1235.
14. Uribe, F. A., Gottesfeld, S. and Zawodzinski, T. A. J. Electrochem. Soc. 2002, 149, A293-A296.

15. Soto, H. J., Lee, W., Van Zee, J. W. and Murthy, M. Electrochem. Solid-State Lett. 2003, 6, A133-A135.
16. Halseid, R., Vie, P. J. and Tunold, R. Effect of ammonia on the performance of polymer electrolyte membrane fuel cells. J. Power Sources. 2006, 154, 343-350.
17. Jung, R. M., Cho, H., Park, S. and Van Zee, J. W. J. Power Sources. 2015, 275, 14-21.
18. Poynton, S. D., Zeng, R., Kizewski, J., Ong, A. L., Varcoe, J. R. Development of Alkaline Exchange Ionomers for use in Alkaline Polymer Electrolyte Fuel Cells. ECS Transactions, 2012, 50, 2067-2073.
19. Zhou, J., Unlu, M., Vega, J., Kohl, P. Anionic polysulfone ionomers and membranes containing fluorenyl groups for anionic fuel cells. Journal of Power Sources, 2009, 190, 285-292.
20. Pandey, T., Peters, B., Liberatore, M. and Herring, A. Insight on pure vs air exposed hydroxide ion conductivity in an anion exchange membrane for fuel cell applications. ECS Transactions, 2014, 64, 1195-1200.
21. Unlu, M., Zhou, J. and Kohl, P. Anion Exchange Membrane Fuel Cells: Experimental Comparison of Hydroxide and Carbonate Conductive Ions. Electrochemical and Solid-State Letters, 2009, 12, B27-B30.
22. Vega, J., Shrestha, S., Ignatowich, M. and Mustain, W. Carbonate Selective Ca2Ru2O7-y Pyrochlore Enabling Room Temperature Carbonate Fuel Cells I: Synthesis and Physical Characterization. Journal of The Electrochemical Society, 2012, 159, B12-B17.
23. Rigdon, W., Omasta, T., Lewis, C. and Mustain, W. Reaction Dependent Transport of Carbonate and Bicarbonate through Anion Exchange Membranes in Electrolysis and Fuel Cell Operations. ECS Transactions, 2015, 69, 1-9
24. Aspen compressor performance chart.
25. Possamai, F., Lilie, D., Zimmermann, A., Mongia, R., 2008. Miniature vapor compression system, International refrigeration and air conditioning conference. Purdue University, Paper 963.
26. Danfoss Compressor, Transcritical refrigeration systems with carbon dioxide, how to design and operate a small capacity (<10kW) transcritical CO2 system.
27. Emerson Copeland Compressor data sheet, ZO Scroll Compressor For Subcritical R-744.
28. Danfoss, CO2 A Green Compressor, data sheet.
29. Frascold, cooling solutions CO2 semi-hermetic reciprocating compressors.
30. Wang, X., Hwang, Y. and Radermacher, R. Investigation of potential benefits of compressor cooling, Applied Thermal Engineering, 2008, 28, 1791-1797.
31. Barbir, F., 2005, PEM Fuel Cells : Theory and Practice. San Diego : Elsevier Science, Print.

32. Slade, R., Kizewski, J., Poynton, S., Zeng, R. and Varcoe, J. Alkaline Membrane Fuel Cells. Fuel Cells: Selected Entries from the Encyclopedia of Sustainability Science and Technology, New York, 2013, Print.
33. Luo, Y., Guo, J., Wang, C. and Chu, D. An Acrylate-Polymer Based Electrolyte Membrane for Alkaline Fuel Cell Applications. ChemSusChem, 2011, 11, 1557-1560.
34. Vega, J., Spinner, N., Catanese, M. and Mustain, W. Carbonate Selective Ca2Ru2O7-y Pyrochlore Enabling Room Temperature Carbonate Fuel Cells II: Verification of Carbonate Cycle and Electrochemical Performance. Journal of The Electrochemical Society, 2012, 159, B18-B23.
35. Incropera and Dewitt, 2002
36. Onda, K., Ichihara, K., Nagahama, M., Minamoto, Y., Araki, T., 2007. Separation and compression characteristics of hydrogen by use of proton exchange membrane. Journal of Power Sources 164, 1-8.
37. Mehta, V., Cooper, J., 2002. Review and analysis of PEM fuel cell design and manufacturing. Journal of Power Sources 114, 32 – 53.
38. Wong, T., Girard, F., Vanderhoek, T., 2004. Electrochemical Hydrogen Compressor, United States patent application publication, 2004/0211679 A1.
39. Moton, J., James, B., Colella, W., 2014. Advances in electrochemical compression of hydrogen. Proceedings of the ASME 2014 12th International Conference on Fuel Cell Science, Engineering and Technology, Boston, MA.
40. Bedbak, S. and Gopal, R. Performance analysis of a compressor driven metal hydride cooling system. International Journal of Hydrogen Energy, 2005, 30, 1127-1137.
41. Hopkins, R., Kim, K., 2010. Hydrogen compression characteristics of a dual stage thermal compressor system utilizing LaNi5 and Ca0.6Mm0.4Ni5 as the working metal hydrides. International Journal of Hydrogen Energy 35, 5693-5702.
42. Pehnt, M. Life-cycle assessment of fuel cell stacks, International Journal of Hydrogen Energy. 2001, 26, 91-101.
43. Tao, Y., Lee, H., Hwang, Y., Radermacher, R., Wang C., 2015. Electrochemical compressor driven metal hydride heat pump. International Journal of Refrigeration 60, 278-288.
44. Suzuki, S., Muroyama, H., Matsui, T., and Eguchi, K. J. Power Sources. 2012, 257-262.
45. Eberle, U., Müller, B., and Helmolt, R., 2012. Fuel cell electric vehicles and hydrogen infrastructure: status 2012. Energy and Environmental Science, 5 (10), 8780 - 8798
46. Sathe, A., Groll, E. and Garimella, S. International Compressor Engineering Conference Proceedings. 2008.

47. Tao, Y., Gibbons, W., Hwang, Y., Radermacher, R., Wang, C., 2017. Electrochemical ammonia compression. Chemical Communications 53, 5637.
48. Kaye, G., and Laby, T. Tables of physical and chemical constants and some mathematical functions. Longman, New York. 1986
49. Choi, P., Jalani, N. and Datta, R., 2005. Thermodynamics and proton transport in Nafion II proton diffusion mechanisms and conductivity. Journal of Electrochemical Society. 152, E123-E130.
50. Chen, C., Tse, Y., Lindberg, G., Knight, C., and Voth, G. Hydroxide solvation and transport in anion exchange membranes. Journal of American Chemical Society 2015, 138, 991-1000.
51. Agmon, N., The Grotthus mechanism, Chemical Physics Letters 1995, 244, 456-462.
52. Refrigerator market profile, US DOE 2009
53. Guidance for inspection of atmospheric refrigerated ammonia storage tanks
54. Varcoe, J., Atanassov, P., Dekel, D., Herring, A., Hickner, M., Kohl, P., Kucernak, A., Mustain, W., Nijmeijer, K., Scott, K., Xu, T., Zhuang, L. Anion exchange membranes in electrochemical energy systems. Energy and Environmental Science, 2014, 7, 3135.
55. Adams, L, Poynton, S., Tamain, C., Slade, R. and Varcoe, J. A Carbon Dioxide Tolerant Aqueous Electrolyte Free Anion Exchange Membrane Alkaline Fuel Cell. ChemSusChem, 2008, 1, 79-81.
56. Dekel, D. Review of cell performance in anion exchange membrane fuel cells. Journal of Power Sources, 2017, 1-12
57. Jenkins H and Thakur, K. Reappraisal of Thermochemical Radii for Complex Ions, Journal of Chemical Education, 1979, 56, 9.
58. Larmine, J. and Dicks, A. Fuel Cell Systems Explained, 2nd Ed. John Wiley and Sons Ltd, West Sussex England, 2003, Print.
59. Chung, C., Chen, S., Chiu, P., Chang, M., Hung, T. and Ko, T. Carbon film coated 304 stainless steel as PEMFC bipolar plate, Journal of Power Sources 2008, 176, 276-281.
60. Pozio, A., Zara, F., Masci, A. Bipolar plate materials for PEMFCs: A conductivity and stability study. Journal of Power Sources, 2008, 179, 631-639.
61. Kumagai, M., Myung, S., Kuwata, S., Asaishi, R. and Yashiro, H. Corrosion behavior of austenitic stainless steels as a function of pH for use as bipolar plates in polymer electrolyte membrane fuel cells. Electrochimica Acta, 2008, 53, 4205-4212.
62. Coney, M., Stephenson, P., Malmgren, A., Linnemann, C., Morgan, R., Richards, R., Huxley, R., Abdallah, H., Development of a reciprocating compressor using water injection to achieve quasi-isothermal compression,

Proceedings of the 16th International Compressor Engineering Conference, 1992, pp 541-550.
63. Faghri, A. and Guo, Z. Challenges and opportunities of thermal management issues related to fuel cell technology and modeling. International Journal of Heat and Mass Transfer, 2005, 48, 3891-3920.
64. Taherian, R. A review of composite and metallic bipolar plates in proton exchange membrane fuel cell: Materials, fabrication and material selection. Journal of Power Sources, 2014, 265, 370-390.
65. Zhang, G. and Kandlikar, S. A critical review of cooling techniques in proton exchange membrane fuel cell stacks. International Journal of Hydrogen Energy, 2012, 37, 2412-2429.
66. Schmidt, H., Buchner, P., Datz, A., Dennerlein, K., Lang, S. and Waidhas, M. Low-cost air cooled PEFC stacks. Journal of Power Sources, 2002, 105, 243-249.
67. Sohn, Y., Park, G., Yang, T., Yoon, Y., Lee, W., Yim, S. and Kim, C. Operating characteristics of an air cooling PEMFC for portable applications. Journal of Power Sources, 2005, 145, 604-609.
68. Matian, M., Marquis, A., Brandon, N., Model based design and test of cooling plates for an air-cooled polymer electrolyte fuel cell stack. Int. J. Hydrogen Energy 2011; 36: 6051-6066.
69. Garrity, P., Klausner, J., Mei, R., A flow boiling microchannel evaporator plate for fuel cell thermal management. Heat Transfer Eng 2007; 28: 877-884.
70. Boomsma K, Poulikakos D, Zwick F. Metal foams as compact high performance heat exchangers, *Mech Mater* 2003; 35: 1161-1176.
71. Odabaee, M., Mancin, S., Hooman, K., Metal foam heat exchangers for thermal management of fuel cell systems- An experimental study. *Exp Therm Fluid Sci* 2013; 51: 214-219.
72. COSIA SAGD Reference Facilities, Candor Engineering Ltd. March 24, 2017
73. Joo, S., Park, J., Renzas, J., Butcher, D., Huang, W. and Somorjai, G. Size effect of ruthenium nanoparticles in catalytic carbon monoxide oxidation. Nano Letters, 2010, 10, 2790-2713.
74. Shafiee, S. and McCay, M. Different reactor and heat exchanger configurations for metal hydride hydrogen storage systems- A review. International Journal of Hydrogen Energy, 2016, 41, 9462-9470.